AD 739823

0

TECHNICAL REPORT

ANALYTICAL STUDIES OF IMPACT-GENERATED SHOCK PROPAGATION - SURVEY AND NEW RESULTS

By: William J. Rae

CAL No. AI-2456-A-1

June 1968

CORNELL AERONAUTICAL LABORATORY, INC.
OF CORNELL UNIVERSITY, BUFFALO, N. Y. 14221

(1)

CORNELL AERONAUTICAL LABORATORY, INC.
BUFFALO, NEW YORK 14221

ANALYTICAL STUDIES OF IMPACT-GENERATED SHOCK PROPAGATION-SURVEY AND NEW RESULTS

CAL REPORT NO. AI-2456-A-1

JUNE 1968

PREPARED BY: William J. Rae
William J. Rae

APPROVED BY: J. Gordon Hall
J. Gordon Hall, Head
Aerodynamic Research Department

FOREWORD AND ACKNOWLEDGEMENT

This report will appear as a chapter of the book: High Velocity Impact Phenomena, edited by R. Kinslow, to be published by Academic Press. The preparation of this report was supported by the Cornell Aeronautical Laboratory Internal Research Program.

The writer is very grateful to Drs. Ronald G. Rehm and T. R. Sundaram for many helpful comments.

TABLE OF CONTENTS

LIST OF FIGURES

LIST OF TABLES

LIST OF SYMBOLS

a	-	speed of sound
a, b	-	constants related to plane-wave loading history, Eq. (67)
A^2	-	normalized sound speed (squared), Eq. (185)
A	-	constant in power-law shock trajectory
B	-	amplitude coefficient, Eq. (65)
A_1, A_2	-	constants in the asymptotic solution of the plane-wave, perfect-gas case, at large negative ζ
B_1, B_2	-	constants in the solution near the shock/free-surface intersection
c	-	weak-wave speed in the linear shock-speed, particle-speed relation
c_p	-	specific heat at constant pressure
$D(\tilde{M}; s, \delta)$	-	function defined in Eq. (160)
e	-	internal energy per unit mass
$\hat{e}_3$	-	unit vector normal to the z, y plane
E	-	projectile kinetic energy, axisymmetric case
$\mathcal{E}$	-	kinetic energy per unit area, plane-wave case
f	-	normalized pressure, $p/\rho_0 \dot{z}_{so}^2$
$F(\gamma)$	-	amplitude of power-law shock trajectory, axisymmetric case
$F(p, \rho)$	-	functional form of equation of state
$F(z, y, t)$	-	function whose zero locus is the shock location

F_1, F_2, F_3, F_4	- similitude functions, defined in Eqs. (164)-(166)
$fcn(\cdot\cdot,\cdot\cdot,\cdot\cdot)$	- denotes functional dependence on the arguments displayed
$\mathcal{g}$	- normalized internal energy, $e/\dot{z}_{so}^2$
$G(\gamma)$	- function defined in Eq. (62)
$\mathcal{G}(\cdot\cdot)$	- loading function, Eq. (66)
$H(\gamma)$	- function defined in Eq. (A-21)
$I(\gamma)$	- Integral defined in Eq. (141)
k_1, k_2, k_3	- constants in shock-shape expression
K	- constant in approximate off-axis pressure distribution, Eq. (135)
K_1	- constant used in specifying boundary of neglected mass, Appendix
ℓ	- coordinate giving distance from shock/free-surface intersection
$\mathcal{L}_0$	- axisymmetric scaling length, Eq. (29)
$\mathcal{L}_1$	- plane-wave scaling length, Eq. (64)
L_0	- projectile scale, $(M/\rho_0)^{1/3}$. Also used as the thickness of the impacting slab in the plane-wave case.
L_1	- initial depth of a plane of particles whose trajectories are found in Sec. IV C. 3.
m_0	- neglected mass
M	- projectile mass
M_s	- shock Mach number, $\mathcal{g}_s/c$

M_{so} - shock Mach number along symmetry axis, $\dot{z}_{so}/c$

$\tilde{M}$ - value which the shock Mach number had when the shock crossed a particle of given entropy

N - characteristic exponent in power-law shock trajectory; also used (Sec. IV C. 4) to denote the component, normal to a constant-β line, of the pseudovelocity vector

p - pressure

$p_L(t)$ - loading function, Eq. (66)

P - projectile momentum, axisymmetric case

P_{max} - amplitude of loading function, Eq. (66)

$\mathcal{P}$ - momentum per unit area, plane-wave case

q - particle velocity

q_s - shock velocity

r - spherical radius

R - y/L_o

R_o - scaling length for spherically symmetric explosions, Eq. (187)

R_s - spherical radius of shock

s - slope parameter in linear shock-speed, particle-speed relation

t - time

t_s - time when a given particle is processed by the shock

t_1 - time when z_{so} is equal to L_1

T - component of pseudovelocity vector tangent to constant-β lines

T_{max} - duration of loading function, Eq. (66)

u - z-component of particle velocity

U - projectile speed before striking the target

v - y-component of particle velocity

V - $=(\partial w/\partial \tau)_{\tau=0}$

x - parameter in Enig's equation of state, Eq. (155)

y - cylindrical radius

z - axial coordinate

z_{so} - distance from origin to the shock, along the symmetry axis

$\dot{z}_{so}$ - shock speed along the symmetry axis

Z_1 - $= z/L_0$

α - similitude parameter

$\bar{\alpha}$ - coefficient of volume expansion

β - angle measured from free surface

γ - specific-heat ratio

Γ - Grüneisen factor

δ - $= \rho c_p / \bar{\alpha} \rho_0 c^2$, Eq. (161)

$\Delta(\rho)$ - function defined in Eq. (148)

ζ - normalized axial coordinate, z/z_{so}

η - normalized spherical radius, r/z_{so}

θ - spherical polar angle

λ	- similitude parameter. See Eqs. (68) or (87) for connection between λ and N in the plane and axisymmetric cases, respectively
ρ	- mass density
σ	- normalized cylindrical radius, y/z_{so}
σ_1	- value of σ at the shock/free-surface intersection
τ	- $= Ut/L_o$
ϕ	- normalized axial component of particle velocity, $u/\dot{z}_{so}$
$\Phi(\Psi)$	- function defined in Eqs. (153)-(155)
$\varphi(\rho)$	- used in Eq. (24) to denote general density dependence in state equation that allows self-similar solutions
ψ	- normalized density, ρ/ρ_o
Ψ	- function defined in Eqs. (153)-(155)
ω	- normalized radial component of particle velocity, $v/\dot{z}_{so}$
$(\ )_c$	- denotes cohesive contribution
$(\ )_H$	- denotes evaluation on the Hugoniot
$(\ )_{UL}$	- denotes upper limit of integration
$(\ )_{cs}$	- denotes conditions at a control surface
$(\ )_R$	- denotes head of rarefaction fan
$(\ )_{so}$	- denotes conditions at the shock, along the axis of symmetry
$(\ )_s$	- denotes conditions at a general point on the shock
$(\ )_{o,1}$	- denotes conditions ahead of, behind, the shock

$(\ )^{(0)}, ^{(1)}, \ldots$	- denotes order of the coefficient in an expansion in powers of ℓ
$(\dot{\ })$	- denotes d/dt
$(\hat{\ })$	- denotes a unit vector

I. INTRODUCTION

Many authors have treated the motion of a half-space of a condensed medium caused by the impact of a high-speed projectile, or by the detonation of an explosive at the surface. Most of the available data are the results of experiments or of computer calculations. The purpose of the present work is to present a synthesis of what is known, based on the analytical properties of the governing differential equations.

In some theoretical treatments of shock propagation, the phenomena occurring are represented by an extremely simplified model, for which a solution can be written down without difficulty. Papers of this sort, which Eichelberger classified as "quasi-theoretical" in his 1963 review (1), are mentioned only briefly in the present work. The primary emphasis is given to theoretical studies that start from a full formulation of the problem, and then proceed through a sequence of approximations to a simpler set of equations whose relation to the original problem can be clearly understood.

When solids collide at speeds on the order of several kilometers per second, the pressures generated reach megabar proportions. Because these pressures exceed the strengths of materials by many factors of ten, there is a regime where it is possible to neglect the effect of strength, and to treat the solid as an inviscid, compressible fluid. The steps leading to this approximation, and the resulting set of differential equations, are reviewed in Section II. The entire content of this work is devoted to the solution of these equations under a variety of further approximations. Thus the solutions described here apply only to that portion of the impact process where strength can be neglected. In any impact, of course, the pressures eventually decay, and the material strength then becomes the dominant factor, determining the final configuration in which the material comes to rest. The inviscid solutions of the present work offer no direct information on this final configuration. In some cases, they have been used to infer information about the final deformation, but a clear distinction must be made between what is found from the inviscid solution in its regime of validity, and what is inferred about the subsequent, strength-dominated response of the solid.

Much of our present understanding of the propagation of strong shock waves in gases was provided by the methods of self-similarity. Perhaps the most famous example of this approach is the treatment of the point-source explosion problem, by von Neumann (2), Sedov (3), Taylor(4), and others. In seeking solutions of the impact problem, it is natural to turn again to the similarity method. Unfortunately, there are two features of the impact problem that prevent this method from enjoying the same degree of success that it achieved in the earlier blast-wave problems. The first is that the flow contains two spatial dimensions, and thus is described by a set of partial differential equations, even when similarity is assumed. The second is that the intensity of impact-generated shock waves is usually too small to permit a similarity assumption; flows of this type are characteristically non-self-similar. The full set of requirements for self-similarity is discussed in Section III.

One case for which self-similarity can be assumed occurs when the equation of state of the target is taken to be that of a perfect gas. A solution for this case was calculated by Walsh et. al. (5). These numerical results were very generously made available to the present writer by Dr. Walsh, and have been used to determine the full two-dimensional, self-similar solution. This solution, described in Section IV, provides a great deal of information about the two-dimensional properties of the flow field, for the self-similar case.

The effects of nonsimilarity are considered in Section V. These effects can be attributed to the form of the state equation appropriate for a solid; thus the section begins with a review of various expressions for the equation of state. Following this, exact solutions are considered. It is shown that the "late-stage equivalence" similitude discovered by Walsh (5, 6, 7) holds for very general conditions, and has a rigorous analytical basis. The available details of the solution are reviewed, and several approximate treatments of the nonsimilar problem are discussed.

The concluding remarks, in Section VI, contain a summary of the present state of our knowledge of impact-generated shock propagation, some comments on the application of this knowledge to crater-size predictions, and a list of some of the more important problems that remain to be solved.

Many of the results appearing below are new, and are presented here for the first time. Specifically, the new material includes:

1. The self-similar flowfield functions and associated particle paths (Section IV)

2. The analytic solution for the region near the shock/free-surface intersection point (Section IV)

3. The derivation of the general similitude properties of the basic differential equations (Section V)

II. FORMULATION OF THE PROBLEM

A. RESTRICTION TO AXISYMMETRIC FLOW

The only case considered in this work is that in which the target is a half-space, and the path of the projectile is normal to the original target surface. The projectile is assumed to have an axis of symmetry coincident with its path. Thus, the flow taking place after the initial contact is axisymmetric. This restriction is made for the purpose of simplicity in the mathematical treatment of the problem. In addition, it has been observed experimentally that the crater resulting from an oblique impact has the same shape as that due to a normal impact, for angles of obliquity up to a maximum value that depends on a number of factors(8). Thus the results described here may also be applicable to cases of oblique incidence, although the similarity of the final crater shape does not constitute sufficient proof that the shock-propagation histories are the same in the two cases.

Furthermore, the projectile is represented as a point source of energy and momentum throughout most of this work. Thus the solutions presented can be applied to an actual impact situation only when the main shock has propagated to a depth many times the significant dimension of the projectile.

B. FLUID-MECHANICAL MODEL

The net force acting on a small element of the target material is contributed to by gradients of the normal and shear stresses. The relative magnitudes of these two contributions can be estimated by comparing a typical normal stress with a typical shear stress, since the gradients of these quantities in any two perpendicular directions are of the same order of magnitude.

The proper order for the normal stress is the pressure generated at the shock, which is initially on the order of $\rho_o U^2$, and which decays as the shock spreads out into the target. The ultimate strength of the target material appears to be a suitable order of magnitude for the shear stress. Comparison of these two quantities for impact of typical solids at speeds on the order of several kilometers per second suggests that the material-strength effect is less than the normal-stress contributions by several factors of ten. Thus there is a regime in which the equations used to describe the target response can be taken as the familiar equations of compressible, inviscid-fluid flow*, expressing the conservation of mass, momentum, and energy.

While this approximation has been used for more than a decade, there has always been an awareness that it must fail at sufficiently low pressure (9, 10). Recent years have seen significant advances toward the determination

---

* This approximation is often referred to as the "hydrodynamic" model. Use of this term is avoided in the present work because of its association in many texts with incompressible flow.

of the pressure level at which the strength effect becomes important, as well as useful methods for predicting the effect-- see, for example, Ref. 11. Throughout the present work, however, attention is restricted to results obtained in the zero-strength approximation.

In prescribing the energy equation, energy changes arising from viscous dissipation and heat conduction are omitted; this is consistent with their neglect in the momentum equation. The transport of energy by radiation is also neglected.

C. EQUATIONS OF MOTION

A cylindrical coordinate system is chosen with its axis along the approach path of the projectile:

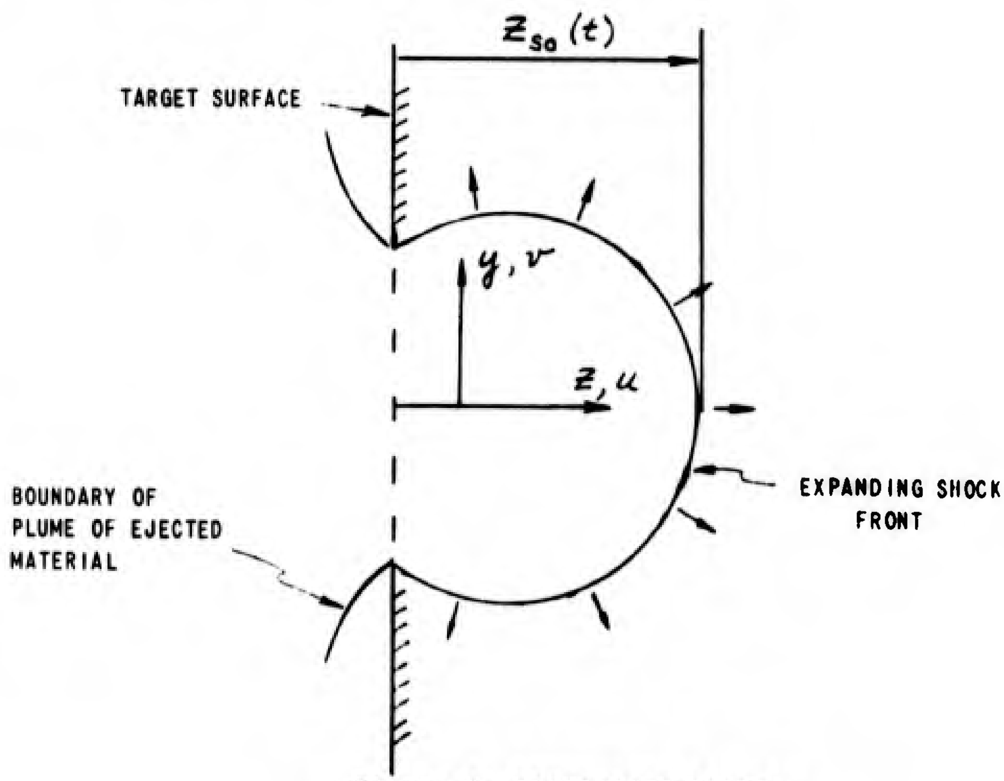

Figure 1 COORDINATE SYSTEM

In these coordinates, the equations of motion are:

$$\frac{\partial \rho}{\partial t} + u \frac{\partial \rho}{\partial z} + v \frac{\partial \rho}{\partial y} + \rho \left(\frac{\partial u}{\partial z} + \frac{v}{y} + \frac{\partial v}{\partial y} \right) = 0 \tag{1}$$

$$\frac{\partial u}{\partial t} + u \frac{\partial u}{\partial z} + v \frac{\partial u}{\partial y} + \frac{1}{\rho} \frac{\partial p}{\partial z} = 0 \tag{2}$$

$$\frac{\partial v}{\partial t} + u \frac{\partial v}{\partial z} + v \frac{\partial v}{\partial y} + \frac{1}{\rho} \frac{\partial p}{\partial y} = 0 \tag{3}$$

$$\frac{\partial e}{\partial t} + u \frac{\partial e}{\partial z} + v \frac{\partial e}{\partial y} - \frac{p}{\rho^2} \left(\frac{\partial \rho}{\partial t} + u \frac{\partial \rho}{\partial z} + v \frac{\partial \rho}{\partial y} \right) = 0 \tag{4}$$

$$e = F(p, \rho) \tag{5}$$

The specific functional dependence appearing in the equation of state is left arbitrary for the moment. The use of an equation of state implies an assumption of thermodynamic equilibrium; thus kinetic processes such as condensation or phase change are excluded from consideration.

D. BOUNDARY CONDITIONS

Along the shock, the Rankine-Hugoniot conditions apply. For a small planar element of the shock, moving at speed q_s into a medium at rest, these conditions are

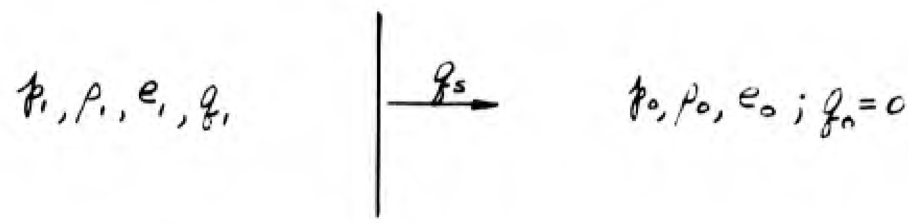

Figure 2 SHOCK-WAVE NOTATION

$$\rho_0 q_s = \rho_1 (q_s - q_1) \tag{6}$$

$$p_1 - p_0 = \rho_0 q_s q_1 \tag{7}$$

$$e_1 - e_0 = \frac{1}{2} (p_0 + p_1) \left(\frac{1}{\rho_0} - \frac{1}{\rho_1} \right) \tag{8}$$

A second boundary condition is that, at the edge of the plume of fluid being ejected from the target, the pressure in the plume should equal the ambient static pressure surrounding the target (usually this pressure is taken to be zero). These boundary conditions are very difficult to apply, since the time-dependent location and shape of the shock and of the plume boundary cannot be specified in advance.

III. SIMILARITY REQUIREMENTS

A. GENERAL CONSIDERATIONS

In studying a problem as complex as the present one, it is useful to see whether there are any similitudes that might be used to correlate solutions for different impact situations. The purpose of this section is to discuss the conditions under which a similitude can be found.

In its most general form, a similitude identifies scaling factors for both the dependent variables (pressure, density, particle velocity) and the independent ones (two spatial coordinates and the time), such that for different impacts the scaled pressure distribution (for example) would be the same function of the scaled spatial coordinates, provided the same scaled time were chosen for both impacts. At a later value of the scaled time, the two scaled pressure distributions would again be identical to each other, although different from the distribution that existed earlier.

A simpler similitude is sometimes found in which the scaled distributions are the same for all values of the scaled time; solutions of this type are said to be self-similar. It is shown below that a self-similar solution can be found when the state equation of the target is approximated by that of a perfect gas. If an equation of state more realistic for a solid is used, the solution is not self-similar, but a more complex similitude can be shown to exist.

B. NORMALIZATION

As a first step in deriving the similitude properties of the solution, it is useful to normalize the spatial coordinates by the distance $z_{so}(t)$ to which the shock has propagated along the axis of symmetry:

$$\zeta = \frac{z}{z_{so}(t)} \quad , \quad \sigma = \frac{y}{z_{so}(t)} \tag{9}$$

The time variable is replaced by the Mach number of the shock along the axis of symmetry:

$$M_{so}(t) = \dot{z}_{so}/c \tag{10}$$

Here c is the speed at which small disturbances travel into the undisturbed medium. The dependent variables are redefined as follows:

$$u(z, y, t) = \dot{z}_{so}(t)\, \phi(\zeta, \sigma, M_{so}) \tag{11}$$

$$v(z, y, t) = \dot{z}_{so}(t)\, \omega(\zeta, \sigma, M_{so}) \tag{12}$$

$$p(z, y, t) = \rho_o \left[\dot{z}_{so}(t)\right]^2 f(\zeta, \sigma, M_{so}) \tag{13}$$

$$\rho(z, y, t) = \rho_0 \psi(\zeta, \sigma, M_{so}) \tag{14}$$

$$e(z, y, t) = \left[\dot{z}_{so}(t)\right]^2 g(\zeta, \sigma, M_{so}) \tag{15}$$

In writing the functional dependences on the right-hand sides of these equations, the point-source assumption has been made. If this were not done, it would be necessary to add a separate dependence on the scale of the projectile $L_0/z_{so}(t)$.

In terms of these variables, the equations of motion become

$$(\phi - \zeta)\frac{\partial \psi}{\partial \zeta} + (\omega - \sigma)\frac{\partial \psi}{\partial \sigma} + \psi\left(\frac{\partial \phi}{\partial \zeta} + \frac{\omega}{\sigma} + \frac{\partial \omega}{\partial \sigma}\right) = \tag{16}$$

$$= \frac{d \ln \dot{z}_{so}}{d \ln z_{so}} \frac{\partial \psi}{\partial \ln M_{so}}$$

$$\frac{d \ln \dot{z}_{so}}{d \ln z_{so}} \phi + (\phi - \zeta)\frac{\partial \phi}{\partial \zeta} + (\omega - \sigma)\frac{\partial \phi}{\partial \sigma} + \frac{1}{\psi}\frac{\partial f}{\partial \zeta} = \tag{17}$$

$$= -\frac{d \ln \dot{z}_{so}}{d \ln z_{so}} \frac{\partial \phi}{\partial \ln M_{so}}$$

$$\frac{d \ln \dot{z}_{so}}{d \ln z_{so}} \omega + (\phi - \zeta)\frac{\partial \omega}{\partial \zeta} + (\omega - \sigma)\frac{\partial \omega}{\partial \sigma} + \frac{1}{\psi}\frac{\partial f}{\partial \sigma} = \tag{18}$$

$$= -\frac{d \ln \dot{z}_{so}}{d \ln z_{so}} \frac{\partial \omega}{\partial \ln M_{so}}$$

$$2\frac{d\ln \dot{z}_{so}}{d\ln z_{so}}\, g + (\phi-\zeta)\frac{\partial g}{\partial \zeta} + (\omega-\sigma)\frac{\partial g}{\partial \sigma} - \frac{f}{\psi^2}\left\{(\phi-\zeta)\frac{\partial \psi}{\partial \zeta} + (\omega-\sigma)\frac{\partial \psi}{\partial \sigma}\right\} =$$

$$= -\frac{d\ln \dot{z}_{so}}{d\ln z_{so}}\left\{\frac{\partial g}{\partial \ln M_{so}} - \frac{f}{\psi^2}\frac{\partial \psi}{\partial \ln M_{so}}\right\} \tag{19}$$

The Rankine-Hugoniot conditions become

$$\psi_1\left(1 - \frac{\dot{z}_{so}}{g_s}\frac{g_1}{\dot{z}_{so}}\right) = 1 \tag{20}$$

$$f_1 - \frac{p_o}{\rho_o \dot{z}_{so}^2} = \frac{g_s}{\dot{z}_{so}}\frac{g_1}{\dot{z}_{so}} \tag{21}$$

$$g_1 - \frac{e_o}{\dot{z}_{so}^2} = \frac{1}{2}\left(f_1 + \frac{p_o}{\rho_o \dot{z}_{so}^2}\right)\left(1 - \frac{1}{\psi_1}\right) =$$

$$= \frac{F\left(\rho_o \dot{z}_{so}^2 f_1,\ \rho_o \psi_1\right)}{\dot{z}_{so}^{\,2}} \tag{22}$$

C. REQUIREMENTS FOR SELF-SIMILARITY

If the flow is to be self-similar, it must have the same normalized spatial distributions at all times. The conditions necessary for this to occur can be seen by inspection of the above equations.

The first requirement is the point-source assumption, i.e., that $L_0/z_{so}(t)$ be negligible. This assumption has already been made. The second requirement is that the quantity $d \ln \dot{z}_{so} / d \ln z_{so}$ be a constant; this is satisfied if the shock scale grows as a power of the time:

$$z_{so} = At^N \tag{23}$$

The third, fourth and fifth sources of time dependence enter through the boundary conditions at the shock. The third is introduced by the function $g_s/\dot{z}_{so}$; the flow can be self-similar only if this quantity is independent of the time. Thus the shock must preserve the same shape as it grows. The fourth condition for self-similarity is that the pressure ahead of the shock be negligible in comparison to $\rho_0 \dot{z}_{so}^2$. The latter quantity is of the order of the pressure behind the shock, and is large compared with p_0 whenever the fluid-mechanical approximation is valid. The fifth possibility of time dependence enters by way of the state equation. As pointed out by Kynch (12) and Sedov (13), self-similar solutions are possible when the equation of state has the form

$$e = p\,\varphi(\rho) \tag{24}$$

where $\varphi(\rho)$ is any function of the density. When the state equation is of this form, when the term $p_0/\rho_0 \dot{z}_{so}^2$ is negligible, and when the shock shape is constant, it is possible to solve the third of the Rankine-Hugoniot conditions for the density ratio across the shock, ψ_1 , which remains constant

$$2\rho_0 \varphi(\rho_0 \psi_1) - 1 + \frac{1}{\psi_1} = 0 \tag{25}$$

The equation of state of a perfect gas

$$e = \frac{p}{(\gamma-1)\rho} \tag{26}$$

is of the form of Eq. (24). Thus, departures from self-similarity for a perfect gas arise from the counterpressure term $p_0/\rho_0 \dot{z}_{so}^2$. The situation is reversed for shock propagation in a solid. There, the counterpressure term is negligible, but the state equation is not of the proper form, except in the limit of extremely high pressures. Only the very early portion of an impact at extremely high speed will satisfy the self-similarity conditions in a solid. Thus, impact-generated shock propagation in solids is characteristically non-self-similar.

If all of the conditions for self-similarity are met, then the functions f, ψ, g, ϕ, and ω depend only on the two similarity coordinates ζ and σ *:

$$\frac{p}{\rho_0 \dot{z}_{so}^2}, \frac{\rho}{\rho_0}, \frac{e}{\dot{z}_{so}^2}, \frac{u}{\dot{z}_{so}}, \frac{v}{\dot{z}_{so}} = fcns(\zeta, \sigma) \tag{27}$$

* They also depend on any constants appearing in the state equation, such as γ in the perfect-gas case.

The theoretical existence of this similarity is of little use, however, until the actual dependence of f and the other functions on ζ and σ has been found, and until the constant A and the exponent N appearing in the shock trajectory, Eq. (23), have been related to the energy and momentum of the projectile. Dimensional analysis can be used to construct a characteristic length and time from the quantities E and P. It is convenient to include the quantities ρ_o and c in this formulation as well. The result is the following form of the power-law shock trajectory:

$$\frac{z_{so}}{\mathcal{L}_o} = F(\gamma)\left(\frac{ct}{\mathcal{L}_o}\right)^N \tag{28}$$

where the scaling length $\mathcal{L}_o$ is defined as

$$\mathcal{L}_o = \left\{ \frac{E}{\rho_o c^2}\left(\frac{P}{\rho_o c}\right)^{\frac{2-5N}{4N-1}} \right\}^{\frac{4N-1}{3(1-N)}} \tag{29}$$

Walsh and his coworkers (5, 7) present a discussion of the self-similar solution from a slightly different point of view. They first observe that a dimensional analysis of the problem, characterized by the initial density ρ_o, the projectile size L_o, the impact speed U, and the specific-heat ratio γ, shows that the solution must be of the form:

$$\frac{p}{\rho_o U^2}, \frac{\rho}{\rho_o}, \frac{u}{U}, \frac{v}{U} = fcns\left(\frac{z}{L_o}, \frac{y}{L_o}, \frac{Ut}{L_o}; \gamma\right) \tag{30}$$

They then show that a simpler scaling can be found if one introduces the assumption of "late-stage equivalence". This assumption states that the solutions for two different impacts will be identical, after early transient differences have died out, provided the quantity $L_o \mathcal{U}^{\alpha}$ is the same for the two impacts, α being a constant. The "late" aspect of this statement is identical with the point-source assumption, i.e., it simply requires that the shock scale be large compared with the projectile scale. The requirement that $L_o \mathcal{U}^{\alpha}$ be a constant is the same as the statement that the scaling length $\mathcal{L}_o$ be the same in the two cases, where α and N are related by

$$\alpha = \frac{N}{1-N} \tag{31}$$

Thus, for the perfect-gas case, late-stage equivalence is the same as self-similarity.

The functional dependences employed by Walsh et al. are

$$\frac{p Z^{2/\alpha}}{\rho_o \mathcal{U}^2}, \frac{\rho}{\rho_o}, \frac{u Z^{1/\alpha}}{\mathcal{U}}, \frac{v Z^{1/\alpha}}{\mathcal{U}} = fcns\left(\frac{Z^{1+\alpha}}{\tau^{\alpha}}, \frac{R^{1+\alpha}}{\tau^{\alpha}}; \gamma\right) \tag{32}$$

where

$$\tau = \frac{\mathcal{U}t}{L_o}, \quad Z = \frac{z}{L_o}, \quad R = \frac{y}{L_o} \tag{33}$$

It will be seen in Section IV that this form of the solution is identical with the self-similar form described above.

D. SIMILITUDE FOR FINITE SHOCK SPEED

The equation of state of a solid approaches that of a perfect gas only at very high pressures. Thus the self-similarity described above can be expected to apply to solids only under the limiting condition of very large shock strength $(M_{so} \rightarrow \infty)$. As M_{so} becomes finite, the equation of state no longer approximates that of a perfect gas, and the flow becomes non-self-similar. (Specifically, the second, third, and fifth of the requirements listed above are not met.) However, the only new parameter that must be considered is M_{so} *; the quantity $d \ln \dot{z}_{so} / d \ln z_{so}$, the shock shape, and the boundary values at the shock depend only on M_{so}. Thus the solution can be written as

$$\frac{p}{\rho_0 \dot{z}_{so}^2}, \frac{\rho}{\rho_0}, \frac{e}{\dot{z}_{so}^2}, \frac{u}{\dot{z}_{so}}, \frac{v}{\dot{z}_{so}} = fcns\left(\zeta, \sigma, M_{so}, \cdots\right) \tag{34}$$

where the shock trajectory is of the form

$$\frac{z_{so}}{\mathcal{L}_0}, M_{so} = fcns\left(\frac{ct}{\mathcal{L}_0}, \cdots\right) \tag{35}$$

* In addition, parameters other than γ appear in the equation of state. The similitude described here can in principle be used only to correlate solutions for a given material. Actually, the evidence described in Section V indicates that the differences between various materials are relatively minor, at least in axisymmetric flows.

Here the three dots indicate the presence of various constants from the equation of state.

The important feature of these results is that no new scaling lengths enter the problem when M_{so} becomes finite. The scaling length $\mathcal{L}_o$, which originates in the self-similar limit, continues to be the appropriate similtude parameter throughout the non-self-similar part of the flow. In particular, the parameter N (or equivalently α) in the formula for $\mathcal{L}_o$ depends only on the high-pressure limit of the state equation.

The similitude expressed in Eqs. (34) and (35) was first observed by Walsh et. al. (6), who called it "late-stage equivalence". These authors pointed out that dimensional analysis would yield the following form of the solution:

$$\frac{p}{\rho_o \mathcal{U}^2}, \frac{\rho}{\rho_o}, \frac{u}{\mathcal{U}}, \frac{v}{\mathcal{U}} = \text{fcns}\left(\frac{z}{L_o}, \frac{y}{L_o}, \frac{\mathcal{U}t}{L_o}, \frac{\mathcal{U}}{c}\right) \tag{36}$$

They demonstrated numerically that in two impacts for which $L_o \mathcal{U}^{\alpha}$ is the same (where α is the same constant that produces self-similarity in the perfect-gas limit) the solution is the same function of time in both cases. The solution common to both is different at different times, of course, since this flow is not self-similar. They went on to show that the existence of this similitude implies that the solution can be rewritten in the form:

$$\frac{p Z^{2/\alpha}}{\rho_o \mathcal{U}^2}, \frac{\rho}{\rho_o}, \frac{u Z^{1/\alpha}}{\mathcal{U}}, \frac{v Z^{1/\alpha}}{\mathcal{U}} = \text{fcns}\left(\frac{Z^{\alpha+1}}{\tau^{\alpha}}, \frac{R^{\alpha+1}}{\tau^{\alpha}}, \frac{(\mathcal{U}/c)^{\alpha+1}}{\tau}\right) \tag{37}$$

The connection between this correlation and that of Eqs. (34) and (35) is discussed in Section V.

Rather than use the same term (late stage equivalence) for the self-similar and the non-self-similar portions of the flow, it seems preferable to speak of both of these equivalences as "point-source similitude", noting that the similitude has self-similar behavior in the limit $M_{so} \rightarrow \infty$. This terminology is adopted throughout the present work.

It should be noted that the point-source assumption is not related to any assumptions made regarding the equation of state. All the solutions discussed in the present work employ the point-source model, but different forms of the equation of state are used in various places.

IV. THE PERFECT-GAS CASE

The purpose of this section is to present a complete picture of the two-dimensional character of the flow, in a case where self-similarity applies. Self-similarity is possible with any equation of state of the form indicated in Eq. (24). The reason for devoting special attention to the perfect-gas case is that it approximates the high-pressure form of the state equation for many solids.

A. BASIC EQUATIONS

Under the conditions of self-similarity, the shock scale grows as a power of the time; thus

$$\frac{d \ln \dot{z}_{so}}{d \ln z_{so}} = -\frac{1-N}{N} \tag{38}$$

If this is used in Eqs. (16)-(19), and if the right-hand sides are set equal to zero, the result is

$$(\phi - \zeta)\frac{\partial \psi}{\partial \zeta} + (\omega - \tau)\frac{\partial \psi}{\partial \sigma} + \psi\left[\frac{\partial \phi}{\partial \zeta} + \frac{\omega}{\sigma} + \frac{\partial \omega}{\partial \sigma}\right] = 0 \tag{39}$$

$$-\frac{1-N}{N}\phi + (\phi - \zeta)\frac{\partial \phi}{\partial \zeta} + (\omega - \sigma)\frac{\partial \phi}{\partial \sigma} + \frac{1}{\psi}\frac{\partial f}{\partial \zeta} = 0 \tag{40}$$

$$-\frac{1-N}{N}\omega + (\phi - \zeta)\frac{\partial \omega}{\partial \zeta} + (\omega - \sigma)\frac{\partial \omega}{\partial \sigma} + \frac{1}{\psi}\frac{\partial f}{\partial \sigma} = 0 \tag{41}$$

$$-2\,\frac{1-N}{N} f + (\phi - \zeta)\frac{\partial f}{\partial \zeta} + (\omega - \sigma)\frac{\partial f}{\partial \sigma} - \frac{\gamma f}{\psi}\left[(\phi - \zeta)\frac{\partial \psi}{\partial \zeta} + (\omega - \sigma)\frac{\partial \psi}{\partial \sigma}\right] = 0 \tag{42}$$

It can be shown that these equations are either elliptic or hyperbolic in character, depending on whether

$$(\phi - \zeta)^2 + (\omega - \sigma)^2 - \frac{\gamma f}{\psi} \lessgtr 0 \tag{43}$$

The reason why a mixed mathematical character arises can be seen by following the path of a small-disturbance front, originating at the point A in Fig. 3a. The front of this wavelet travels at a velocity equal to the vector sum of the local sound speed and particle velocity, and is located, at a succession of later instants, as follows:

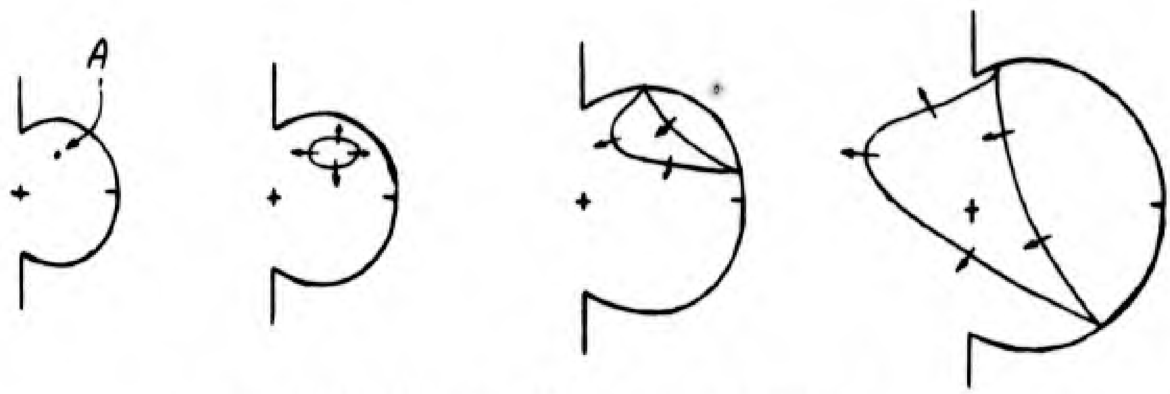

Figure 3a PATH OF DISTURBANCE FRONT, $|q| < a$ INITIALLY

This figure is a schematic illustration of what might happen if the disturbance originates at a point where the particle speed is locally less than the sound speed. In this case, the disturbance can overtake the shock wave, where it is reflected; it is eventually felt at all points in the region enclosed by the shock. If each of the instants in the figure above is now reduced to the same scale, and if the solution in these scaled coordinates is to be the same for each instant, then clearly the governing differential equations must have the property that the solution at point A affects the solution at all the points traversed by the disturbance. The interdependence of the points in part of the flow field is manifested in the partially elliptic character of Eqs. (39)-(42).

If the disturbance originates at the point B (see Fig. 3b) where the sound speed is less than the particle speed, then the disturbance has only a finite zone of influence:

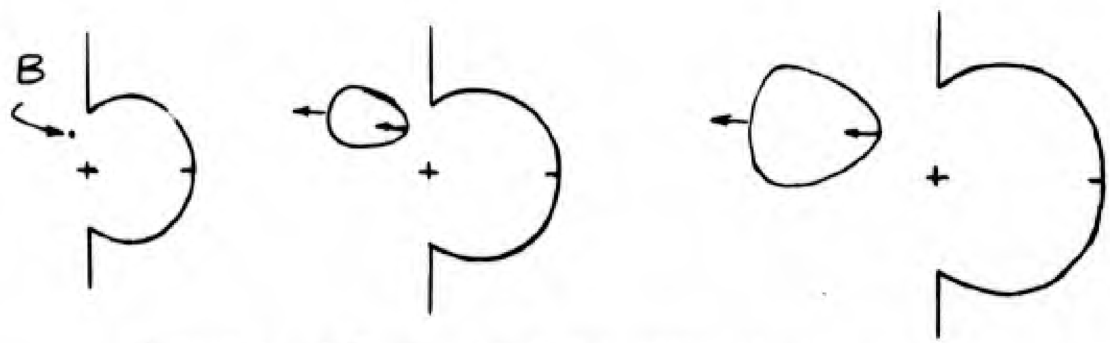

Figure 3b PATH OF DISTURBANCE FRONT, $|q| > a$ INITIALLY

When the transformation of these sketches to the self-similar plane is made, the finite zone-of-dependence property is assured by the partially hyperbolic nature of the solution.

Finally, because disturbances made in the elliptic region are ultimately transmitted to the hyperbolic region, it follows that the solutions in the two regions must be matched along their common boundary. It will be seen below that the matching can be achieved by the proper choice of the parameter N'.

The boundary conditions at the shock are

$$\psi_1 = \frac{\gamma+1}{\gamma-1} \quad , \quad f_1 = \frac{2}{\gamma+1}\left(\frac{q_s}{\dot{z}_{so}}\right)^2 \quad , \quad \frac{q_1}{\dot{z}_{so}} = \frac{2}{\gamma+1}\,\frac{q_s}{\dot{z}_{so}} \qquad (44)$$

The two components ϕ_1 and ω_1 are found from $\vec{g}_1/\dot{z}_{so}$ by taking its components in the ζ and σ directions:

$$\frac{\vec{g}_1}{\dot{z}_{so}} = \phi_1 \hat{\zeta} + \omega_1 \hat{\sigma} \tag{45}$$

The determination of these components cannot be carried out until the shock shape is specified.

At the time of the present writing, no solutions have been calculated directly from Eqs. (39)-(42), because of their mixed hyperbolic-elliptic nature, and also because of the unknown value of N, and the unknown location of the shock surface and the plume boundary. A further problem arises when an attempt is made to satisfy the conservation of the total energy and momentum. Because of its crucial importance, this subject is discussed fully in the paragraphs below.

B. CONSERVATION OF ENERGY AND MOMENTUM

1. The Axisymmetric Case

The integrals expressing the total energy and momentum of the system are

$$E = 2\pi \int_{z=-\infty}^{z_{so}(t)} \int_{y=0}^{y_{UL}(z,t)} \left[e - e_0 + \frac{1}{2}(u^2 + v^2) \right] \rho y \, dy \, dz \tag{46}$$

$$P = 2\pi \int_{z=-\infty}^{z_{so}(t)} \int_{y=0}^{y_{UL}(z,t)} \rho u y \, dy \, dz \tag{47}$$

The upper limit for the integration on y is the shock surface, for $z > 0$ and the plume boundary, for $z < 0$.

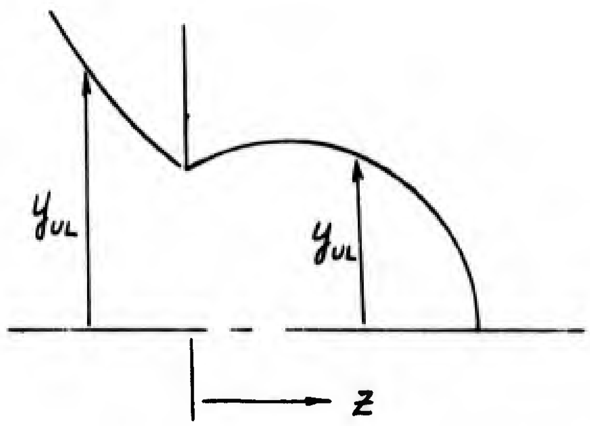

Figure 4 INTEGRATION LIMITS

The choice of the lower limit $z = -\infty$ requires some explanation. In an actual impact with a projectile of nonzero size, the particles lying originally on the free surface would be located at a finite value of z , for any finite time after the impact. An upper limit to their distance from the free surface can be calculated by assuming that, at $t = 0$, they immediately begin moving to the left at the full escape speed, which for a perfect gas has the value

$$u_{escape} = \frac{2}{\gamma - 1} \left(\frac{\gamma p_1}{\rho_1} \right)^{1/2} \tag{48}$$

Here p_1 and ρ_1 are the pressure and density generated at the impact point. This estimate represents an upper limit to their distance from the free surface since these particles are actually carried below the free surface at first; only later do they reverse their velocity, and asymptotically approach the escape speed in the minus- z direction. If the point-source idealization is now made, then the projectile, of vanishing size, must carry a nonzero amount of energy and momentum. To do this, its velocity must be infinite; thus the pressure generated at impact, as well as the speed of the escape front, will also be infinite. For this reason, the lower limit in the integrals above is set at $z = -\infty$.

If the self-similar functions are now introduced into Eqs. (46) and (47), the result is

$$E = 2\pi \rho_0 \dot{z}_{so}^2 z_{so}^3 \int_{-\infty}^{1} \int_{0}^{\sigma_{UL}(\zeta)} \left[\frac{f}{(\gamma-1)\psi} + \frac{1}{2}(\phi^2 + \omega^2) \right] \psi \sigma \, d\sigma \, d\zeta \qquad (49)$$

$$P = 2\pi \rho_0 \dot{z}_{so} z_{so}^3 \int_{-\infty}^{1} \int_{0}^{\sigma_{UL}(\zeta)} \phi \psi \sigma \, d\sigma \, d\zeta \qquad (50)$$

It is clear that a single value of N cannot render both of these expressions independent of time. Constancy of energy would require $N = 2/5$, while constant momentum requires $N = 1/4$. The solution of this dilemma was provided, for the one-dimensional case, by Zeldovich (14). It was subsequently extended to the axisymmetric problem by Rayzer (15) and by the present writer (16). Zeldovich's solution is given below.

2. The One-Dimensional Case

If the projectile is assumed to be a slab of infinite length in the y- direction, or if the disturbance is caused by an explosive slab of infinite length in the y-direction, the response of the target can be assumed to be a function only of z and t. The solution of this problem has been discussed in several papers (14, 16-22). An excellent review is given by Mirels (23). The features important for the present case are repeated below.

The equations of motion are Eqs. (1), (2), and (4), with the y-derivates omitted, and the term v/y absent from the continuity equation. The self-similar forms of these equations are found by dropping their right-hand sides, to yield:

continuity: $$(\phi - \zeta)\psi' + \psi\phi' = 0 \tag{51}$$

momentum: $$-\frac{1-N}{N}\phi + (\phi-\zeta)\phi' + \frac{f'}{\psi} = 0 \tag{52}$$

energy: $$-2\frac{1-N}{N}f + (\phi-\zeta)f' - \frac{\gamma f}{\psi}(\phi-\zeta)\psi' = 0 \tag{53}$$

Here the prime denotes $d/d\zeta$, and the boundary conditions are

$$\psi(1) = \frac{\gamma+1}{\gamma-1} \quad ; \quad \phi(1) = f(1) = \frac{2}{\gamma+1} \tag{54}$$

In both the impact and explosive-slab cases, the target acquires a nonzero energy and momentum. For the impact case, the magnitudes of these quantities can be related to the energy and momentum of the projectile. In the explosive case, the energy and momentum acquired by the target depend on particulars of the loading history at the surface.

The integrals expressing the conservation of the total energy and momentum (per unit area in the plane of the target surface) are

$$\mathcal{E} = \rho_o \dot{z}_{so}^{2} z_{so} \int_{-\infty}^{1} \left(\frac{f}{\gamma - 1} + \frac{\psi \phi^2}{2} \right) d\zeta \tag{55}$$

$$\mathcal{P} = \rho_o \dot{z}_{so} z_{so} \int_{-\infty}^{1} \psi \phi \, d\zeta \tag{56}$$

The lower limits in these integrals have been taken at minus infinity, since the projectile or explosive slab is considered to be of vanishing thickness. Note that the one-dimensional problem presents the same dilemma regarding the choice of N : the energy integral requires $N = {}^2/_3$, while the momentum integral requires $N = {}^1/_2$.

However, there is a much more important consideration affecting the choice of N, namely, that Eqs. (51)-(53) have an acceptable solution only for one value of N . The reason for this can be seen by solving them for the derivatives:

$$\phi' = - \frac{1-N}{N} \frac{\frac{2f}{\psi} - \phi(\phi - \zeta)}{(\phi - \zeta)^2 - \gamma f/\psi} \tag{57}$$

$$\psi' = - \frac{1-N}{N} \frac{(\phi - \zeta)\psi\phi - 2f}{(\phi - \zeta)\left[(\phi - \zeta)^2 - \gamma f/\psi\right]} \tag{58}$$

$$f' = - \frac{1-N}{N} f \frac{\gamma\phi - 2(\phi - \zeta)}{(\phi - \zeta)^2 - \gamma f/\psi} \tag{59}$$

These equations become singular at the point where $(\phi - \zeta)^2 - \frac{\gamma f}{\psi}$ changes sign. This point divides the zones in the similarity plane in which small disturbances can or cannot be felt all the way to the shock wave. For a given value of γ, Eqs. (57)-(59) have nonsingular solutions only for a single value of N. For that value, the numerators of these equations are also zero at the singular point; resolution of the indeterminate form yields the slope of the solution that passes smoothly through the singularity. Table I lists the values of $N(\gamma)$ that lead to regular solutions. The distributions of density, pressure, and velocity that are obtained are shown in Fig. 5 for the case $\gamma = 1.4$, which has the closed-form solution (17, 18)

$$\psi = 6(5-4\zeta)^{-5/2}, \quad \phi = \frac{5}{6}(2\zeta - 1), \quad f = \frac{5}{6}(5-4\zeta)^{-3/2} \tag{60}$$

There can be no question that the nonsingular solutions are the only acceptable ones. But if N is chosen so as to achieve a smooth crossing of the singularity, it is then impossible to satisfy either of Eqs. (55) and (56). The problem involved in the choice of N is not created simply by the fact that there is a second quantity (the momentum) to be conserved. Even if the total momentum were to be zero, the constant-energy value $N = 2/3$ still would not produce a physically acceptable solution.

A resolution of this difficulty was proposed by Zeldovich (14); it is also discussed in the recent text by Zeldovich and Rayzer (24). Their suggestion is that a small portion of the mass be omitted in calculating the total energy and momentum. This small mass initially lies at the free surface and is strongly compressed during the initial stages of the impact or

TABLE I

$\mathcal{N}(\gamma)$ FOR ONE-DIMENSIONAL BLAST WAVES

γ	$\mathcal{N}$	Source
1	0.5	Ref. 23
1.1	0.56888	"
1.4	0.6	"
5/3	0.61073	"
2.8	0.626704	"
∞	0.6416	"
1.001	0.5106	Ref. 16
1.1	0.5683	"
1.2	0.5843	"
1.3	0.5935	"
1.4	0.6000	"
1.8	0.6143	"
2.0	0.6182	"
2.5	0.6244	"
3.0	0.6279	"
4.0	0.6321	"
5.0	0.6341	"
7.0	0.6365	"
10.0	0.6385	"
100.0	0.6412	"
1000.0	0.6416	"

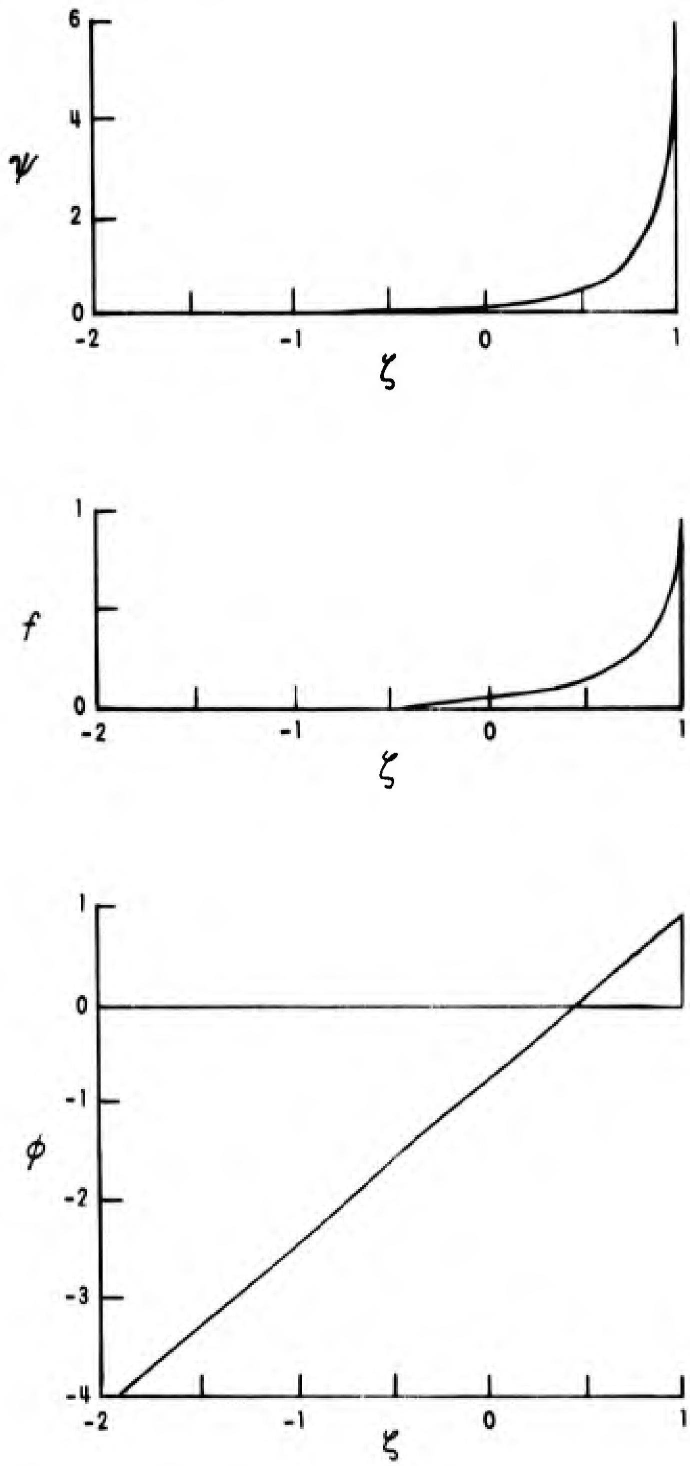

Figure 5 SELF-SIMILAR, PLANE-WAVE SOLUTION (PERFECT GAS, $\gamma = 1.4$)

explosion. It acquires a certain entropy during this compression, which it retains thereafter, since the flow is particle-isentropic. However, the entropy acquired during the initial stages is in general different from the entropy that would be assigned by the self-similar solution. That solution depends only on conditions at the shock and on the properties of the self-similar differential equations; it contains no information about the details of how the shock was initiated. The small amount of mass processed during the early phase always bears the imprint of this phase, and is never correctly described by the self-similar solution. Zeldovich's argument is that, in seeking a self-similar solution, only that mass should be included whose motion is expected to be properly described by such a solution.

An analogous interpretation has been developed in recent years for the problem of hypersonic flow over a blunted slender body (see, for example, Refs. 23, 25, and 26)*. Far downstream of the nose, the flow near the shock can be self-similar if the coordinates, transverse to the freestream direction, of the body and the shock grow as a power of the streamwise coordinate. The layers of fluid near the body, however, are those which have passed through the blunt part of the bow shock; there they acquired an entropy distribution that reflects the details of the shock shape near the nose. This distribution is in general different from that given by the self-similar solution.

To correctly account for the effect of the entropy layer,

---

* The writer is very grateful to his colleague, Dr. T. R. Sundaram, for calling his attention to this analogy, and for many interesting discussions of its application to the impact problem.

separate analyses must be carried out for the high-entropy region and the self-similar region, and the two analyses must then be joined, for example by the method of matched asymptotic expansions (27).

If an analysis of this type were done for the present problem, it would be possible to derive a formula for the shock trajectory which at large time would be of the form $z_{so} = At^N$. The exponent N would be that given by the nonsingular solution of the self-similar equations, while the amplitude A would reflect the details of the shock-initiation process--i. e., A would depend on the amount of mass neglected. Zeldovich outlined this approach in his original paper, recommending that the amplitude A be determined by matching the self-similar solution to a numerical solution of the complete, nonsimilar, partial differential equations at some intermediate time. Since the appearance of Zeldovich's paper, the method of matched asymptotic expansions has undergone considerable development, and could now be used to derive an explicit formula for the amplitude coefficient A in terms of the loading history at the target surface. To the writer's knowledge, the full details of this approach have not yet been carried out.

Zeldovich's result can be expressed in the form (see Appendix 1)

$$z_{so}(t) = H(\gamma) \frac{m_o}{\rho_o} \left[\frac{\rho_o^2 \varepsilon t^2}{m_o^3} \right]^{N/2} \tag{61}$$

where the indeterminate length scale has been expressed in terms of the neglected mass m_o. The present writer observed (16) that a determinate result could be found by making a slight modification to Zeldovich's analysis. This result was presented in Ref. 16 with the erroneous indication that it was an exact solution of the problem, equivalent to what would be derived by the method of matched asymptotic expansions. Further study has made it clear that such is not the case; however, the results derived in this manner have been found to be a very accurate and simple approximation, and are worthy of mention.

If the length scale is made determinate in the manner indicated above, the solution for the slab-impact case has the form (see Appendix 1 for details)

$$z_{so}(t) = G(\gamma)\frac{P^2}{\rho_o \mathcal{E}}\left[\frac{t}{P^3/\rho_o \mathcal{E}^2}\right]^N \tag{62}$$

This can be rewritten in terms of a scaling length $\mathcal{L}_1$ as:

$$\frac{z_{so}}{\mathcal{L}_1} = G(\gamma)\left(\frac{ct}{\mathcal{L}_1}\right)^N \tag{63}$$

where

$$\mathcal{L}_1 = \left\{\frac{\mathcal{E}}{\rho_o c^2}\left(\frac{P}{\rho_o c}\right)^{\frac{2-3N}{2N-1}}\right\}^{\frac{2N-1}{1-N}} \tag{64}$$

For $\gamma = 1.4$, the **constant** $G(\gamma)$ has the value $\left(12\mathcal{E}/9\right)^{1/5}$

The accuracy of this formula can be estimated by comparing its predictions with the numerical results of Zhukov and Kazhdan (21). These authors calculated the response of a half-space of gas, with $\gamma = 1.4$, to a square-wave pressure loading on the surface. At late time, their solution displayed the same behavior as that of the self-similar solution, and they determined the amplitude coefficient from their numerical results. In terms of the peak pressure at the shock, Zhukov and Kazhdan designate this amplitude by the symbol B :

$$p_1 = B\,P_{max}\left(\frac{T_{max}}{Z_{so}}\sqrt{\frac{P_{max}}{\rho_0}}\right)^{2\frac{1-N}{N}} \tag{65}$$

Here the symbols P_{max} and T_{max} are parameters that characterize the loading. In the general case, the free surface is considered to be subjected at $t=0$ to a sharply rising pressure pulse $p_L(t)$ of peak amplitude P_{max} and duration T_{max} :

$$p_L(t) = P_{max}\,\mathcal{G}\left(t/T_{max}\right) \tag{66}$$

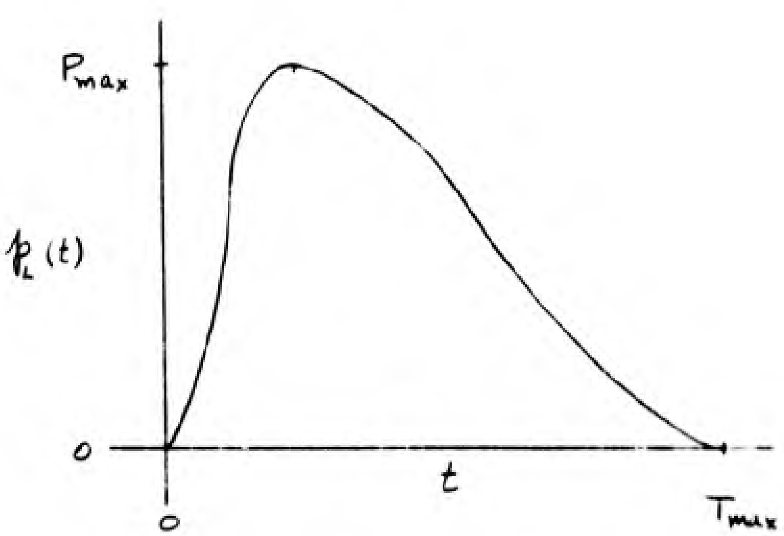

Figure 6 SURFACE-LOADING FUNCTION

The momentum and energy imparted to the target during this loading are

$$\mathcal{P} = a\, P_{max} T_{max} \quad ; \quad a = \int_0^1 \mathcal{G}\left(t/T_{max}\right) d\left(t/T_{max}\right)$$

$$\mathcal{E} = b\, T_{max} \frac{P_{max}^{3/2}}{\rho_0^{1/2}} \quad ; \quad b = \int_0^1 \mathcal{G}\left(t/T_{max}\right) \frac{u_L\left(t/T_{max}\right)}{\sqrt{P_{max}/\rho_0}}\, d\left(t/T_{max}\right) \tag{67}$$

where u_L denotes the velocity of the loaded surface. In particular, for a square-wave loading, $a = 1$, $b = \left(\frac{2}{\gamma+1}\right)^{1/2}$. Use of these values in Eq. (62) leads to the prediction that $\mathcal{B} = 1.657$. The number actually found by Zhukov and Kazhdan is 1.8224.* Thus the approximation presented above is in error by about ten percent in pressure, or about five percent in shock location.

Other evidence for the accuracy of this solution can be found in the numerical calculations of Dienes (22) and of Chou and Burns (28). The scale of the shock trajectory in both of these calculations is predicted with great accuracy by Eq. (62).**

Dienes' calculations were done for the case of zero initial pressure in the target, an initial density of 1.0 gm/cm^3, and for a slab whose

---

*The amplitude coefficient $\mathcal{B}$ depends only on the shape of the loading function, as expressed in the constants a and b. Thus it would have the same constant value for a slab of any thickness and velocity, and a different constant value for a square-wave loading of any magnitude.

**The agreement, in the case of Dienes' calculations, is partially obscured by the fact that he made a slight shift in the origin of the time scale of the theoretical solution, so as to force the theoretical and numerical shock locations to coincide at 2.0 microseconds. The agreement is still very good, even if no such shift is introduced.

thickness-density product was 1.2 gm/cm^2, moving initially at 10^6 cm/sec. Not only is the shock location accurately given by Eq. (62), but also the distributions of pressure, density, and particle velocity are found to be matched by Eq. (60).

The calculations presented by Chou and Burns were done by the method of characteristics, for a series of six impact conditions. The case singled out for special attention here used a slab thickness of 3.319 cm, traveling initially at 9.144 km/sec. The initial pressure in the target was taken to be one atmosphere, and so the solution at very late time becomes non-self-similar because of the effect of counterpressure. There is a time interval, however, before the onset of the nonsimilar effect, and sufficiently long after the termination of the early impact phase, during which Chou and Burns' calculations are closely matched by Eq. (62). The agreement is shown in Fig. 7, where it can be seen that the error in shock location is less than five percent.

Dienes (22) observed that the approximate solution discussed above could also be derived by assuming that the self-similar solution matches neither $\mathcal{E}$ nor ρ individually, but that it produces a flow having the same value of $\mathcal{E}\rho^{\lambda}$ as did the impacting slab, where λ is defined as

$$\lambda = \frac{2 - 3N}{2N - 1} \tag{68}$$

He too compared this solution with his own numerical results, but, like the present writer, was unaware of the fact that this solution would be shifted slightly in amplitude if used in the correct sense outlined by Zeldovich.

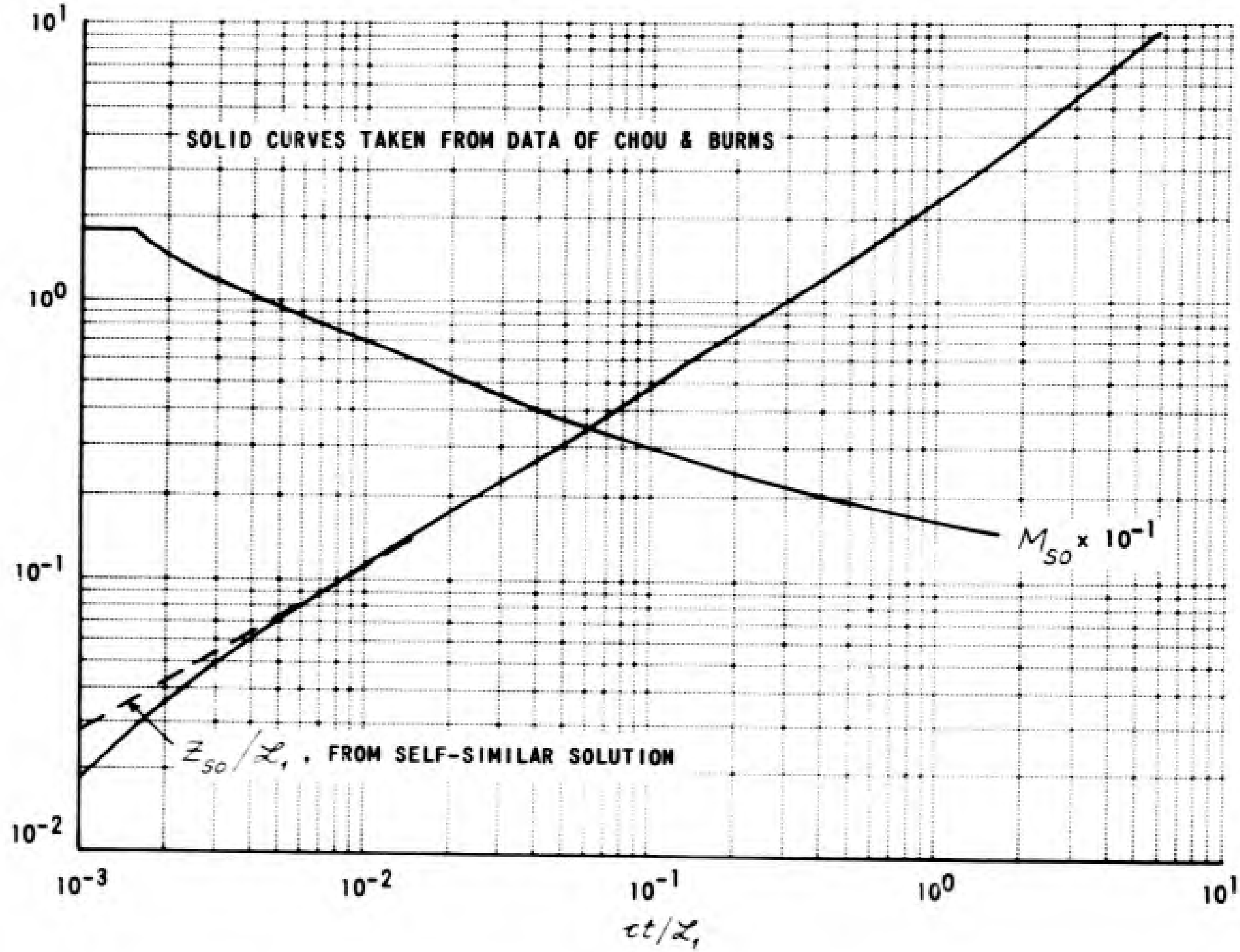

Figure 7 PLANE-WAVE SHOCK-TRAJECTORY SIMILITUDE FUNCTIONS
PERFECT GAS, $\gamma = 1.4$, WITH COUNTERPRESSURE

To summarize this discussion of energy and momentum conservation, it should be repeated that at a large time after the loading of the front surface of a half-space of gas, and before the onset of the effect of counterpressure, the flowfield is correctly described by the nonsingular, self-similar solution, except for those portions that were set in motion during the loading process and shortly afterwards. The power-law dependence of the solution, and its scaling with respect to the parameters ρ_o, $\mathcal{E}$, and $\mathcal{P}$ is that given by Eq. (63). The amplitude coefficient appearing in the solution depends on γ and also on the details of the time history of the loading process.

The considerations given above for one dimension can be extended to the case of two spatial dimensions. The axisymmetric impact case has been considered by the present writer (16), while Rayzer (15) has treated both impacts and explosions of either a point source or a line source. In these cases also, the solution at late time has a self-similar, power-law dependence throughout most of the flowfield. The criterion for selecting the exponent is that it be the value which allows a smooth transition between the hyperbolic and elliptic regions. The scaling with respect to the total energy and momentum, and the initial density are given below. Simultaneous conservation of energy and momentum is achieved by neglecting the small portion of the mass affected during the initiation of the flow (or, more precisely, by finding the correct solution for this part of the flow and by then joining it to the self-similar part of the flow by the matched-asymptotic-expansion procedure). The amplitude coefficient in the expression for the shock trajectory depends on the specific heat ratio γ and also on the details of the loading history.

C. THE AXISYMMETRIC SOLUTION FOR $\gamma = 1.5$

The direct solution of the self-similarity equations for the axisymmetric case is extremely difficult, because of the mixed hyperbolic-elliptic nature of the problem, the unknown value of N, and the unknown shape of the shock and of the plume boundary. At the time of this writing, no direct solution of these equations has been reported.

However, the solution of the original time-dependent equations of motion has been reported by Walsh et al. (5,7) for the case of a right-circular cylinder striking a half space of perfect gas, with $\gamma = 1.5$, zero initial pressure, and density $1.0\ gm/cm^3$. As noted above, these authors observed the development of the self-similar solution, and indicated a functional form which the solution could take. The actual distributions of the self-similar functions were not presented, however. Dr. Walsh made available to the present writer the complete numerical output for this problem; the self-similar distributions have been found, and are described below.

1. Shock Shape

Walsh's calculations were done with a computer code (29) that was an improvement over the particle-in-cell method, in that the mass distribution was represented in a continuous manner, rather than by a number of discrete particles. The projectile was taken to be 36 cm in both length and diameter, travelling initially at 10^6 cm/sec. After the flow becomes self-similar, any instant can be chosen as the one to be used for evaluating the similarity functions. The one chosen here was the largest time for which results were printed (5.40×10^{-3} sec). At this point in the calculation, the cell size was 8 cm in the axial and radial directions. To locate the shock, the pressure was graphed as a function of distance, assuming that the pressure in each cell could be assigned at the midpoint of that cell. Fig. 8 shows the result for the row of cells lying nearest to the symmetry axis. It is characteristic of numerical calculations of this type that the shock is spread out over several cells. The location of the shock was guessed, usually between the second and third points on the front portion of the pressure pulse. The shock-location points, estimated from curves of this type (p versus z , for $y \leq 180$ cm. and p vs. y, for $z \leq 236$ cm. were then graphed, and a curve was faired through these points. This faired curve could be closely approximated by the ellipse:

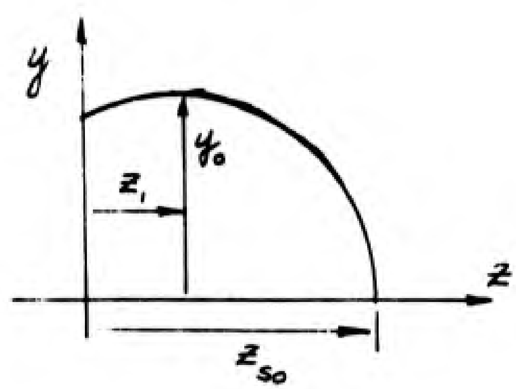

Figure 9 NOTATION USED IN SHOCK-SHAPE FORMULA

$$\left(\frac{z - z_1}{z_{so} - z_1}\right)^2 + \left(\frac{y}{y_0}\right)^2 - 1 = 0 \qquad (69)$$

with $z_{so} = 321$ cm , $z_1 = 96$ cm , and $y_0 = 241$ cm . In terms of the similarity coordinates, this becomes

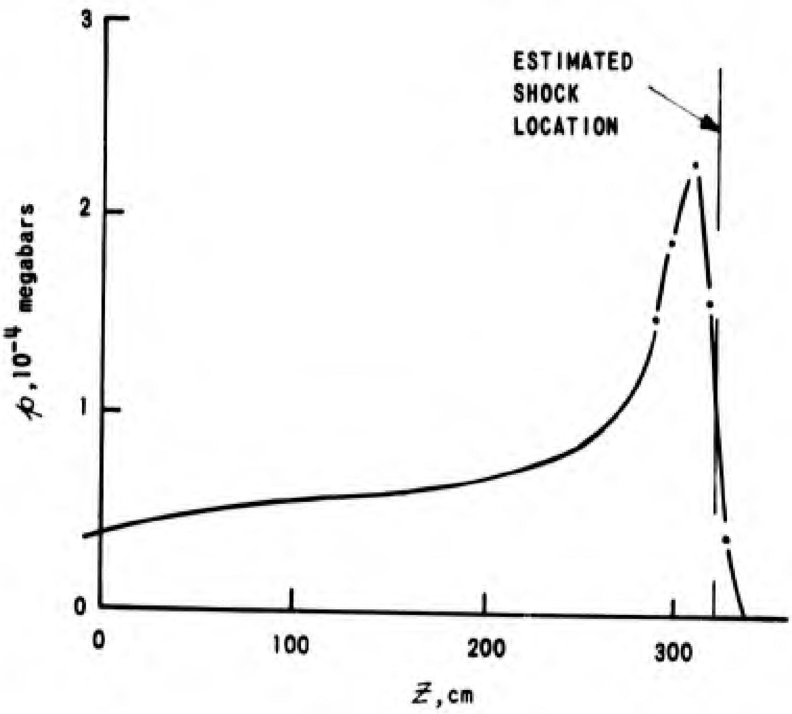

Figure 8 PRESSURE DISTRIBUTION IN THE ROW OF CELLS NEAREST TO THE AXIS OF SYMMETRY

$$\left(\frac{\zeta - k_1}{k_2}\right)^2 + \left(\frac{\sigma}{k_3}\right)^2 = 1 \tag{70}$$

where

$$k_1 = \frac{z_1}{z_{s0}} = 0.2491 \; , \; k_2 = 1 - k_1 = 0.7009 \; , \; k_3 = \frac{y_0}{z_{s0}} = 0.7508 \tag{71}$$

It is possible to find the angle between the shock and the free surface at the point where they meet, independently of the numerical results. The basis for this solution was given in a number of Russian papers, (30-35) which are reviewed by Collins (36) and by Collins and Holt (37). The reasoning is that, if the solution is to be self-similar, then the shock must meet the free surface at an angle such that the wave system generated behind the shock does not cause any change in the shock shape. This condition is satisfied when the speed of the rarefaction front behind the shock just matches the velocity of the point of intersection of the shock and the free surface, a condition which is referred to as "critical reflection". The expansion wavelet emanating at time t from a given point on the free surface would be located, Δt later, as a circle whose radius has grown at the sound speed, and whose center has been carried along at the particle speed behind the shock. Thus, the construction is (38)

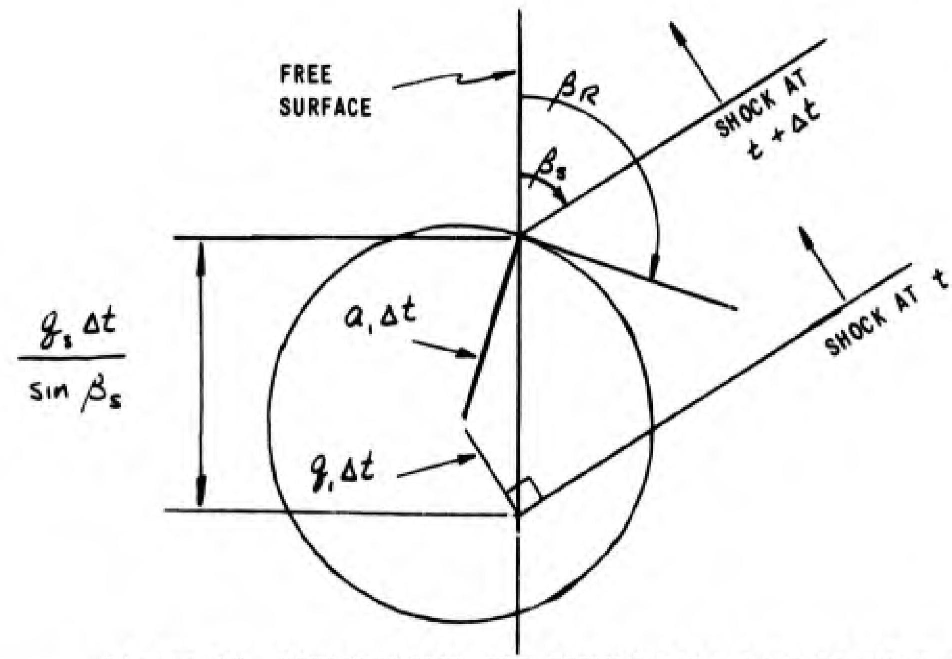

Figure 10 CONSTRUCTION FOR DETERMINING INTERSECTION ANGLE BETWEEN SHOCK AND FREE SURFACE

This leads to the formula

$$\sin \beta_s = \left\{ 2 \frac{g_1}{g_s} - \left(\frac{g_1}{g_s}\right)^2 + \left(\frac{a_1}{g_s}\right)^2 \right\}^{-1/2} \tag{72}$$

For an infinite-strength shock in a perfect gas, this becomes

$$\sin \beta_s = \sqrt{\frac{\gamma+1}{2\gamma}} \tag{73}$$

When $\gamma = 1.5$, $\beta_s = 65.9^\circ$. The value that is found from Eq. (70) is 63.2°. The difference between these numbers is well within the accuracy inherent in the process of fairing the numerical data.*

---

* The writer did not become aware of the formula for β_- until after Eq. (70) had been established. It would be possible to adjust the constants so as to match Eq. (73) exactly, but this has not been done here.

The papers by Collins (36), and Collins and Holt (37) contain an error in the derivation of the formula for β_s . Instead of adding the velocity components q_1 and a_1 vectorially, as in the figure above, these authors equate the sum of the absolute values of these components to the speed of the shock/free-surface intersection point (see Eq. (3.20) of Ref. 36 and 37). Their formula for the shock angle, expressed in the present notation, is:

$$\sin \beta_s \Big]_{\text{COLLINS-HOLT}} = \frac{\gamma+1}{2+\sqrt{2\gamma(\gamma-1)}} \tag{74}$$

For $\gamma = 1.5$, this formula gives $\beta_s = 50.8^\circ$, which differs considerably from Walsh's data.

The shock velocity distribution corresponding to Eq. (69) was found by the usual method (39); Eq. (69) was written in the form

$$F(z, y, t) = 0 \tag{75}$$

The expression for dF/dt can be written as

$$q_{sz} \frac{\partial F}{\partial z} + q_{sy} \frac{\partial F}{\partial y} + \frac{\partial F}{\partial t} = 0 \tag{76}$$

where the components of the shock velocity are

$$\vec{q}_s = q_{sz} \hat{z} + q_{sy} \hat{y} \tag{77}$$

Along lines perpendicular to the shock, the shock-velocity components have the ratio

$$\frac{q_{sy}}{q_{sz}} = \frac{\partial F/\partial y}{\partial F/\partial z} \tag{78}$$

Thus Eqs. (76) and (78) can be rewritten as

$$q_{sz} = -\frac{\dfrac{\partial F/\partial t}{\partial F/\partial z}}{1 + \left(\dfrac{\partial F/\partial y}{\partial F/\partial z}\right)^2} \tag{79}$$

and

$$q_s = q_{sz}\left[1 + \left(\frac{\partial F/\partial y}{\partial F/\partial z}\right)^2\right]^{1/2} = \frac{\dfrac{\partial F}{\partial t}}{\left[\left(\dfrac{\partial F}{\partial y}\right)^2 + \left(\dfrac{\partial F}{\partial z}\right)^2\right]^{1/2}} \tag{80}$$

In terms of the similarity coordinates, then, the shock-velocity distribution is

$$\frac{q_s}{\dot{Z}_{so}} = \frac{\dfrac{\zeta}{k_2}\left(\dfrac{\zeta - k_1}{k_2}\right) + \left(\dfrac{\sigma}{k_3}\right)^2}{\left[\dfrac{1}{k_2^2}\left(\dfrac{\zeta - k_1}{k_2}\right)^2 + \dfrac{1}{k_3^2}\left(\dfrac{\sigma}{k_3}\right)^2\right]^{1/2}} \tag{81}$$

The components are

$$\left\{\frac{q_{sz}}{q_s}, \frac{q_{sy}}{q_s}\right\} = \frac{\left\{\dfrac{\zeta - k_1}{k_2^2}, \dfrac{\sigma}{k_3^2}\right\}}{\left[\dfrac{1}{k_2^2}\left(\dfrac{\zeta - k_1}{k_2}\right)^2 + \dfrac{1}{k_3^2}\left(\dfrac{\sigma}{k_3}\right)^2\right]^{1/2}} \tag{82}$$

Using these velocities, the similarity functions can be evaluated at the shock, from

$$\psi_1 = \frac{\gamma+1}{\gamma-1} \quad , \quad f_1 = \frac{2}{\gamma+1}\left(\frac{q_s}{\dot{z}_{so}}\right)^2 \quad , \quad \phi_1 = \frac{2}{\gamma+1}\,\frac{q_{sz}}{\dot{z}_{so}} \quad , \quad \omega_1 = \frac{2}{\gamma+1}\,\frac{q_{sy}}{\dot{z}_{so}} \tag{83}$$

Elsewhere in the flow field, the similarity functions were found from Eqs. (11)-(14), using as normalizing quantities:

$$\dot{z}_{so} = 2.20 \times 10^4 \ \mathrm{cm/sec} \ , \quad \rho_0 \dot{z}_{so}^2 = 4.84 \times 10^{-4} \ \mathrm{Mbar}$$

The value of $\dot{z}_{so}$ was found from the relation

$$\dot{z}_{so} = \frac{N}{t}\, z_{so} \tag{84}$$

with $N = 0.37$, $t = 5.40 \times 10^{-3}$ sec. , $z_{so} = 321$ cm.

These numbers can also be used to evaluate the constant appearing in the shock trajectory. Analogously to Eq. (62), the formula for the axisymmetric case is

$$z_{so}(t) = F(\gamma)\left(\frac{P^2}{\rho_0 E}\right)^{1/3}\left[\frac{t}{\left(P^5/\rho_0 E^4\right)^{1/3}}\right]^{0.37} \tag{85}$$

From the above data, $F(1.7)$ is found to be 1.6415. As in the plane-wave case, this amplitude coefficient also depends on the details of the initiation process. The figure given above applies for a right-circular cylinder of length-to-diameter ratio unity. The calculations reported by Walsh et al (5, 7) indicate that the coefficient would be essentially the same for a sphere, or for a right-circular cylinder of length-to-diameter ratio between the limits 1/3 and 3.

Equation (85) can be rewritten in terms of a scaling length $\mathcal{L}_o$, as:

$$\frac{z_{so}}{\mathcal{L}_o} = F(\gamma)\left(\frac{ct}{\mathcal{L}_o}\right)^N \tag{86}$$

where

$$\mathcal{L}_o = \left\{\frac{E}{\rho_o c^2}\left(\frac{P}{\rho_o c}\right)^\lambda\right\}^{\frac{1}{3(1+\lambda)}}, \quad \lambda = \frac{2-5N}{4N-1} \tag{87}$$

2. The Similarity Functions

Contour plots, showing the distributions of ψ, f, ϕ, and ω in the ζ, σ plane were prepared from the numerical data. These results are shown in Figs. 11-14.

The density contours show a resemblance to what would be found for a spherically symmetric blast wave (2-4). The density falls very rapidly with distance normal to the shock, but it changes slowly with angular position.

The constant-pressure contours show considerably greater variation with angular position. They also display the feature, in common with the spherically symmetric explosion problem, that the pressure drops rapidly near the shock but quickly levels off to a relatively constant value.

The two velocity components display a linear variation for ζ greater than about 0.6; the distributions become more complicated at lower

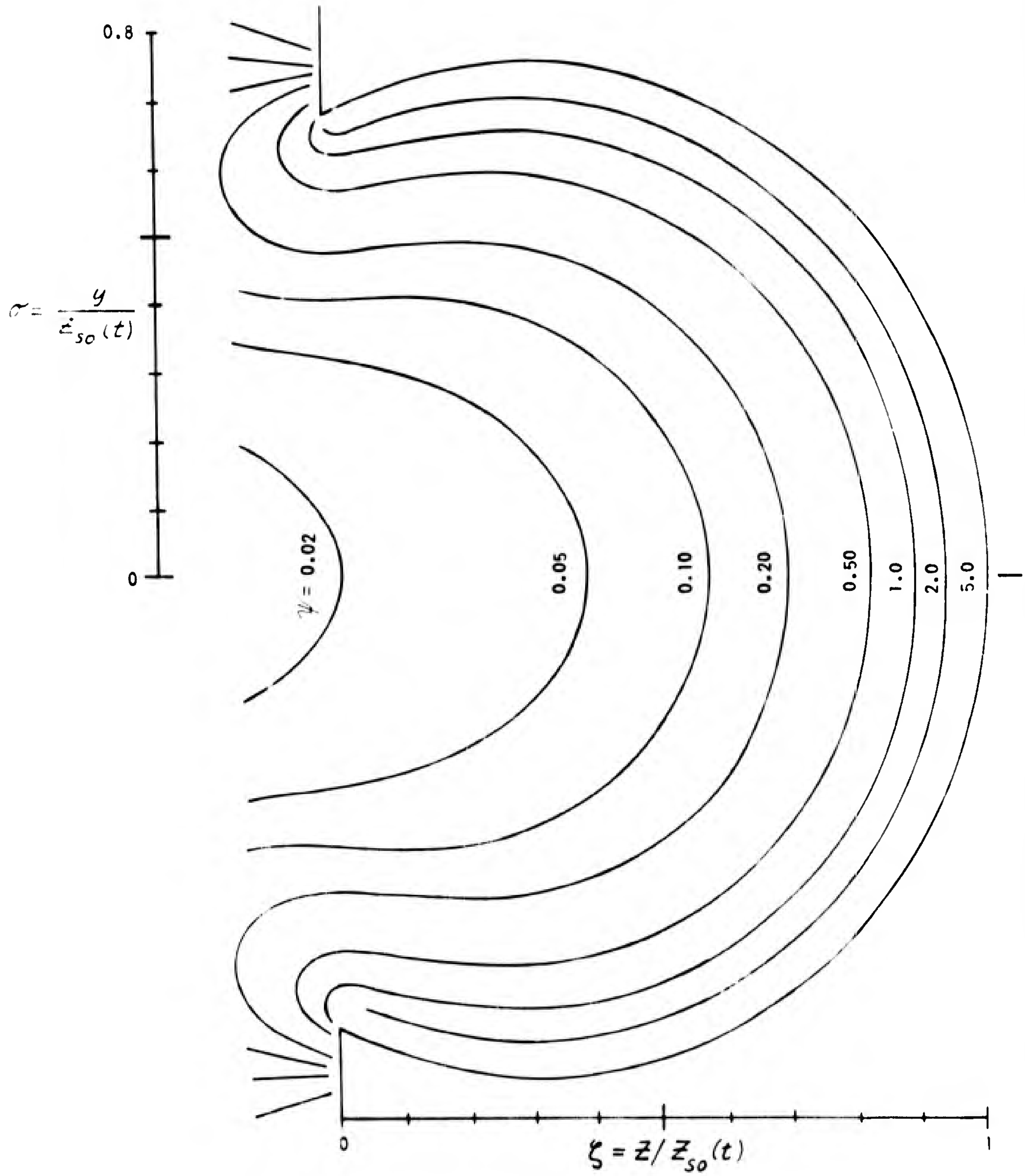

Figure 11 CONTOURS OF CONSTANT DENSITY RATIO, $\psi = \rho/\rho_0$
$\gamma = 1.5$

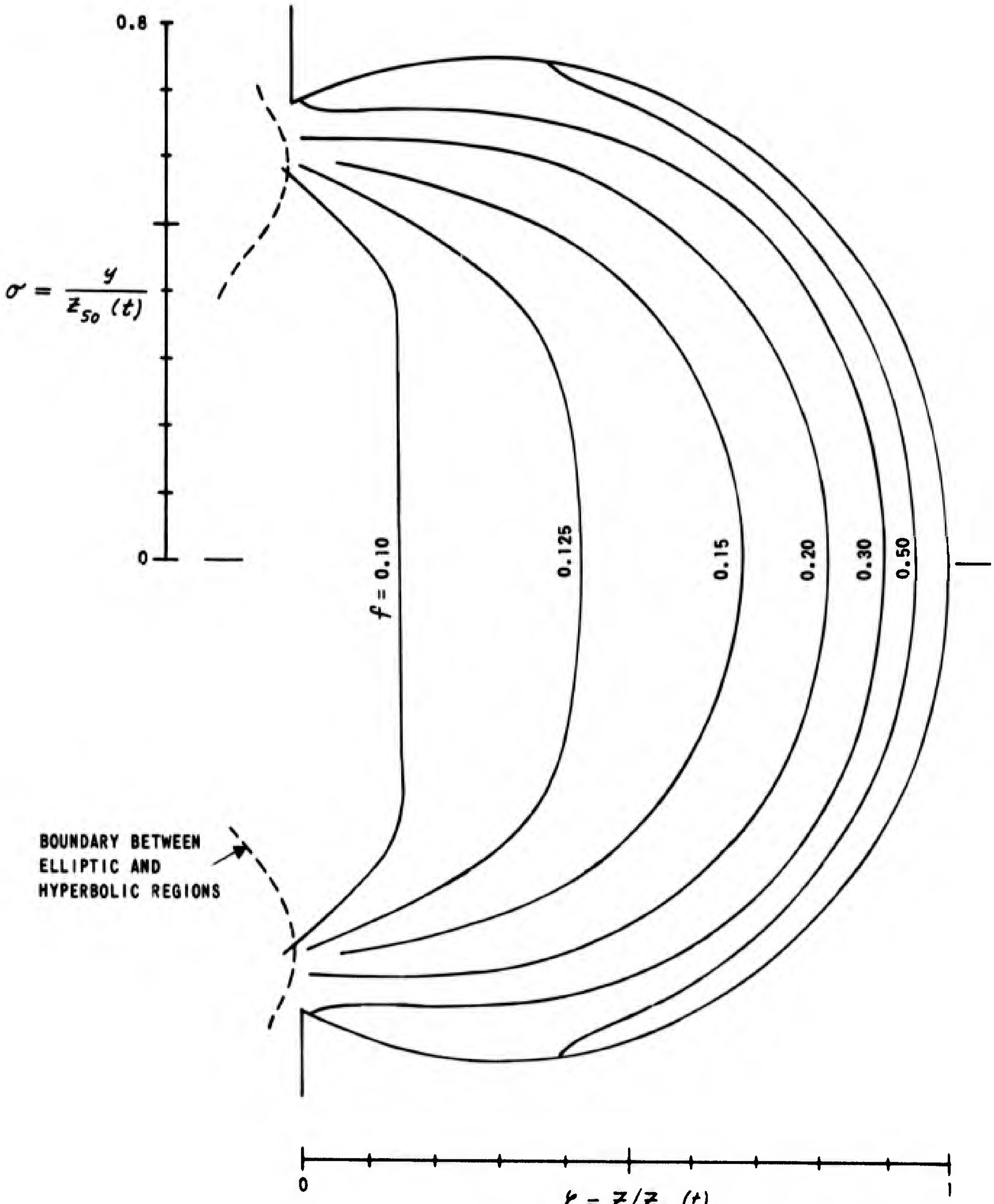

Figure 12 CONTOURS OF CONSTANT PRESSURE, $f = \frac{p}{\rho_0 \dot{z}_{so}^2}$

$\gamma = 1.5$

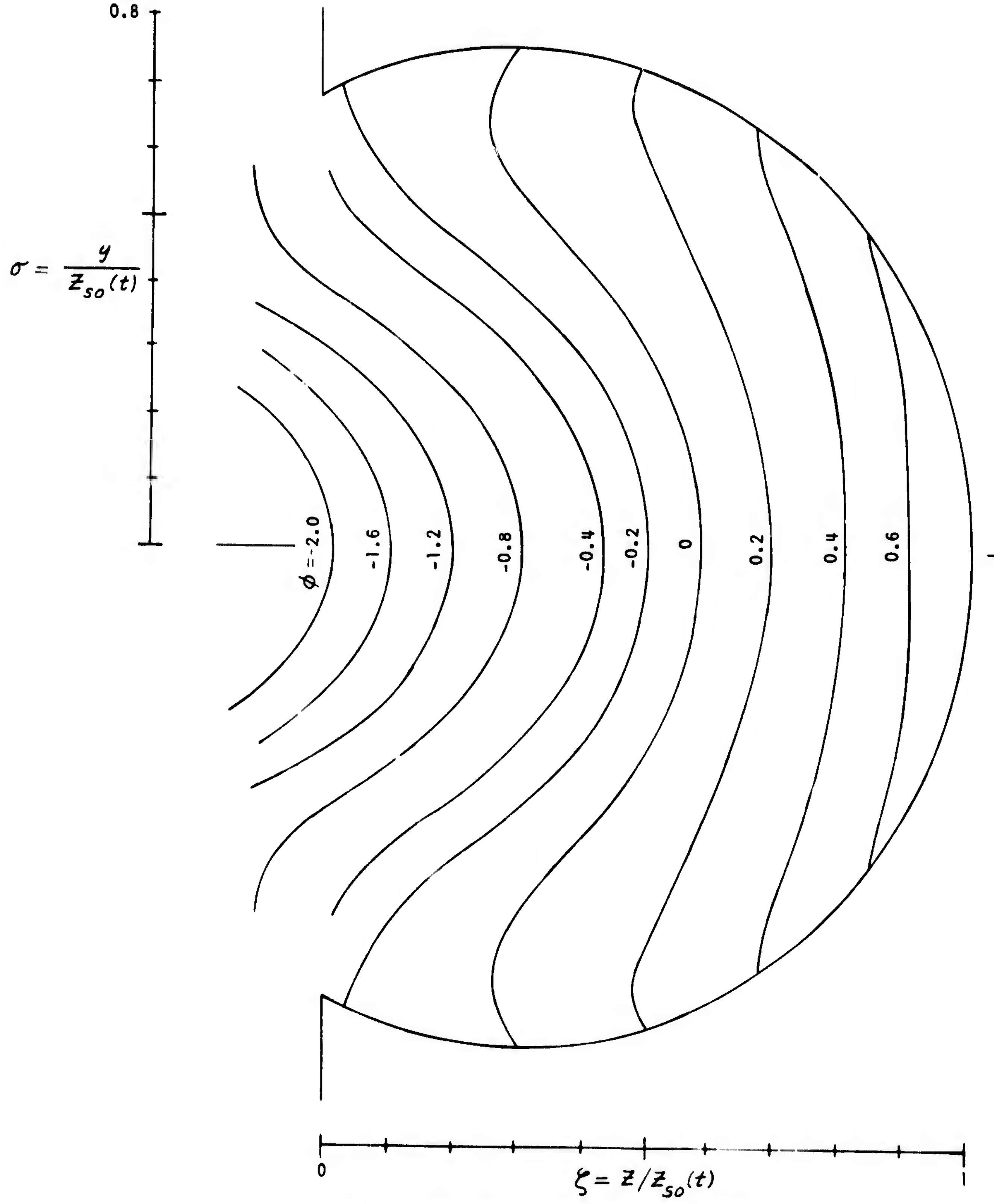

Figure 13 CONTOURS OF CONSTANT AXIAL VELOCITY COMPONENT. $\phi = u/\dot{Z}_{so}$

$\gamma = 1.5$

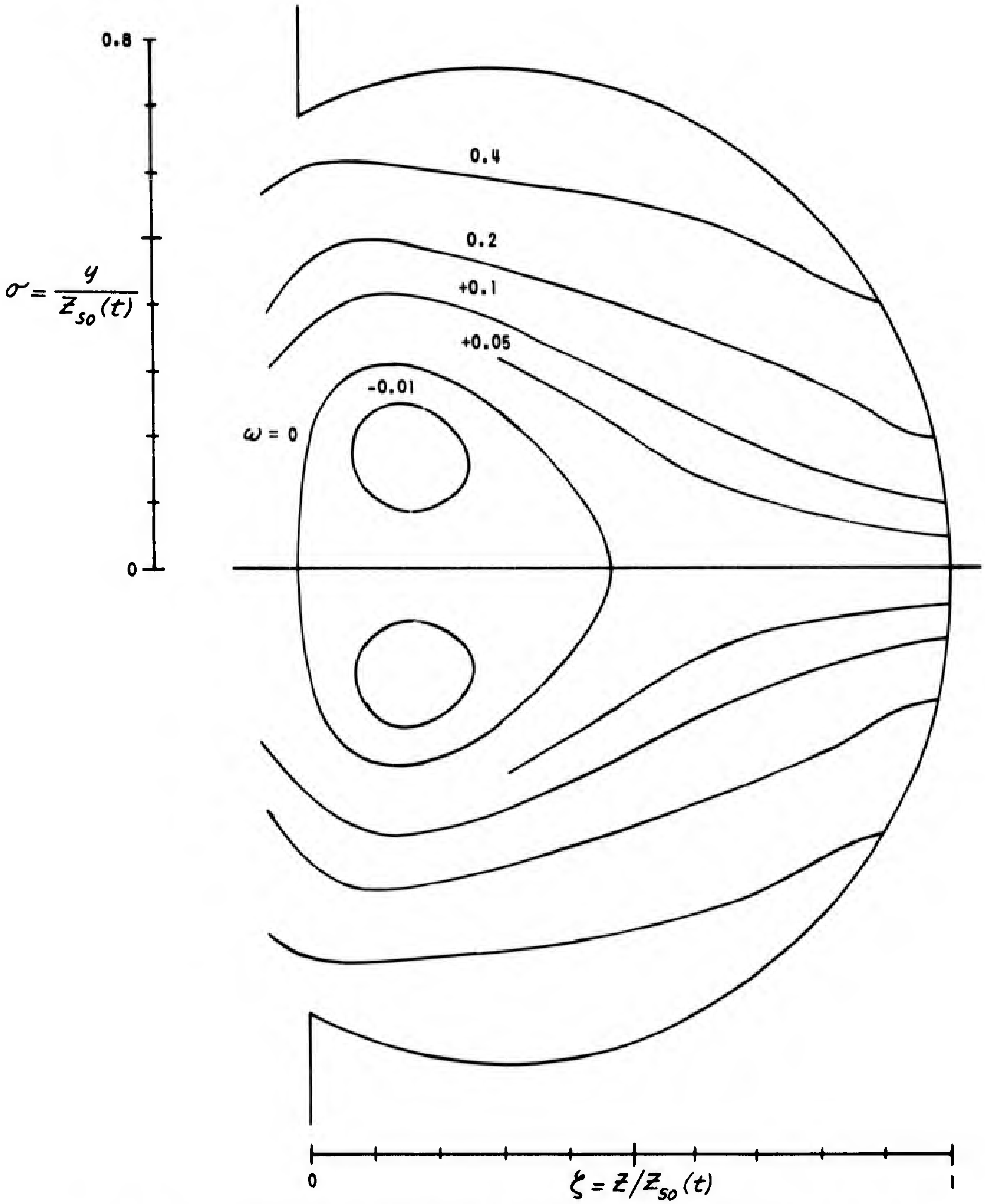

Figure 14 CONTOURS OF CONSTANT RADIAL VELOCITY COMPONENT, $\omega = v/\dot{Z}_{so}$
$\gamma = 1.5$

values of ζ , with the appearance of a region where the radial component is directed toward the axis.

The numerical method produces a nonzero value for all of the dependent variables along the free surface, outside the target. It will be seen below that the solution near the shock/free-surface intersection should be of the centered-wave type, and that the plume boundary, along which the pressure and density fall to zero, should not coincide with the free surface for $\gamma = 1.5$. The centered-wave nature of the solution is partially masked by the effect of the nonzero grid size.

The numerical result for the boundary between the elliptic and hyperbolic regions is shown in Fig. 12. This boundary should intersect the shock/free-surface juncture. Its failure to do so is another demonstration that the numerical method loses some of the details of the centered-wave flow structure in this region.

It must be emphasized that a considerable amount of fairing and smoothing has gone into this reduction of Walsh's data, and that future research will undoubtedly lead to some adjustments in the locations of these contours. It is not possible to estimate their accuracy from the data on hand.

3. Particle Paths

For the self-similar inviscid flow considered here, it is possible to display the path taken by any particle after it is processed by the shock. This is done by expressing the fact that the entropy of the particle remains constant, and equal to the value it acquired at the shock.* Since the entropy depends

*It is assumed that there are no shock waves other than the main one.

only on p/ρ^γ, this becomes

$$p/\rho^\gamma = p_1/\rho_1^\gamma \tag{88}$$

where the subscript denotes conditions immediately after passage through the shock. In terms of the similarity functions, the relation is

$$\left(\frac{\dot{z}_{so1}}{\dot{z}_{so2}}\right)^2 = \frac{f}{f_1}\left(\frac{\psi_1}{\psi}\right)^\gamma \tag{89}$$

Here $\dot{z}_{so2}$ denotes the shock speed at the present instant, when the particle being considered has the dimensionless pressure and density f and ψ (without subscripts), and $\dot{z}_{so1}$ refers to the earlier time t_s when the particle in question was processed by the shock. This equation can be rewritten as

$$\frac{t}{t_s} = \left[\frac{f/\psi^\gamma}{f_1/\left(\frac{\gamma+1}{\gamma-1}\right)^\gamma}\right]^{\frac{1}{2(1-N)}} \tag{90}$$

Along the axis of symmetry, this relation alone can be used to find t/t_s at each value of ζ, since the axis is also a particle path. At points off the axis of symmetry, the particle path must be found explicitly. In a time interval dt, the position of the particle changes by $dy = v\,dt$ and $dz = u\,dt$; in terms of the similarity functions, these become

$$\begin{aligned} dy &= \sigma\, dz_{so} + z_{so}\, d\sigma = \omega\, \dot{z}_{so}\, dt = \omega\, dz_{so} \\ dz &= \zeta\, dz_{so} + z_{so}\, d\zeta = \phi\, \dot{z}_{so}\, dt = \phi\, dz_{so} \end{aligned} \tag{91}$$

Thus displacements in the similarity plane take place at a rate proportional to the pseudovelocity components $\omega - \sigma$ and $\phi - \zeta$:

$$d\sigma = (\omega - \sigma)\, d \ln z_{so} \quad , \quad d\zeta = (\phi - \zeta)\, d \ln z_{so} \tag{92}$$

and the particle paths are the family of lines satisfying

$$\frac{d\tau}{d\zeta} = \frac{\omega - \sigma}{\phi - \zeta} \tag{93}$$

Solutions of this equation were found by the method of isoclines, and are shown as the dashed lines in Fig. 15. Contours of constant t/t_s are shown as solid lines. Table II lists the conditions at the points where the particles enter the shock.

TABLE II

INITIAL CONDITIONS FOR PARTICLE PATHS

Path No.	1	2	3	4	5	6	7	8	9
ζ_s	1.0	0.984	0.930	0.832	0.709	0.567	0.418	0.245	0.040
σ_s	0	0.160	0.330	0.488	0.612	0.697	0.742	0.751	0.700

Several interesting features can be observed in Fig. 15. The first is the time history of the path of a particle which lies on the axis of symmetry, at a distance L_1 below the free surface, before being shocked at $t = t_s$. This particle follows the shock with decreasing speed, until $\frac{t}{t_s} = 24.5$, at which time its velocity changes sign. This occurs (see Fig. 13) at $\zeta = 0.585$; thus the maximum depth to which this particle travels is

$$\frac{z_{max}}{L_1} = \frac{z_{max}}{z_{so}(t)} \cdot \frac{z_{so}(t)}{z_{so}(t_s)} = 0.555\,(24.5)^{0.37} = 1.91 \tag{94}$$

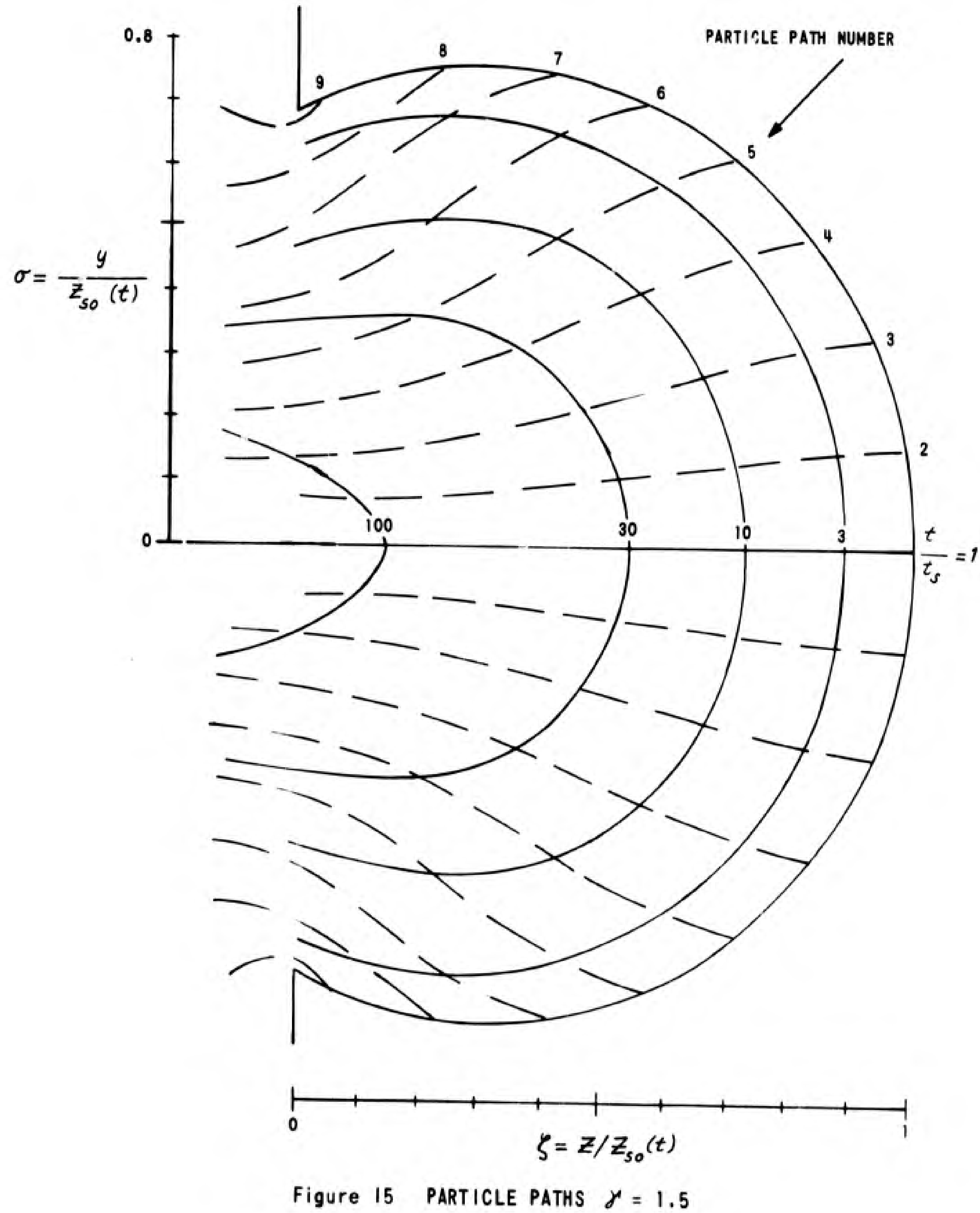

Figure 15 PARTICLE PATHS γ = 1.5

Thereafter the particle moves toward the free surface, crossing it at $t/t_s = 125$. For comparison, the exact solution of the one-dimensional problem for $\gamma = 1.4$ shows that the maximum penetration of $2.60\, L_1$ occurs at $t/t_s = 15.6$, and that the particle crosses the original free surface when $t/t_s = 55.9$.

Next, it is of interest to follow the motion of a layer of particles, all of which lie initially in a plane a distance L_1 below the free surface. Let t_1 denote the instant when the center of the shock arrives at $z = L_1$. (For a chosen value of L_1 the quantity t_1 can be related to the mass and velocity of the projectile for any specific case by using Eq. (85)). Somewhat later, the point on the shock at which particle path number 2 begins (i.e., $\zeta = 0.984$, $\sigma = 0.160$) will reach the depth L_1, i.e., the shock scale at that instant will be

$$\frac{z_{so}(t_s)}{L_1} = \frac{1}{0.984} = 1.018$$

Thus the y-coordinate of this point will be

$$\frac{y_s}{L_1} = \frac{y_s}{z_{so}(t_s)} \cdot \frac{z_{so}(t_s)}{L_1} = \frac{0.160}{0.984} = 0.163$$

The time at which this particle is shocked is

$$\frac{t_s}{t_1} = \left[\frac{z_{so}(t_s)}{z_{so}(t_1)}\right]^{1/N} = \left[\frac{z_{so}(t_s)}{L_1}\right]^{1/N} = (1.018)^{1/0.37} = 1.049$$

The location of this particle at any subsequent time can now be found. For instance, if a later time t is chosen such that $\frac{z_{so}(t)}{L_1} = 5$ (i.e., $\frac{t}{t_1} = (5)^{1/0.37} = 77$), then the time after shock crossing for this particle would be

$$\frac{t}{t_s} = \frac{t/t_1}{t_s/t_1} = \frac{77}{1.049} = 73.5$$

The location of this particle can then be found, from Fig. 15, as $\zeta = 0.25$, $\sigma = 0.08$, which gives $z/L_1 = 1.25$, $y/L_1 = 0.40$.

Calculations of this type were carried out for all nine particle paths, and for times such that $\frac{z_{so}(t)}{L_1}$ was equal to 2, 3, 4, and 5 (the corresponding times are $t/t_1 = 6.5$, 19.5, 42.2, and 77). The results are shown in Fig. 16. The layer of particles is carried down into the target initially. Later on, particles which are sufficiently far from the axis begin to acquire a significant radial component, with those at very large values of y_s/L_1 being carried toward the free surface by the shock itself. At this later time, the particles which originally lay near the axis have reversed their downward motion and are traveling toward the free surface.

This motion bears a resemblance to the type of deformation observed by Frasier and Karpov (40) in a target composed of alternate light and dark layers of wax. At some time before the motion was brought to rest by the strength effects, the particles near the axis were carried downward, while those away from the axis were sheared into a wave-like pattern. The present results display, at least qualitatively, the same sort of behavior, although they obviously have no quantitative relation to the wax experiments (which involve both nonsimilarity and strength effects). However, it is interesting to note that an inviscid treatment contains a mechanism for generating the type of deformation observed. The question of how this pattern is affected, and ultimately arrested, by the effects of nonsimilarity and of material strength remains a subject for further study.

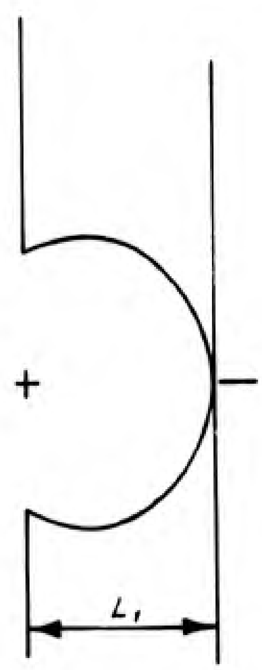

Figure 16a POSITIONS, AT $t = t_1$ ($z_{so} = L_1$) OF PARTICLES IN THE PLANE $z = L_1$

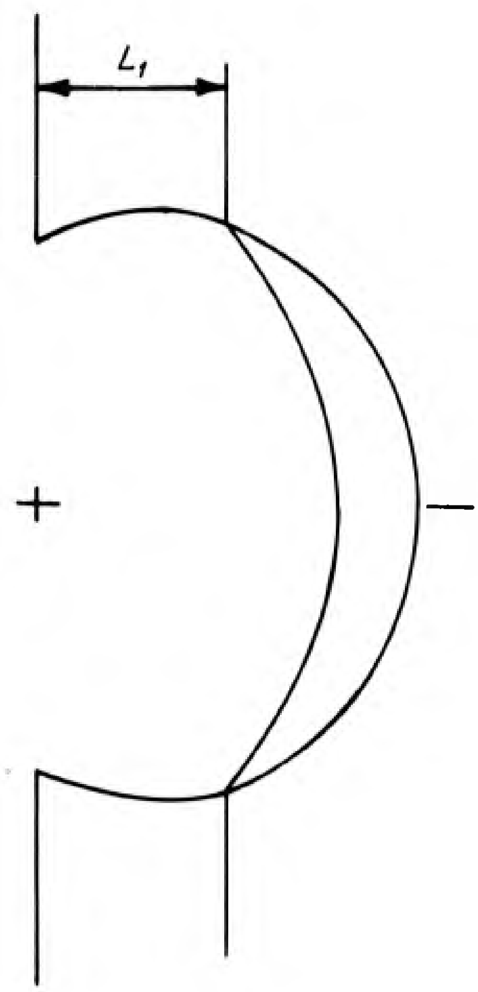

Figure 16b POSITIONS, AT $t = 6.5\, t_1$ ($z_{so} = 2L_1$) OF PARTICLES LOCATED INITIALLY IN THE PLANE $z = L_1$

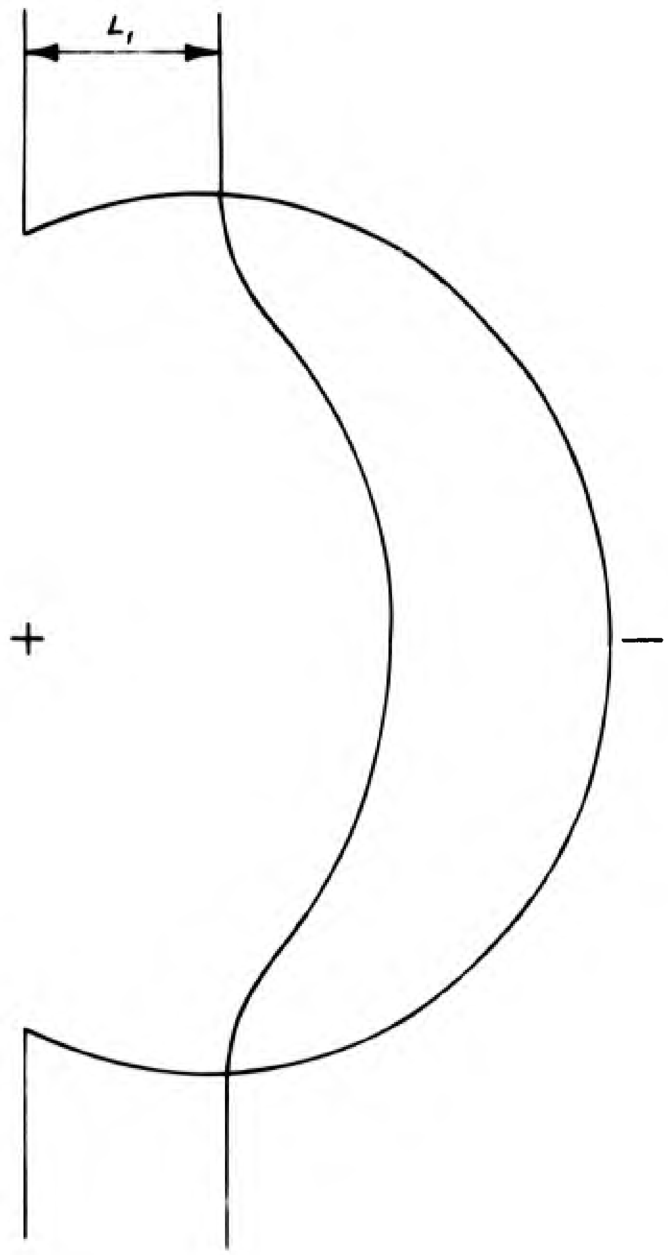

Figure 16c POSITIONS, AT $t = 19.5\,t_1$ ($z_{so} = 3L_1$) OF PARTICLES LOCATED INITIALLY IN THE PLANE $z = L_1$

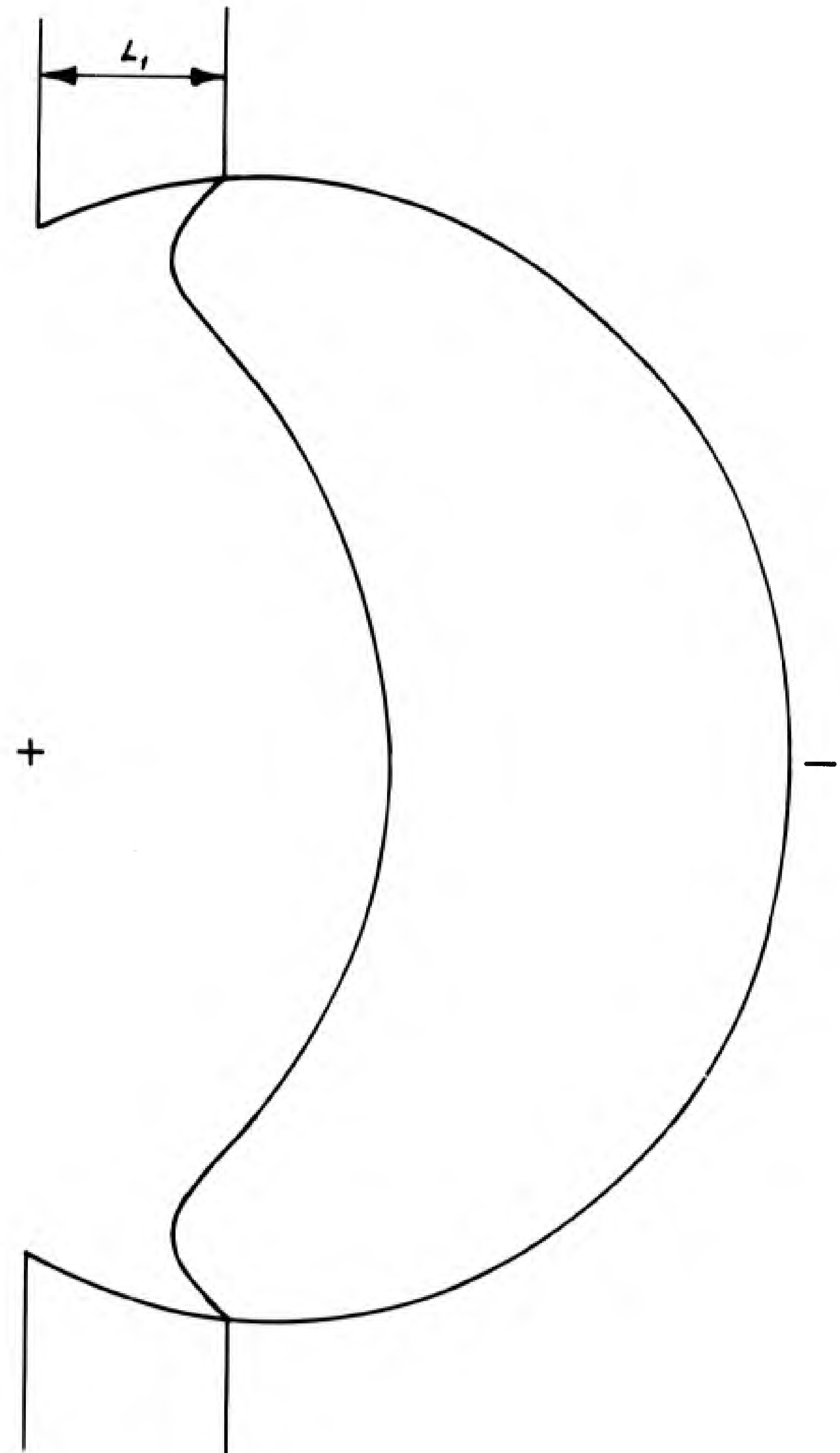

Figure 16d POSITIONS, AT $t = 42.2\,t_1$ ($z_{so} = 4L_1$) OF PARTICLES LOCATED INITIALLY IN THE PLANE $z = L_1$

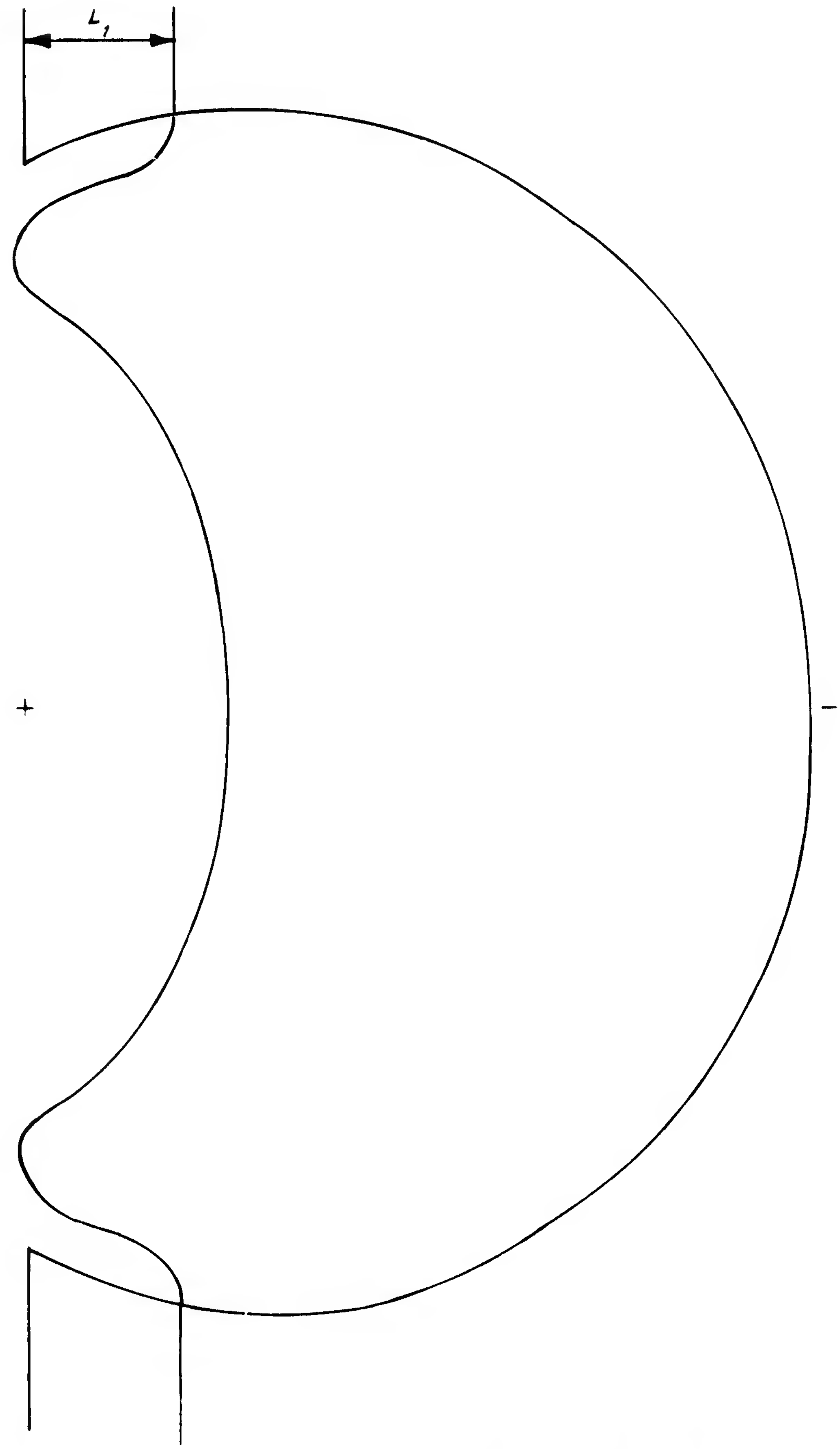

Figure 16e POSITIONS. AT $t = 77t_1$ ($z_{so} = 5L_1$) OF PARTICLES LOCATED INITIALLY IN THE PLANE $z = L_1$

4. Solution Near the Shock/Free-Surface Intersection

It is possible to derive an exact solution for the properties of the flow in the vicinity of the point where the shock meets the free surface. The derivation below follows that given in Section 108 of Courant and Friedrichs (41).

a. Differential Equations

The similarity equations are expressed in a coordinate system whose origin is located at the shock/free-surface intersection:

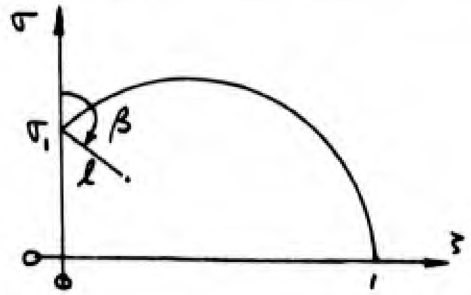

$$\zeta = \ell \sin\beta$$

$$\sigma = \sigma_1 + \ell \cos\beta \qquad (95)$$

Figure 17 COORDINATE SYSTEM NEAR THE SHOCK/FREE-SURFACE INTERSECTION

All of the dependent variables are expanded as a series in ℓ ; for example:

$$\phi(\ell,\beta) = \phi_{(0)}(\beta) + \ell\,\phi_{(1)}(\beta) + \ell^2\phi_{(2)}(\beta) + \cdots \qquad (96)$$

If these expansions are now substituted into the full similarity equations (Eqs. (39)-(42)) the leading terms (coefficients of ℓ^{-1}) are found to be (a prime denotes $d/d\beta$)

Continuity:

$$\left[\phi_{(0)}\cos\beta - (\omega_{(0)} - \sigma_1)\sin\beta\right]\psi'_{(0)} + \psi_{(0)}\left[\phi'_{(0)}\cos\beta - \omega'_{(0)}\sin\beta\right] = 0 \qquad (97)$$

Axial Momentum:

$$\left[\phi_{(0)} \cos\beta - (\omega_{(0)} - \tau_1) \sin\beta\right] \phi'_{(0)} + \frac{f'_{(0)}}{\psi_{(0)}} \cos\beta = 0 \tag{98}$$

Radial Momentum:

$$\left[\phi_{(0)} \cos\beta - (\omega_{(0)} - \tau_1) \sin\beta\right] \omega'_{(0)} - \frac{f'_{(0)}}{\psi_{(0)}} \sin\beta = 0 \tag{99}$$

Energy:

$$\left[\phi_{(0)} \cos\beta - (\omega_{(0)} - \tau_1) \sin\beta\right]\left[f'_{(0)} - \frac{\gamma f_{(0)}}{\psi_{(0)}} \psi'_{(0)} \right] = 0 \tag{100}$$

Since these equations are homogeneous in the derivatives, they will have a nontrivial solution only if the determinant of the coefficients vanishes. This condition is

$$N_{(0)}^2 \left[N_{(0)}^2 - \frac{\gamma f_{(0)}}{\psi_{(0)}} \right] = 0 \tag{101}$$

where

$$N_{(0)} = \phi_{(0)} \cos\beta - (\omega_{(0)} - \tau_1) \sin\beta \tag{102}$$

This notation is prompted by the fact that the quantity on the right-hand side of Eq. (102) is just the zeroth - order component, normal to a constant-β line, of the vector whose components are $\phi - \zeta$ and $\omega - \tau$ (τ is the tangential component):

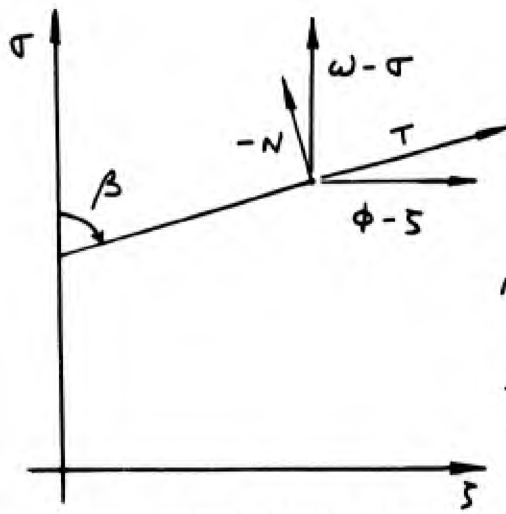

$$N = (\phi - \zeta)\cos\beta - (\omega - \sigma)\sin\beta$$
$$T = (\phi - \zeta)\sin\beta + (\omega - \sigma)\cos\beta \qquad (103)$$

Figure 18 SIGNIFICANCE OF THE QUANTITIES N AND T

To make the determinant of the coefficients zero, the choice is made

$$N_{(0)}^{2} = \frac{\gamma f_{(0)}}{\psi_{(0)}} \qquad (104)$$

This expression is the counterpart, for the present problem, of the usual Prandtl-Meyer relation, which states that the velocity component normal to the rays is sonic (42).

Since $N_{(0)}$ is in general not zero, the energy equation can be written as

$$f_{(0)}' - \frac{\gamma f_{(0)}}{\psi_{(0)}} \psi_{(0)}' = 0 \qquad (105)$$

whose solution is the isentropic relation

$$f_{(0)} = \text{const}\ \psi_{(0)}^{\gamma} \qquad (106)$$

The continuity equation can be written

$$N_{(0)} \, \psi'_{(0)} \big/ \psi_{(0)} + \left(N'_{(0)} + T_{(0)} \right) = 0 \tag{107}$$

The quantity $\psi'_{(0)} \big/ \psi_{(0)}$ appearing here is evaluated from Eqs. (104) and (106), giving

$$\frac{\psi'_{(0)}}{\psi_{(0)}} = \frac{2}{\gamma - 1} \; \frac{N'_{(0)}}{N_{(0)}} \tag{108}$$

Thus the continuity equation becomes

$$N'_{(0)} = - \frac{\gamma - 1}{\gamma + 1} \; T_{(0)} \tag{109}$$

A second relation between $N_{(0)}$ and $T_{(0)}$ can be derived by adding the axial momentum equation, multiplied by $\sin\beta$, to the radial momentum equation, multiplied by $\cos\beta$; the result is

$$T_0{}' = N_{(0)} \tag{110}$$

This is just a statement of the irrotationality condition, i. e.,

$$\mathrm{curl}\,\vec{q} = \hat{e}_3 \, \frac{\dot{z}_{s0}}{\ell \, z_{s0}} \left\{ \omega'_{(0)} \cos\beta + \phi'_{(0)} \sin\beta \right\} + O(\ell^{0}) \tag{111}$$

Equations (109) and (110) can now be combined to give

$$T''_{(0)} + \frac{\gamma - 1}{\gamma + 1} \; T_{(0)} = 0 \tag{112}$$

Thus

$$T_{(0)} = B_1 \sin\sqrt{\frac{\gamma-1}{\gamma+1}}\,\beta + B_2 \cos\sqrt{\frac{\gamma-1}{\gamma+1}}\,\beta \tag{113}$$

$$N_{(0)} = T_{(0)}' = \sqrt{\frac{\gamma-1}{\gamma+1}}\left\{ B_1 \cos\sqrt{\frac{\gamma-1}{\gamma+1}}\,\beta - B_2 \sin\sqrt{\frac{\gamma-1}{\gamma+1}}\,\beta \right\} \tag{114}$$

b. Boundary Conditions

In order to determine B_1 and B_2, boundary conditions on $N_{(0)}$ and $T_{(0)}$ must be assigned at some value of β. Immediately behind the shock, where $\beta = \beta_s$ and where the component of the shock velocity along the surface is $\sigma_1 \dot{z}_{s_0}$, the dependent variables have the values (see Eq. (83))

$$\psi_{(0)} = \frac{\gamma+1}{\gamma-1} \tag{115}$$

$$f_{(0)} = \frac{2}{\gamma+1}\left(\sigma_1 \sin\beta_s\right)^2 = \frac{\sigma_1^{\,2}}{\gamma} \tag{116}$$

$$\phi_{(0)} = -\frac{2\sigma_1}{\gamma+1}\sin\beta_s\cos\beta_s = -\frac{\sigma_1}{\gamma}\sqrt{\frac{\gamma-1}{\gamma+1}} \tag{117}$$

$$\omega_{(0)} = \frac{2\sigma_1}{\gamma+1}\sin^2\beta_s = \frac{\sigma_1}{\gamma} \tag{118}$$

The quantities ψ, f, ϕ, and ω remain constant at these values, for the region between the shock and the head of the expansion wave, i.e., for $\beta_s < \beta < \beta_R$. Thus, in this region, $N_{(0)}$ and $T_{(0)}$ vary with β according to

$$N_{(0)} = \sigma_1\left\{ -\frac{1}{\gamma}\sqrt{\frac{\gamma-1}{\gamma+1}}\cos\beta - \left(\frac{1}{\gamma}-1\right)\sin\beta \right\} \tag{119}$$

$$T_{(0)} = \sigma_1\left\{ -\frac{1}{\gamma}\sqrt{\frac{\gamma-1}{\gamma+1}}\sin\beta + \left(\frac{1}{\gamma}-1\right)\cos\beta \right\} \tag{120}$$

The value of β_R can be found, as the tangent to the rarefaction-wave circle in Fig. 10

$$\sin \beta_R = \left\{ 1 - \left(\frac{q_1}{a_1} \cos \beta_s \right)^2 \right\}^{1/2} , \quad \cos \beta_R = - \frac{q_1}{a_1} \cos \beta_s \tag{121}$$

For an infinite-strength shock in a perfect gas, this becomes

$$\sin \beta_R = \frac{\sqrt{\gamma^2 - 1}}{\gamma} , \quad \cos \beta_R = - \frac{1}{\gamma} \tag{122}$$

Thus, the initial conditions are

$$T_{(0)} (\beta_R) = 0 , \quad N_{(0)} (\beta_R) = \sigma_1 \sqrt{\frac{\gamma - 1}{\gamma + 1}} \tag{123}$$

After determining the constants B_1 and B_2 to match these boundary conditions, the solution can be written in the form

$$T_{(0)} = \sigma_1 \sin \left\{ \sqrt{\frac{\gamma - 1}{\gamma + 1}} (\beta - \beta_R) \right\} \tag{124}$$

$$N_{(0)} = \sigma_1 \sqrt{\frac{\gamma - 1}{\gamma + 1}} \cos \left\{ \sqrt{\frac{\gamma - 1}{\gamma + 1}} (\beta - \beta_R) \right\} \tag{125}$$

c. Properties of the Solution

The two components of the particle velocity can now be found from these relations. To find the density and pressure, the constant in Eq. (106) is evaluated, from conditions at β_R :

$$f_{(0)} = \frac{\sigma_1^2}{\gamma} \left(\frac{\gamma - 1}{\gamma + 1} \right)^{\gamma} \psi_{(0)}^{\gamma} \tag{126}$$

Then, using Eq. (104), the density is found as

$$\psi_{(0)} = \left\{ \left(\frac{\mathcal{N}_{(0)}}{\sigma_1} \right)^2 \left(\frac{\gamma+1}{\gamma-1} \right)^{\gamma} \right\}^{\frac{1}{\gamma-1}} \tag{127}$$

and the pressure is calculated from Eq. (126).

The value of β at which the density and pressure fall to zero is found by setting $\mathcal{N}_{(0)} = 0$, i.e.:

$$\sqrt{\frac{\gamma-1}{\gamma+1}}\,(\beta - \beta_R) = \frac{\pi}{2} \tag{128}$$

Thus the "vacuum" boundary is

$$\beta_{VACUUM} = \beta_R + \sqrt{\frac{\gamma+1}{\gamma-1}}\,\frac{\pi}{2} \tag{129}$$

The total change in β from the front of the rarefaction fan to the vacuum boundary is $\sqrt{\frac{\gamma+1}{\gamma-1}}\,\frac{\pi}{2}$, in complete correspondence to the total Mach-angle change for a steady Prandtl-Meyer flow (43).

The variations of β_S, β_R, and β_{VACUUM} with γ are shown in Fig. 19; it is interesting to note that the vacuum boundary interacts with the free surface for γ less than about 1.37, and lies above it for values of γ greater than 1.37.

The above solution reveals the angle along which the various contours in Figs. 11-14 should approach the shock/free-surface intersection. These angular locations are in reasonable agreement with the results inferred from Walsh's solution, except in the region outside the target, as noted earlier. The singular characteristic, which divides the elliptic and hyperbolic regions,

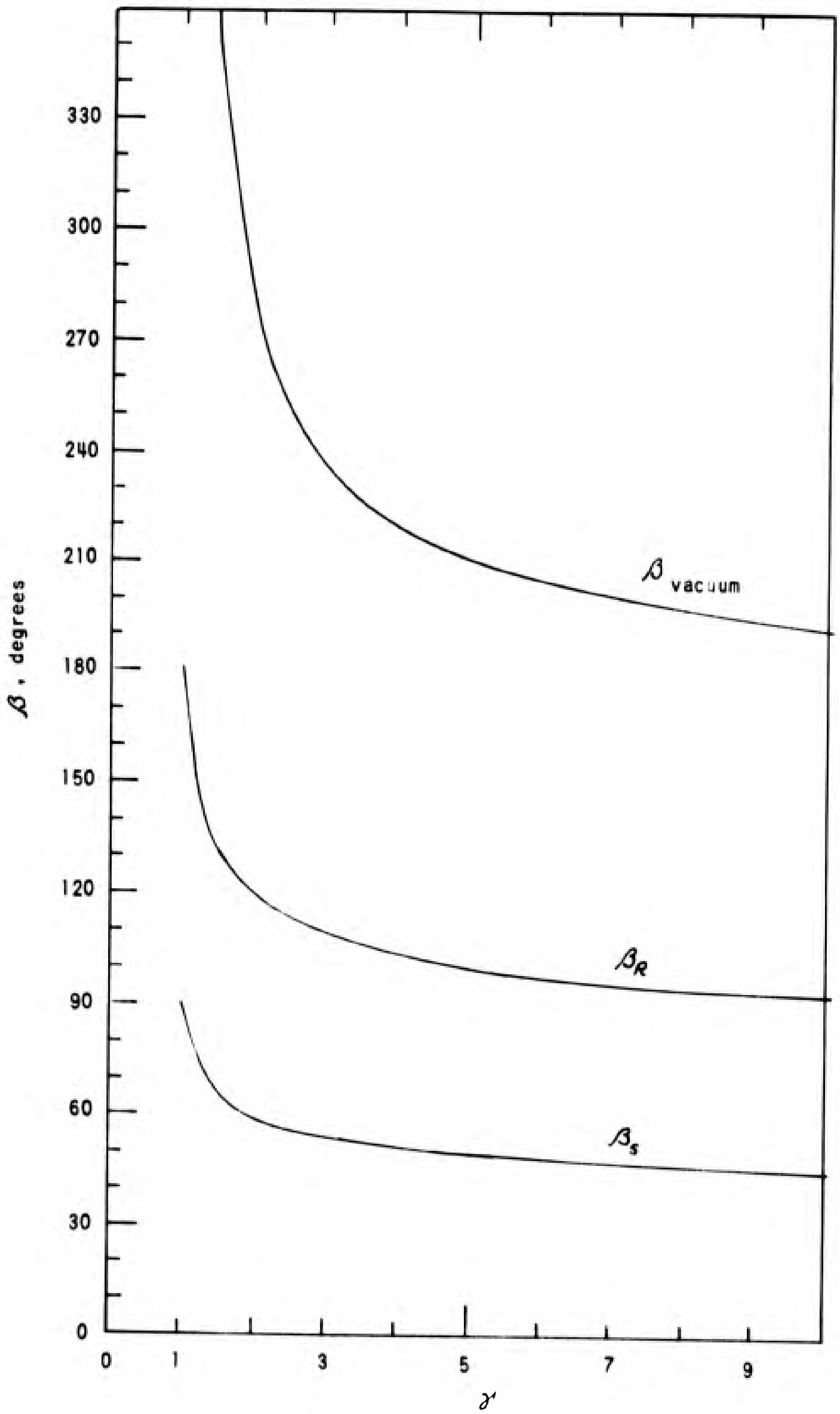

Figure 19 ANGULAR POSITION OF SHOCK, RAREFACTION FRONT, AND ZERO-PRESSURE SURFACE

can be shown from the solution above to lie along $\beta = \beta_R$. As mentioned in the discussion of Fig. 12, the numerical data do not recover this location very well.

It would be of interest to extend this solution to the next order in ℓ , as done for steady isentropic flow by Johannesen and Meyer, (44) and for flows having entropy gradients* and discontinuities of streamline curvature by Hakkinen (45, 46). The solution is required to this order, if the details of the free-surface trajectory are to be found.

D. APPROXIMATE SOLUTIONS

Many authors have attempted to uncover some of the features of the perfect-gas solution by resorting to various approximations. The most significant of these is the work of Rayzer (15), who identified the analogy with the one-dimensional case, and extended Zeldovich's arguments (14) concerning the simultaneous conservation of energy and momentum. He worked out an axisymmetric solution based on the approximation that (in the present notation) ϕ and ω should be linear functions of ζ and σ , respectively. This assumption produces a constant value (in the similarity coordinates) for the divergence of the velocity field, a condition which Rayzer suggests as a suitable generalization of the nearly constant value of $d\phi/d\zeta$ that is found in the plane-wave case (it is exactly constant for $\gamma = 1.4$). To work out the details of the solution, he assumes a crude shape for the shock, and is able to find a pair of values of

---

* Dr. Sundaram has pointed out the interesting possibility that the solution to this order might reveal the existence of a lip shock, which is known to occur in steady supersonic flow when a highly vortical region undergoes a sudden expansion (47).

ν and γ . The point-impact case he presents has $\nu = 0.386$, for $\gamma = 1.205$.

The distributions which he obtains for the various functions are admittedly crude, but they resemble in many respects the numerical solution described earlier. For example, the density ratio ψ is predicted as 0.0187 along the $\zeta = 0$ plane; reference to Fig. 11 shows that this is a reasonable value.

Rayzer presents a sketch of the shock shape that resembles the one found by Walsh, but he does not cite any numerical evidence for this shape.

Finally, it should be mentioned that Rayzer has also studied the line-impact case. His results again reveal a shock-trajectory law that is very close to the constant-energy solution. In connection with the line-explosion problem, mention should be made of the experiments reported by Deribas and Pokhozhaev (48), who used an exploding wire at the surface of a tank of water. They present a brief discussion of some theoretical scaling concepts and indicate that their results favor a similitude based on the momentum acquired by the fluid. Later experiments by Minin (49), however, indicate that the effects of gravity were important in the Deribas-Pokhozhaev data. Minin's measurements showed that when this effect is eliminated the growth rate of the funnel, or plume (essentially $\sigma_1 z_{so}(t)$) has a power-law dependence, with the exponent 0.47, which is just slightly less than the value 0.5 that would apply for a constant-energy, self-similar solution. In addition, Minin observed a growth rate of $t^{0.38}$ for the case when the exploding wire was arranged as a small flat coil, so as to generate essentially a point explosion.

Another approximate treatment of the point-source, perfect-gas problem was given by the present writer (16). In that work, the similarity equations were written along the axis of symmetry*

$$(\phi - \zeta)\psi' + \psi(\phi' + 2V) = 0 \tag{130}$$

$$-\frac{1-N}{N}\phi + (\phi - \zeta)\phi' + \frac{f'}{\psi} = 0 \tag{131}$$

$$-2\frac{1-N}{N}f + (\phi - \zeta)f' - \frac{\gamma f}{\psi}(\phi - \zeta)\psi' = 0 \tag{132}$$

Here the prime denotes $d/d\zeta$, and the function V is defined as

$$V = \left(\partial\omega/\partial\sigma\right)_{\sigma=0} \tag{133}$$

If information could now be provided about the function V, the solution near the axis of symmetry could be carried out in complete analogy to the one-dimensional case. In particular, Eqs. (130)-(132) become singular at the point where $(\phi - \zeta)^2 = \frac{\gamma f}{\psi}$, which is obviously the point where the boundary between the elliptic and hyperbolic zones intersects the axis of symmetry.

In order to provide an estimate of the function V, the radial momentum equation was differentiated, giving

$$-\frac{1-N}{N}V + (\phi - \zeta)V' + (V-1)V + \frac{1}{\psi}\left(\frac{\partial^2 f}{\partial\sigma^2}\right)_{\sigma=0} = 0 \tag{134}$$

---

* This approach was motivated by the success of analogous methods in treating the hypersonic flow over a blunt body (50).

The off-axis pressure distribution was approximated by

$$\left(\frac{\partial^2 f}{\partial \sigma^2}\right)_{\sigma=0} = \frac{f'}{\zeta} - \frac{K}{\zeta^2}(1-\zeta)f \qquad (135)$$

where the parameter K is a measure of the rate of decrease of the pressure with distance from the axis. In the blunt-body case, this parameter is directly related to the shock shape; in the present problem, it is much more difficult to estimate. The particular form of this approximation corresponds, in a spherical coordinate system, to

$$\left[\left(\frac{\partial^2 f}{\partial \theta^2}\right)_\eta\right]_{\theta=0} = -K(1-\eta)f \qquad (136)$$

where the coordinates are defined as

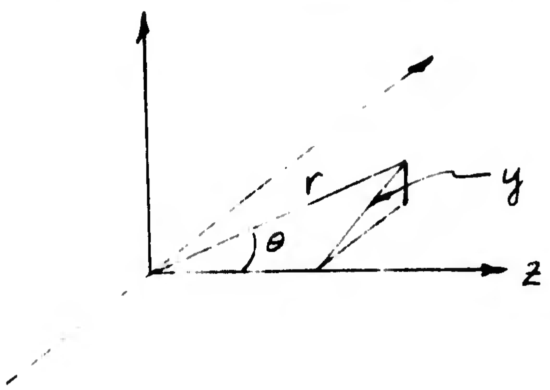

$$\eta = \frac{r}{z_{so}(t)} \qquad (137)$$

$$\zeta = \eta \cos\theta \qquad (138)$$

$$\sigma = \eta \sin\theta \qquad (139)$$

Figure 20 SPHERICAL POLAR COORDINATES

The η-factor in Eq. (136) was chosen so as to make $\partial^2 f/\partial\theta^2$ zero at $\eta = 1$, since it had already been assumed in Ref. 16 that the shock was a hemisphere with origin located at t' e impact point on the free surface.

It was found that for values of γ from 2.0 to 6.0, and K set equal to 1.0 and 10.0, the value of N required for a smooth transition through the singular point of Eqs. (130)-(132) always lay between 0.367 and 0.4. These results are in good agreement with Rayzer's approximate treatment, and with Walsh's calculations. In all three of these papers, the value of $\mathcal{N}$ is found to be near, but slightly less than 2/5, the value that would apply for a symmetric, constant-energy solution.

A direct comparison between the function V predicted by the approximation above and that revealed by Walsh's solution is difficult to make, partly because of the hemispherical shock-shape assumption, and partly because of the loss of accuracy encountered in differencing the numerical data. The general shape and magnitude of the V-distributions are in general agreement, however.

Because of the high density at the shock, most of the mass processed is concentrated in a thin shell at the shock. This fact, together with the closeness of the approximate values of $\mathcal{N}$ to the value 0.4, suggested that the flow could be approximated as one half of a spherically symmetric, constant-energy solution*, and this further approximation is advocated in Ref. 16.

To calculate the shock trajectory in this approximation, it is assumed that all of the the kinetic energy of the projectile goes into the flow behind a hemispherical shock. Then an energy balance gives

$$E = 2\pi \rho_0 R_s^3 \dot{R}_s^2 \, I(\gamma) \tag{140}$$

where the radius of the shock (equal to z_{so} along the symmetry axis) is denoted

*In addition, the symmetry-axis distributions of f, ψ and ϕ agree fairly well with those found from the symmetric solution.

by $R_s(t)$, and where

$$I(\gamma) = \int_0^1 \left(\frac{f}{(\gamma-1)\psi} + \frac{1}{2}\phi^2 \right) \psi \eta^2 d\eta \quad ; \quad \eta \equiv r/R_s(t) \tag{141}$$

To evaluate this integral, the distributions of f, ψ, and ϕ must be found. The solution for these quantities was found numerically by G. I. Taylor (4), and a closed-form solution was found by von Neumann (2), and by Sedov (3). (The closed-form solution was also derived, somewhat later, by J. L. Taylor (51), Latter (52), and Sakurai (53)). Values of $I(\gamma)$ based on these papers can be found in Ref. 54 for $1.2 \leq \gamma \leq 100$.

The solution of Eq. (140) for the shock trajectory is

$$R_s(t) = \left(\frac{25}{8\pi I(\gamma)} \frac{E t^2}{\rho_0} \right)^{1/5} \tag{142}$$

Using the value $I(1.5) = 0.\ldots$, and using a projectile of mass M and velocity U would give

$$R_s(t) \Big|_{\gamma=1.5} = 2.25 \left(\frac{2M}{\rho_0} \right)^{1/3} \left[\frac{Ut}{(2M/\rho_0)^{1/3}} \right]^{0.4} \tag{143}$$

For comparison, Walsh's data (see Eq. (85)) give

$$z_{so}(t) \Big|_{\gamma=1.5} = 1.270 \left(\frac{2M}{\rho_0} \right)^{1/3} \left[\frac{Ut}{(2M/\rho_0)^{1/3}} \right]^{0.37} \tag{144}$$

Thus, the symmetric-solution approximation overestimates the shock penetration depth, except for extremely small values of t.

The first application of the symmetric solution to the impact problem was made by Davids et al (55), and by Davids and Huang(56). At the time of those papers, the relation of the symmetric model to the true solution was not clear, and consequently the proper basis for choosing the parameter $\mathcal{N}$ was not appreciated. As a result, some of the effort in Refs. 55 and 56 was directed toward finding solutions for $\mathcal{N} \neq 0.4$. However, it appears that the only nonsingular solution of the symmetric problem is that for $\mathcal{N} = 0.4$.

V. THE REAL-FLUID CASE

Impact-generated shock propagation in solids rarely takes place at speeds large enough to permit the idealization that the material behaves thermodynamically like a perfect gas. There is a large range of conditions for which the inviscid-fluid model is still valid, but where a more realistic state equation is needed. In this section, some of the equations of state that more accurately describe a compressed solid are described. Following this, exact numerical solutions are discussed, with special reference to similitude considerations. Finally, some approximate solution methods are given.

A. THE EQUATION OF STATE

For the range of thermodynamic conditions encountered in hypervelocity impact, the Mie-Grüneisen equation of state (see, for instance, Ref. 57) provides a suitable description. Workers at various laboratories in the United States have evolved fairly complicated expressions of this equation, especially for metals. (See, for example, the equations used by Bjork (58), Tillotson (59), and Riney (60), and the comparison of these given in Ref. 54). For the purposes of this article, a somewhat simpler expression will suffice.

1. General Form

The Mie-Grüneisen equation is usually written as (57)

$$e\,(p, \rho) - e_c\,(\rho) = \frac{p - p_c(\rho)}{\rho\Gamma(\rho)} \tag{145}$$

where the subscript c denotes the cohesive contributions, and where $\Gamma(\rho)$ is the Grüneisen factor, which depends weakly on ρ .

Along the Hugoniot, Eq. (145) takes the form

$$e_H(\rho) - e_c(\rho) = \frac{p_H(\rho) - p_c(\rho)}{\rho\Gamma(\rho)} \tag{146}$$

Subtracting the left and right sides of this from the corresponding sides of Eq. (145) gives

$$e = \frac{p}{\rho\Gamma(\rho)} - \Delta(\rho) \tag{147}$$

where

$$\Delta(\rho) = \frac{p_H(\rho)}{\rho\Gamma(\rho)} - e_H(\rho) = \frac{p_c(\rho)}{\rho\Gamma(\rho)} - e_c(\rho) \tag{148}$$

The presence of the second term in Eq. (147) precludes a self-similar solution (compare with Eq. (24)) except in the limit of extremely high pressure where the quantity $\Delta(\rho)$ is negligible compared to the leading term.

If this state equation is now substituted into the Rankine-Hugoniot conditions, the result is

$$\left[1 + \frac{2\Delta(\rho_1)}{g_s^2}\right]\left(\frac{\rho_1}{\rho_0}\right)^2 - 2\left[\frac{1}{\Gamma(\rho_1)} + 1\right]\frac{\rho_1}{\rho_0} + 1 + \frac{2}{\Gamma(\rho_1)} = 0 \tag{149}$$

This relation could be used to find the dependence of ρ_1/ρ_0 on g_s , if information were available about the functions $\Gamma(\rho_1)$ and $\Delta(\rho_1)$.

2. Specific Form for a c, s Material

This process can be reversed and the measured Hugoniot data used to infer information about $\Gamma(\rho_1)$ and $\Delta(\rho_1)$. These relations take on a simple form for a substance whose Hugoniot displays a linear relation between the shock speed and particle speed

$$q_s = c + s q_1 \tag{150}$$

The weak-wave speed c is approximately equal to the bulk dilatational wave speed in many cases (57). Such a substance is referred to here as a c, s material. Many solids are well approximated by this relation; Reference 57, for example, lists values of c and s for various substances.

The shock-wave relations for a c, s material can be written in terms of the shock Mach number $M_s = \frac{q_s}{c}$ as:

$$\begin{aligned} \frac{\rho_1}{\rho_0} &= \frac{s M_s}{1 + (s-1) M_s} \quad , \quad & \frac{e_1 - e_0}{c^2} &= \frac{(M_s - 1)^2}{2 s^2} \\ \frac{p_1}{\rho_0 c^2} &= \frac{M_s (M_s - 1)}{s} \quad , \quad & \frac{q_1}{c} &= \frac{M_s - 1}{s} \end{aligned} \tag{151}$$

These relations can now be used to evaluate $\Delta(\rho)$; the resulting form of the equation of state is

$$\frac{e_1 - e_0}{c^2} = \frac{p/\rho_0 c^2}{\frac{\rho}{\rho_0}\,\Gamma\left(\frac{\rho}{\rho_0}\right)} - \frac{\left(\frac{\rho}{\rho_0} - 1\right)\left[\frac{2}{\Gamma(\rho/\rho_0)} + 1 - \frac{\rho}{\rho_0}\right]}{2\left[s - (s-1)\frac{\rho}{\rho_0}\right]^2} \tag{152}$$

At very high shock strengths, the Grüneisen factor must be taken as $2(s-1)$, in order to match the limiting density ratios of Eqs. (149) and (151). In the work reported in Ref. 54, this same constant value was used for all densities, although it would be more appropriate to allow Γ to vary with ρ in such a way as to reach the value $2s-1$ at normal density (57).

Whatever dependence is chosen for $\Gamma\left(\frac{\rho}{\rho_0}; s\right)$, Eq. (152) reveals that equation-of-state data for many materials can be correlated in terms of the quantities $p/\rho_0 c^2$, ρ/ρ_0, and $\frac{e - e_0}{c^2}$, with only s remaining as a parameter. Correlations of this type have been presented by Walsh (6), Gylden (61), and Gogolev et al (62), among others.

It was observed earlier that the Mie-Grüneisen equation approaches the perfect-gas equation of state whenever the pressure becomes large enough that the leading term dominates. Eq. (152) can be used to make a quantitative assessment of the pressure level required. In particular, at the shock, use of Eqs. (151) shows that, as $M_s \to \infty$, the leading term is of order M_s^2 while the second term is of order M_s. At points removed from the shock, the relative order of the leading term is even greater (M_s^2 times as large) than that of the term $\Delta(\rho)$ (see Eq. (183) below). Thus in the infinite-Mach-number limit, Eq. (152) can be replaced by the perfect-gas equation of state, with γ equal to $2s-1$.

Strictly speaking, Eq. (152) is not valid at pressures so high that the linear q_s, q_1 relation ceases to apply. A more serious limitation is that it sometimes leads to negative values of the pressure* and the square of the sound speed, for points along the isentropes at less than normal density (54). However, it does provide an adequate and simple representation for the high-pressure regions of the flow.

3. Enig's Formulations

Two other expressions for the state equation of a C, S material have been presented by Enig (63), and by Enig and Petrone (64). These expressions are more satisfactory, at densities below normal, than the one described above. However, they appear to have escaped the attention of workers in the field of hypervelocity impact.

The basis of the first expression (63) was to pursue the logical consequences of the "mirror-image" approximation, which states that the pressures and velocities experienced by a particle in an isentropic expansion process lie along a mirror image of the Hugoniot curve:

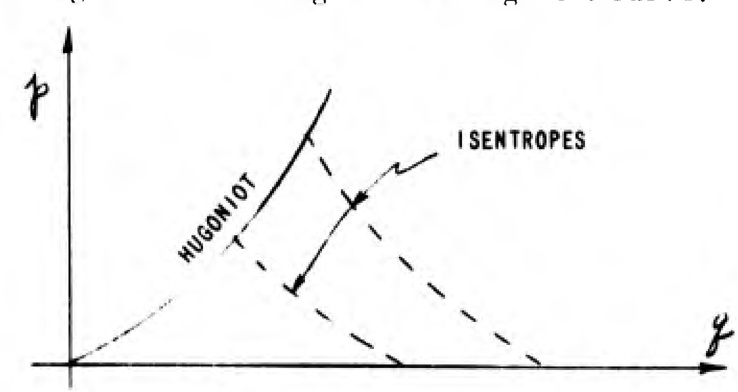

Figure 21 THE MIRROR-IMAGE APPROXIMATION

---

* Negative pressures are also predicted for some conditions by the state equations of Bjork (58), Tillotson (59), and Riney (60).

This construction is consistent with the well-established approximation that the escape speed acquired by isentropic expansion from a point on the Hugoniot is close to twice the particle speed on the Hugoniot (65). Enig noted that the mirror-image assumption implies an equation of state, and he derived a closed-form expression of this equation for the case of a c , s material. In the present notation, his result (63) is

$$4s^2 \frac{e - e_o}{c^2} = \frac{s p}{\rho_o c^2} + s\left(\frac{\rho_o}{\rho} - 1\right) + \Phi(\Psi) \tag{153}$$

where

$$\Psi = \left(1 + 4\frac{s p}{\rho_o c^2}\right) \exp\left[4s\left(\frac{\rho_o}{\rho} - 1\right)\right] \tag{154}$$

and wnere the functional dependence of Φ on Ψ is given parametrically by

$$\Psi = (2x+1)^2 \exp\left[-\frac{4x}{1+x}\right] \; ; \quad \Phi = \frac{x^3}{1+x} \tag{155}$$

The parameter x is a monotonic function of the entropy; specifically, it denotes the velocity that a particle of given entropy had immediately after being processed by the shock:

$$x = \frac{s q_1}{c} = \tilde{\mathcal{M}} - 1 \tag{156}$$

Here the symbol $\tilde{\mathcal{M}}$ stands for the value of the shock Mach number at the instant when the particle in question was processed by the shock.

Enig observed that, in calculating the temperature, the simultaneous assumptions of the mirror-image approximation, the linear q_s, q_1 relation, and the constancy of the thermal coefficient of volume expansion at low pressure lead to a rather singular behavior for the specific heat at constant pressure. The latter problem does not, however, affect the usefulness of the expression involving only e, p, and ρ.

The state equation developed by Enig and Petrone (64) employs the isentropes that had previously been shown by Walsh and Christian (65) to yield the maximum possible free-surface velocity for expansion from a given point on the Hugoniot. These isentropes are based on the approximation that the quantity $-\rho^2\left(\frac{\partial e}{\partial \rho}\right)_p$ is a constant. This quantity is related to the density ρ, the specific heat at constant pressure C_p, and the coefficient of volume expansion $\bar{\alpha}$ by

$$-\rho^2\left(\frac{\partial e}{\partial \rho}\right)_p = \frac{\rho\, c_p}{\bar{\alpha}} \tag{157}$$

In the present notation, this second equation of state is

$$\frac{\rho_0}{\rho} - 1 = -\frac{\tilde{M}-1}{s\tilde{M}} - D(\tilde{M}; s, \delta)\,\frac{p/\rho_0 c^2 - \tilde{M}(\tilde{M}-1)/s}{p/\rho_0 c^2 + \delta} \tag{158}$$

$$\frac{e-e_0}{c^2} = \frac{\tilde{M}-1}{s\tilde{M}}\left[\frac{\tilde{M}(\tilde{M}-1)}{2s} - \frac{p}{\rho_0 c^2}\right] - \frac{p}{\rho_0 c^2}\left(\frac{\rho_0}{\rho} - 1\right)$$
$$- D(\tilde{M}; s, \delta)\left\{\frac{p}{\rho_0 c^2} - \frac{\tilde{M}(\tilde{M}-1)}{s} - \left[\frac{\tilde{M}(\tilde{M}-1)}{s} + \delta\right] \ln \frac{\frac{p}{\rho_0 c^2} + \delta}{\frac{\tilde{M}(\tilde{M}-1)}{s} + \delta}\right\} \tag{159}$$

The function D is defined as

$$D(\tilde{M}; s, \delta) = -\frac{\tilde{M}-1}{s\tilde{M}}\,\frac{\delta + \frac{\tilde{M}(\tilde{M}-1)}{2s}}{\delta + \frac{\tilde{M}(\tilde{M}-1)}{s}\ln\left(1 + \frac{\tilde{M}(\tilde{M}-1)}{s\delta}\right)} \tag{160}$$

and

$$\delta = \frac{\rho c_p}{\bar{\alpha} \rho_o c^2} \tag{161}$$

Both of these formulations lead again to the conclusion that equation-of-state data are correlated by the quantities $(e - e_o)/c^2$, $p/\rho_o c^2$, and ρ/ρ_o, with ς and δ as parameters. They have the advantages of being relatively simple, and of describing the less-than-normal-density states in a manner consistent with observed free-surface behavior. The second equation has been applied successfully to the problem of shock initiation of liquid explosives. However, to the writer's knowledge, neither of these equations has yet been applied to the hypervelocity impact problem.

B. EXACT SOLUTIONS

The particle-in-cell method (66) and various modifications of it (67) have been used successfully to calculate the response of a half-space to either an impact or an explosion at the surface. Such calculations have been reported by Bjork (68), Brode and Bjork (69), Walsh et at (5, 6, 7) and by Riney and Heyda (70)-(76). These calculations have included various projectile shapes and have covered a wide range of impact speeds and types of material. In general, the response begins with a phase during which the shock propagates at a constant speed, and with a shape that is dictated by the shape of the projectile. Later, the shock takes on a roughly hemispherical shape, after the projectile itself has been severely deformed, and the shock has engulfed an amount of mass several times t[illegible]t of the projectile. Throughout the process, the particle-in-cell method sp[illegible]ads the shock over several cell widths. Except for this region and the vincinity of the shock/free-surface intersection, the solutions are satisfactory. In some cases, severe oscillations of the solution are encountered, particularly at low density. These erratic distributions can be partially eliminated by reducing the cell size, and an improvement is achieved by the continuous transport-of-mass modification (29).

1. Similtude; Late-Stage Equivalence

The solutions described above can be applied to conditions other than those for which they were specifically done, by using the similitude discovered by Walsh (6), which he named "late-stage equivalence". The general features of this similitude were described earler in Section IIID; they are formally derived in this section, in order to show their general applicability.

a) Functional Forms

The "late-stage" aspect of the similtude is simply the point-source assumption, i.e., the scaling law will accurately represent the flow caused by a projectile of nonzero size only when z_{so} is large compared to the scale of the projectile. The fact that the similtude is that appropriate to a point source means that a nonzero amount of energy and momentum are deposited at $t=0$ over an area of vanishing size. The early stages of the target's response to this excitation are characterized by self-similar behavior in which M_{so} is infinite, the equation of state is approximated by that of a perfect gas with $\gamma = 2s-1$, and the quantity $d \ln \dot{z}_{so} / d \ln z_{so} = (N-1)/N$ is the constant that will permit a smooth joining of the elliptic and hyperbolic regions.

When the solution enters the non-self-similar phase, the only new parameter that appears is M_{so} . The shock shape and the boundary values of f , ψ , ϕ, etc., change, but they depend only on M_{so}. The quantity $d \ln \dot{z}_{so} / d \ln z_{so}$ also changes as a function of M_{so} , and is found as a part of the numerical solution of Eqs. (16)-(19).

One specific way of finding $d \ln \dot{z}_{so} / d \ln z_{so}$ is the following: an increment in $1/M_{so}$ is chosen (thus giving the value that M_{so} will have at the end of the step) and an average value for $d \ln \dot{z}_{so} / d \ln z_{so}$ over the step is assumed. The method of characteristics can be used to calculate the entire flow field at the end of the step. In particular, one part of the solution is a new value for M_{so} ; if this new value does not agree with the value corresponding to the end of the step, a new value of $d \ln \dot{z}_{so} / d \ln z_{so}$ (which affects the slopes of the characteristics) is used, and the process is repeated until satisfactory agreement is achieved.

After the solution is determined down to a desired minimum value of M_{so} , the shock trajectory to that point must then be found, as indicated in Eq. (35). This is done by integrating the distribution found for $d \ln \dot{z}_{so} / d \ln z_{so}$:

$$z_{so} = \left(z_{so} \right)_{INIT} \exp \left\{ \int_{(M_{so})_{INIT}}^{M_{so}} \frac{d \ln z_{so}}{d \ln \dot{z}_{so}} \, d \ln M_{so} \right\} \tag{162}$$

The initial conditions can be evaluated by taking $(M_{so})_{INIT}$ to be very large, so that the self-similar solution applies. Use of Eq. (86) leads to

$$\frac{z_{so}}{\mathcal{L}_o} = \frac{N^{\frac{N}{1-N}} \, F(\gamma)^{\frac{1}{1-N}}}{\left(M_{so} \right)_{INIT}^{N/(1-N)}} \exp \left\{ \int_{(M_{so})_{INIT}}^{M_{so}} \frac{d \ln z_{so}}{d \ln \dot{z}_{so}} \, d \ln M_{so} \right\} \tag{163}$$

The important point to be noted is that, even though the scaling length $\mathcal{L}_o$ originates in the self-similar flow, nevertheless it continues to be the appropriate length throughout the non-similar portions of the flow. Thus the value of N, or equivalently, the value of the parameter α used by Walsh, depends only the limiting perfect-gas solution.

Equation (163) can be written as

$$\frac{z_{so}}{\mathcal{L}_o} = F_1\left(M_{so} ; s, \cdots\right) \tag{164}$$

where the three dots in the argument allow for the presence of any equation-of-state parameters other than s. In principle, this can be solved for $\dot{z}_{so}$:

$$\frac{\mathcal{L}_o}{c} \frac{d\left(z_{so}/\mathcal{L}_o\right)}{dt} = F_2\left(\frac{z_{so}}{\mathcal{L}_o} ; s, \cdots\right) \tag{165}$$

Integration would then give

$$\frac{z_{so}}{\mathcal{L}_o} = F_3\left(\frac{ct}{\mathcal{L}_o} ; s, \cdots\right) \quad ; \quad M_{so} = F_4\left(\frac{ct}{\mathcal{L}_o} ; s, \cdots\right) \tag{166}$$

For $N = 2/5$, the quantity $\mathcal{L}_o$ is proportional to the cube root of the energy release divided by the characteristic pressure, which is the scaling length appropriate in symmetric explosion problems (77).

Walsh et.al, employ the quantities L_o and U, instead of E and P, in presenting the correlation. The correspondence is:

$$\mathcal{L}_o = \left(\frac{1}{2}\right)^{\alpha - \frac{1}{3}} L_o \left(\frac{\mathcal{U}}{c}\right)^{\alpha} \tag{167}$$

where

$$L_o = \left(M/\rho_o\right)^{1/3} \quad , \quad \alpha = \frac{N}{1-N} \tag{168}$$

Thus the similitude variables used by Walsh are related to those of the present treatment by

$$\frac{\tau}{(\mathcal{U}/c)^{\alpha+1}} = \left(\frac{1}{2}\right)^{\frac{1}{3}-\alpha} \frac{ct}{\mathcal{L}_o} \; ; \; \frac{\{Z, R\}^{\alpha}}{\tau^{\alpha}} = \{\zeta, \sigma\}^{\alpha+1} \left(\frac{1}{2}\right)^{\alpha - \frac{1}{3}} \left(\frac{\mathcal{L}_o}{ct}\right)^{\alpha} \left(\frac{Z_{so}}{\mathcal{L}_o}\right)^{\alpha+1} \tag{169}$$

The last two factors in this expression depend on M_{so} and S . Finally, the correspondence of the dependent variables is

$$\frac{p Z^{2/\alpha}}{\rho_o \mathcal{U}^2} = f(\zeta, \sigma; M_{so}) M_{so}^2 \; \zeta^{2/\alpha} \left(\frac{1}{2}\right)^{2 - 2/3\alpha} \left(\frac{Z_{so}}{\mathcal{L}_o}\right)^{2/\alpha} \tag{170}$$

$$\frac{\{u, v\} Z^{1/\alpha}}{\mathcal{U}} = \{\phi, \omega(\zeta, \sigma; M_{so})\} M_{so} \zeta^{1/\alpha} \left(\frac{1}{2}\right)^{1 - 1/3\alpha} \left(\frac{Z_{so}}{\mathcal{L}_o}\right)^{1/\alpha} \tag{171}$$

In both of these, the final factor on the right is a function of M_{so}, S, and the other parameters in the state equation.

To conclude this discussion of the point-source similitude, it should be repeated that other equation-of-state parameters, in addition to S, may be important for some materials. Even when they are, different impacts into a single material will all be correlated by $\mathcal{L}_o$, since the other parameters remain the same for each of the different impacts. If different impacts into a series of <u>different</u> materials are considered, and if each of these materials has different values for its other equation-of-state parameters, then there is no guarantee that $\mathcal{L}_o$ alone will succeed in correlating the results. It appears that the effect of these parameters is stronger in the plane-wave case than in axisymmetric flow, but a quantitative estimate of their importance requires further study.

b) Evaluation of the Similitude Functions

The published shock-trajectory data can be used to estimate the function F_3 . Figure 22 shows a selection of the available results.* All of these trajectories begin with a constant-speed phase, during which the projectile is being deformed. The trajectory then makes a transition to the point-source type of behavior. If the impact speed is extremely large (such that M_{so} is initially on the order of 30 to 100), then the point-source solution will lie in the self-similar range, where the slope $d \ln z_{so} / d \ln t$ is around 0.37. For impacts at more moderate speed, (such that M_{so} is initially on the order of 10 to 30), the early-time trajectory joins the point-source solution in a region where the logarithmic slope is more nearly 0.5 or 0.6. Finally, if the impact speed is such that M_{so} is initially on the order of 3, the late-stage or point-source phase of the solution will lie very close to

*The numerical data were taken from the collection given in Ref. 54. The results of Bjork et al. for porous aluminum striking solid aluminum at 72 km/sec were taken directly from Ref. 78. The original calculations are presented only at certain discrete points. For purposes of clarity in this presentation, solid lines faired through the data points are shown.

CURVE	SOURCE	PROJECTILE/TARGET	M, gms	U, km/sec	$\mathcal{L}_o$, cm	c, km/sec
a	BJORK	IRON/TUFF	1.065×10^{10}	30	7.12×10^{3}	2.21
b	WALSH & TILLOTSON	IRON/IRON	38.6	40	5.45	4.0
c	HEYDA & RINEY	ALUMINUM/ALUMINUM	0.1525	60	1.247	5.85
d	BJORK ET. AL.	POROUS ALUMINUM/ SOLID ALUMINUM	345	72	18.2	5.85
e	HEYDA & RINEY	ALUMINUM/ALUMINUM	0.1525	20	0.659	5.85

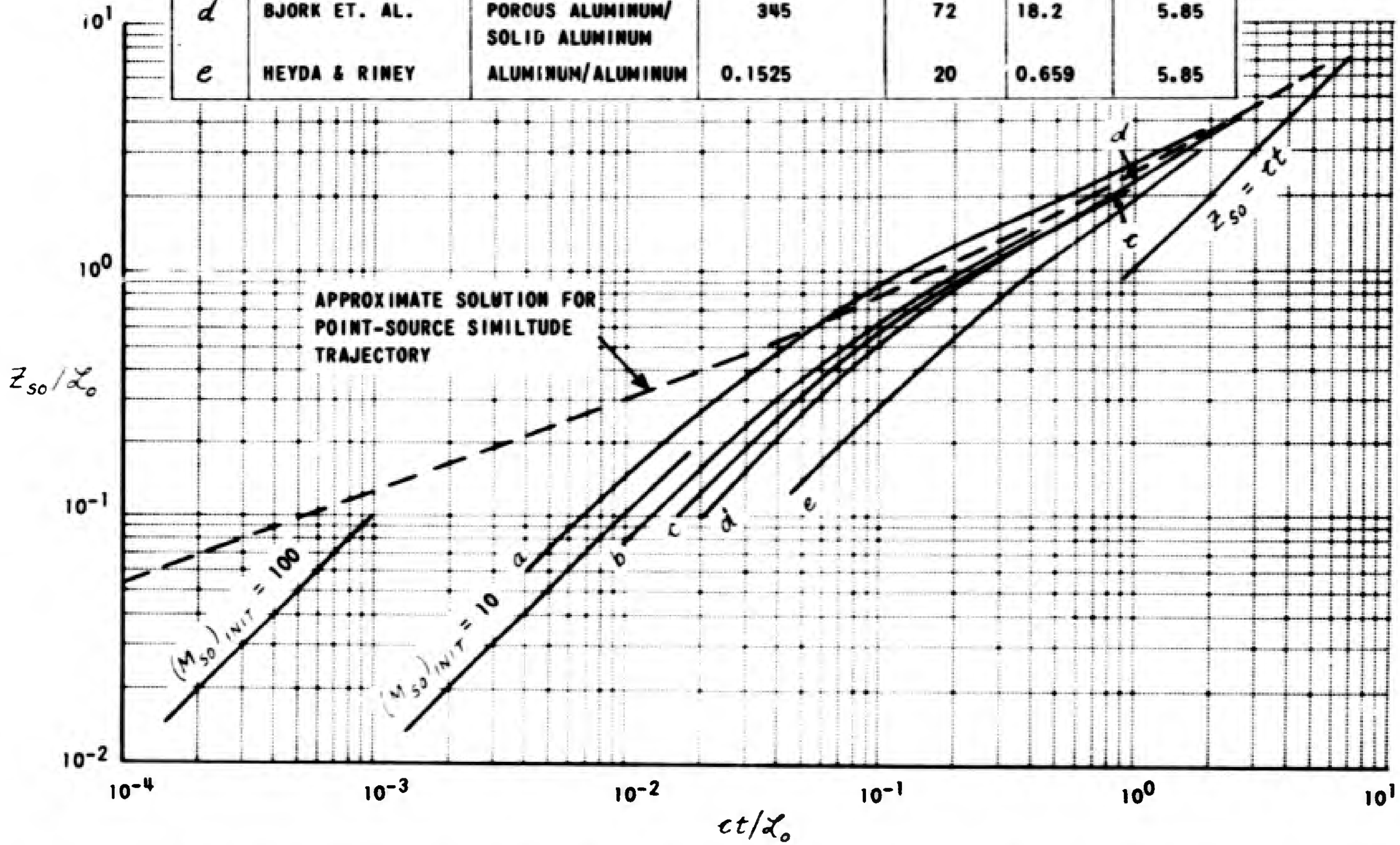

Figure 22 APPROXIMATE SHOCK TRAJECTORY FOR POINT-SOURCE SIMILITUDE. COMPARED WITH NUMERICAL CALCULATIONS

the weak-wave limit, in which $z_{s0} \sim t$. The effectiveness of the correlation derived above can be seen by comparing Walsh's data for iron striking iron at 40 km/sec with those of Heyda and Riney for aluminum-aluminum impact at 60 km/sec.

It appears that the self-similar phase is limited to the regime $ct/t_0 < 10^{-2}$, while the weak-wave limit is reached when $ct/t_0 > 10$. Unfortunately, there are not enough data available in published form to evaluate the complete point-source trajectory. The dashed curve in Fig. 22 is based on an approximation described in Section V C 1.

There are also not enough published data to evaluate the contour plots of the dimensionless functions, such as $f\,(\xi, \sigma\,;\, M_{s0})$. This lack is particularly unfortunate, since it leaves unresolved the question of what portions of the flow are correctly represented by the point-source solution, as a function of the time after impact. Most of the evidence on which the point-source similitude is based consists of quantities like the shock trajectory or the total momentum. The integrals which enter these quantities are dominated by the high-density layers near the shock, however. Thus, as pointed out in Refs. 54 and 78, the possibility remains that two flows whose shock trajectories have converged to the point-source behavior might still contain large regions in which the flow patterns differ, and still reflect the details of the initial impact phase. Walsh et al (5, 7) have presented some data* which show that similitude is achieved if one waits long enough, but there is still a need for a more precise definition of the manner in which the transition from the early phase to the similitude phase occurs.

---

*See Figs. 14, 15, 17, and 18 of Ref. 5.

A second consequence of the lack of these contour plots for finite $\mathcal{M}_{so}$ is that the similitude cannot be used to yield results for cases that have not yet been calculated. If, for example, one wanted to know the pressure distribution in the y-direction, at a depth of 10 cm in a beryllium target, at 100 microseconds after being struck by an aluminum sphere one centimeter in diameter moving at 60 km/sec, there would be no recourse other than to do the calculation ab initio. However, if the contour plots mentioned above were available, the desired information could be taken directly from them.

Thus, the present state of the exact solution for the axisymmetric, nonsimilar case can be summarized by stating that a powerful similitude exists, which can be derived directly from the differential equations for nonsimilar motion due to a point source, and is an extension of the self-similar, perfect-gas solution. However, the detailed structure of the nonsimilar solutions has not been published in sufficient detail to allow its application to a general set of conditions.

c) The Plane-Wave Case

The propagation of plane waves in real materials has been studied extensively (see, for example, Ref. 57), chiefly for the purpose of interpreting measurements of shock waves driven by explosives or by impacting slabs. Most of the attention in these studies has been devoted to the early time interval during which effects of the rarefactions coming from the loading side are not yet felt. Later studies (Ref. 79, for example) have examined the attenuation of the shock due to these rarefactions, and the possible influence of material strength on this attenuation at lower shock intensities (80).

If one waits long enough after the impact of a slab of finite thickness, the solution approaches a planar, "thin-sheet" similitude analogous to the point-source similitude that applies in the axisymmetric case. The existence of this similitude follows directly from the equations for nonsimilar plane-wave motion (i.e., Eqs. (16)-(19), with ω, and derivatives with respect to σ set equal to zero) once the scale of the impacting slab is neglected. Following an analysis similar to that of Eqs. (162)-(166), it can be shown that

$$\frac{z_{so}}{\mathcal{L}_1},\ M_{so} = fcns\left(\frac{ct}{\mathcal{L}_1},\ \gamma,\ \cdots\right) \tag{172}$$

where γ is the specific-heat ratio appropriate to the high-pressure limit of the equation of state, and where the three dots denote the presence of equation-of-state parameters other than γ.

The scaling length $\mathcal{L}_1$ is defined as

$$\mathcal{L}_1 = \left\{\frac{\mathcal{E}}{\rho_o c^2}\left(\frac{\rho}{\rho_o c}\right)^{\frac{2-3N}{2N-1}}\right\}^{\frac{2N-1}{1-N}} = \left(\frac{1}{2}\right)^{\alpha-1} L_o\left(\frac{U}{c}\right)^{\alpha}\ ;\ \alpha = \frac{N}{1-N} \tag{173}$$

Here N is the characteristic exponent that produces a nonsingular solution in the high-pressure, or self-similar limit, where the solution (Eq. (62)) can be written in the power-law form shown in Eq. (63).

Chou and Burns (28) presented method-of-characteristics calculations for a perfect gas, with $\gamma = 1.4$. The pressure ahead of the shock was taken as one atmosphere, and consequently the solution ultimately becomes non-self-similar, because of counterpressure. At sufficiently early time, and after termination of the impact phase, the solution is self-similar, and the values of N and $G(\gamma)$ are corroborated by the numerical results, as noted earlier. Chou and Burns reported the results of six calculations, which showed that, except for the early impact phase, the entire solution, all the way to the acoustic limit, is correlated by the thin-sheet similitude of Eqs. (172) and (173), where the parameter α is the same as that given by the limiting self-similar solution. The results of the particular case in which U was equal to 9.144 km/sec was used to determine the similitude functions for the shock trajectory. These are shown in Fig. 7.

These authors also presented calculations for the case of aluminum and copper, using part of the equation of state developed by Tillotson (59), namely

$$p = \left(a + \frac{b}{\frac{e}{E_0}\left(\frac{\rho_0}{\rho}\right)^2 + 1} \right) e\rho + A\left(\frac{\rho}{\rho_0} - 1\right) + B\left(\frac{\rho}{\rho_0} - 1\right)^2 \qquad (174)$$

The values used for the parameters a, b, E_0, A and B are listed in Ref. 28. At very high pressure, this equation approaches that of a pefect-gas, with $a = \gamma - 1$, as pointed out by Tillotson (59). Chou and Burns use the value $a = 0.5$ for both aluminum and copper. The analysis above predicts that the similitude parameter α would be that corresponding to $\gamma = 1.5$, which is found by interpolating in Table I to be 1.53. The results for copper are correlated by the value $\alpha = 1.50$, in satisfactory agreement with this prediction.

Their results for aluminum are anamalous, however, for they show that similitude is most nearly approached for the range of their calculations if α is 1.28. This result agrees with the earlier calculations, and experiments as well, of Chou and Allison (81).

In summary, it can be said that the calculations of Chou and Allison (81) and of Chou and Burns (28) comply with the thin-sheet similitude outlined above, both for a perfect gas with counterpressure, and for copper. The similitude which they found for aluminum, however, is not the same as the one that originates in the high-pressure limit. Further study of aluminum, including a direct comparison with the thin-sheet similitude solution itself, is required for an understanding of these results.

2. Method of Characteristics

Recently, the method of characteristics has been successfully applied to axisymmetric hypervelocity impact problems by Madden (82), and by Madden and Chang (83). These calculations have thus far been limited to relatively early times, where the shock travelling back into the projectile has not yet encountered its rear face. The results compare favorably with those of Walsh, and they provide considerable detail about the structure of the flow field. Future applications of this technique can be expected to add significant information in regions where the particle-in-cell and associated methods tend to smear out the details of the flow. The method should prove to be of particular value in sorting out the differences in the amplitude coefficient associated with various loading histories.

C. APPROXIMATE SOLUTIONS

There have been many attempts to develop an approximate theory for the nonsimilar phase of impact-generated shock propagation. Several of these, which have enjoyed some success, are briefly described below.

1. Oshima's Method

Oshima (84)-(86) developed a method for approximating the nonsimilar effect due to counterpressure in a perfect gas.* The present writer (54) adapted this method to the conditions of the impact problem, where the nonsimilarity arises from the form of the state equation.

The only cases to which Oshima's method has been applied are those in which the problem is specialized to the axis of symmetry. For this case, Eqs. (16)-(19) can be written as

$$(\phi - \zeta)\frac{\partial \psi}{\partial \zeta} + \psi\left(\frac{\partial \phi}{\partial \zeta} + 2\nu\right) = -\frac{d \ln \dot{z}_{so}}{d \ln z_{so}} \frac{\partial \psi}{\partial \ln M_{so}} \tag{175}$$

$$\frac{d \ln \dot{z}_{so}}{d \ln z_{so}} \phi + (\phi - \zeta)\frac{\partial \phi}{\partial \zeta} + \frac{1}{\psi}\frac{\partial f}{\partial \zeta} = -\frac{d \ln \dot{z}_{so}}{d \ln z_{so}} \frac{\partial \phi}{\partial \ln M_{so}} \tag{176}$$

$$2\frac{d \ln \dot{z}_{so}}{d \ln z_{so}} g + (\phi - \zeta)\frac{\partial g}{\partial \zeta} - \frac{f}{\psi^2}(\phi - \zeta)\frac{\partial \psi}{\partial \zeta} = -\frac{d \ln \dot{z}_{so}}{d \ln z_{so}}\left\{\frac{\partial g}{\partial \ln M_{so}} - \frac{f}{\psi^2}\frac{\partial \psi}{\partial \ln M_{so}}\right\} \tag{177}$$

The essential part of Oshima's method is to make what amounts to a "local-similarity" approximation of the derivatives with respect to M_{so}

* Applications of the method are given by Lewis (87), and some comments on the approximation are made in Ref. 54. The method has recently been extended to imploding shocks and detonations by Lee (88).

$$\left.\frac{\partial \ln \mathcal{F}}{\partial M_{so}}\right)_{\text{any }\zeta} = \left.\frac{\partial \ln \mathcal{F}}{\partial M_{so}}\right)_{\zeta=1} \tag{178}$$

where $\mathcal{F}$ is any of the functions f, ψ, g, ϕ or ω.

In Ref. 54, these terms are evaluated for a material having a linear shock speed-particle speed relation:

$$f(1,0;M_{so}) = \phi(1,0,M_{so}) = \frac{1}{s}\left(1 - \frac{1}{M_{so}}\right)$$

$$\psi(1,0;M_{so}) = \frac{sM_{so}}{1+(s-1)M_{so}}; \quad g(1,0;M_{so}) = \frac{1}{2s^2}\left(1-\frac{1}{M_{so}}\right)^2 \tag{179}$$

For this case, Eqs. (175)-(177) become:

$$(\phi-\zeta)\frac{d\psi}{d\zeta} + \psi\left(\frac{d\phi}{d\zeta} + 2V\right) = -\frac{d\ln \dot{Z}_{so}}{d\ln Z_{so}} \; \frac{\psi}{1+(s-1)M_{so}} \tag{180}$$

$$\frac{d\ln \dot{Z}_{so}}{d\ln Z_{so}}\phi + (\phi-\zeta)\frac{d\phi}{d\zeta} + \frac{1}{\psi}\frac{df}{d\zeta} = -\frac{d\ln \dot{Z}_{so}}{d\ln Z_{so}} \; \frac{\phi}{M_{so}-1} \tag{181}$$

$$2\frac{d\ln \dot{Z}_{so}}{d\ln Z_{so}} g + (\phi-\zeta)\frac{dg}{d\zeta} - \frac{f}{\psi^2}(\phi-\zeta)\frac{d\psi}{d\zeta} =$$

$$= -\frac{d\ln \dot{Z}_{so}}{d\ln Z_{so}}\left\{\frac{2g}{M_{so}-1} - \frac{f/\psi}{1+(s-1)M_{so}}\right\} \tag{182}$$

The function g can now be expressed in terms of f and ψ by using the equation of state*. In Ref. 54, this was taken as Eq. 152 with Γ replaced by $2(s-1)$:

---

*It should be noted that the right-hand side of Eq. (182) was obtained by applying Eq. (178) to the boundary value of g. The final result would be different if the state equation had first been used to eliminate g, and if Eq. (178) had then been applied to the boundary values of f and ψ. Thus, the form of the energy equation in Oshima's method is not unique.

$$g = \frac{1}{2(s-1)}\left\{\frac{f}{\psi} - \frac{\psi - 1}{M_{so}^2\left[s-(s-1)\psi\right]}\right\} \tag{183}$$

With this choice, Eq. (182) becomes

$$\frac{df}{d\zeta} - A^2\frac{d\psi}{d\zeta} =$$

$$= - \frac{d \ln \dot{z}_{so}}{d \ln z_{so}} \cdots \frac{2\frac{M_{so}}{M_{so}-1} g(f,\psi) - \frac{f}{\psi\left[1+(s-1)M_{so}\right]}}{(\phi-\zeta)\left(\frac{\partial g}{\partial f}\right)_\psi} \tag{184}$$

where A^2 is a dimensionless sound speed:

$$A^2 = \frac{a^2}{\dot{z}_{so}^2} = \frac{\frac{f}{\psi^2} - \left(\frac{\partial g}{\partial \psi}\right)_f}{\left(\frac{\partial g}{\partial f}\right)_\psi} =$$

$$= (2s-1)\frac{f}{\psi} + \frac{\psi}{M_{so}^2\left[s-(s-1)\psi\right]^2} \tag{185}$$

If an approximation for V is now provided, Eqs. (180), (181), and (184) can be solved by the same method that is used for the plane-wave, perfect-gas equations, i.e., the parameter $d \ln \dot{z}_{so} / d \ln z_{so}$ is adjusted until a solution free of singularities is found. These singularities occur at the points where $(\phi-\zeta)^2 = A^2$ and where $\phi = \zeta$.

The fact that Oshima's form of the nonsimilar equations must be solved by the same method used in the self-similar limit may appear somewhat surprising, since the original equations that apply to the non-self-similar regime can be solved directly by the method of characteristics and the quantity $d \ln \dot{z}_{so} / d \ln z_{so}$ evaluated as part of the solution. However, because Oshima's method makes a local-similarity approximation, the solution acquires the same property manifested by the self-similar solution, i.e., the flow fields at a series of adjacent instants must be related to each other in a manner consistent with the assumed similarity. Consequently, this approximation leads to elliptic and hyperbolic zones, which can be smoothly joined only by proper choice the eigenvalue, $d \ln \dot{z}_{so} / d \ln z_{so}$

Solutions of this type were reported in Ref. 54 for the case $S = 2$, with M_{so} = 8, 4, 2, and 1.5, and with V found from Eqs. (134) and (135), with $k' = 10$. The results* are summarized in Table III, in terms of the quantity $d \ln \dot{z}_{so} / d \ln z_{so}$. The solution for $M_{so} = \infty$ is the perfect-gas solution for $\gamma = 3$.

TABLE III

M_{so}	∞	8	4	2	1.5
$-d \ln z_{so} / d \ln \dot{z}_{so}$	0.600	0.718	0.843	1.22	1.751

These results were used, in Eq. (163), to find the approximate shock trajectory shown in Fig. 22. The initial conditons were taken from Walsh's perfect-gas solution for $\gamma = 1.5$ (although, strictly speaking, this is not the correct perfect-gas limit for $s = 2$):

$$M_{so}\Big)_{INIT} = 50 \;, \left(\frac{z_{so}}{\mathcal{L}_0}\right)_{INIT} = 0.1230 \;, \left(\frac{ct}{\mathcal{L}_0}\right)_{INIT} = 9.09 \times 10^{-4}$$

* Ref. 54 also contains some results for the nonsimilar, spherically symmetric, constant-energy case. The values of $d \ln \dot{z}_{so} / d \ln z_{so}$ for this case have approximately a constant ratio to those for the asymmetric case. The constancy of this ratio was erroneously interpreted in Ref. 54 as evidence for the validity of Walsh's similitude. As noted above, the validity of the similitude for a point-source disturbance follows without approximation directly from the governing differential equations.

The distribution of M_{so} with $z_{so}/\mathcal{L}_o$ is shown in Fig. 23. This figure can be used, in conjunction with the Rankine-Hugoniot relations, to predict the variation of the peak pressure (and other peak quantities on the axis of symmetry) with distance into the target. This prediction is shown in Fig. 24, and is compared with the calculations of Walsh et al. (6), Heyda and Riney (74), and with the experimental data* of Charest (89).

2. Variable - γ Method

One approach to the nonsimilar problem is to treat it as a succession of perfect-gas solutions, in which γ is allowed to vary in such a way as to always produce the correct conditions at the shock. This approximation is usually coupled with an assumption that the shock shape is hemispherical, with center at the impact point; thus variations around the periphery of the shock are neglected. Finally, the approximation is usually carried one step further, by replacing the flow field by one half of a spherically symmetric, constant-energy solution.

When all of these approximations are made, the only remaining problem is that of choosing the rule for allowing γ to vary. Davids et al (55), (56), chose a constant value of γ, in the vicinity of 7.0, to represent

* All of the data in Fig. 24 are shown as discrete symbols. Only Charest's results are experimental, however, while the other symbols are the results of numerical calculations.

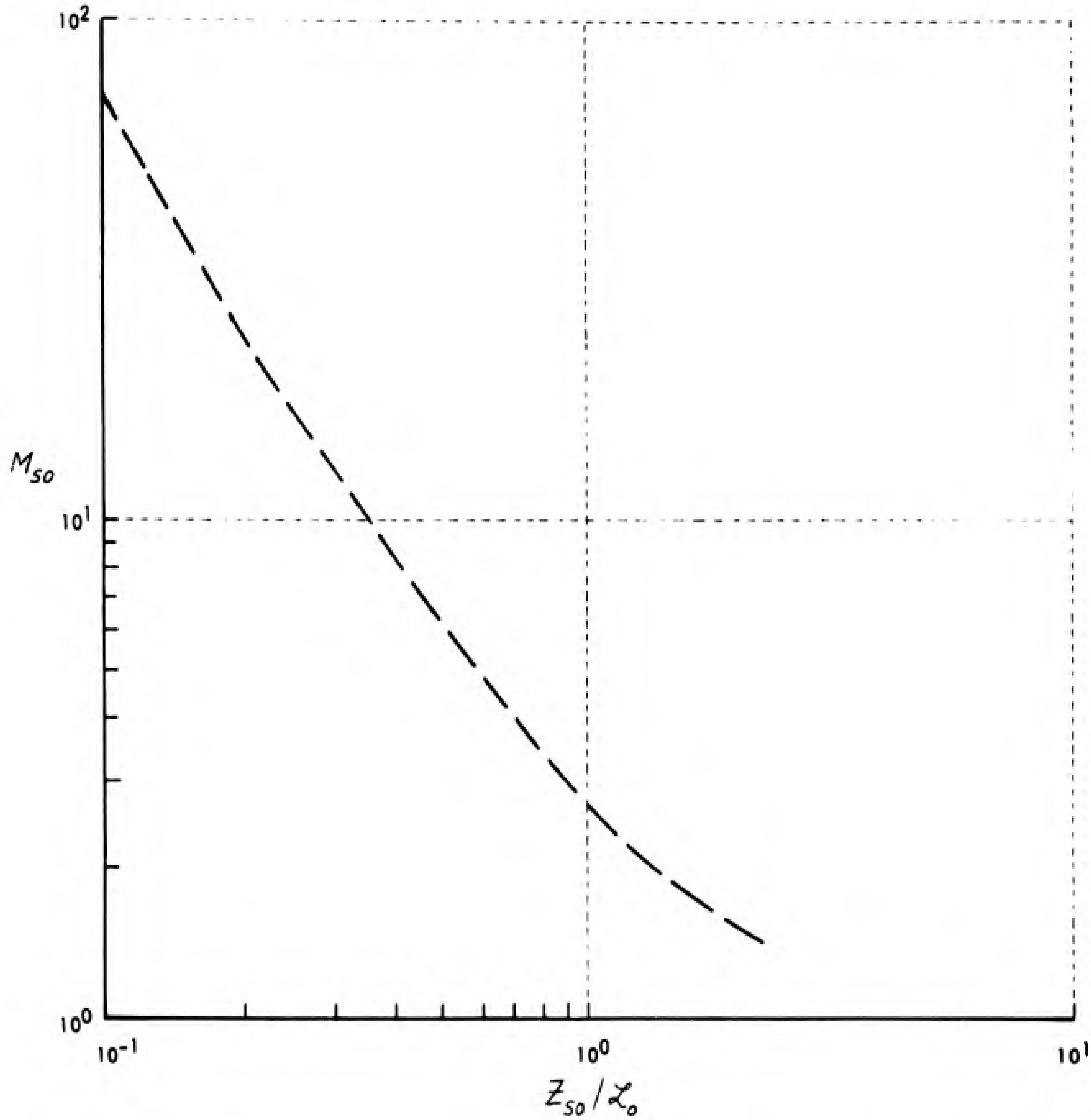

Figure 23 APPROXIMATE PREDICTION OF THE SHOCK MACH NUMBER ALONG THE SYMMETRY AXIS FOR POINT-SOURCE SIMILITUDE

SYMBOL	SOURCE	PROJECTILE/TARGET	M, gms	U, km/sec	$\mathcal{L}_o$, cm	$\rho_o c^2$, Mbar
○	WALSH & TILLOTSON	IRON/IRON	38.6	40	5.45	1.259
▷	HEYDA & RINEY	ALUMINUM/ALUMINUM	0.1525	20	0.659	0.924
⌓	CHAREST	ALUMINUM/ALUMINUM	0.1525	7.32	0.368	0.924
◖	HEYDA & RINEY	LEAD/LEAD	0.641	20	1.208	0.484

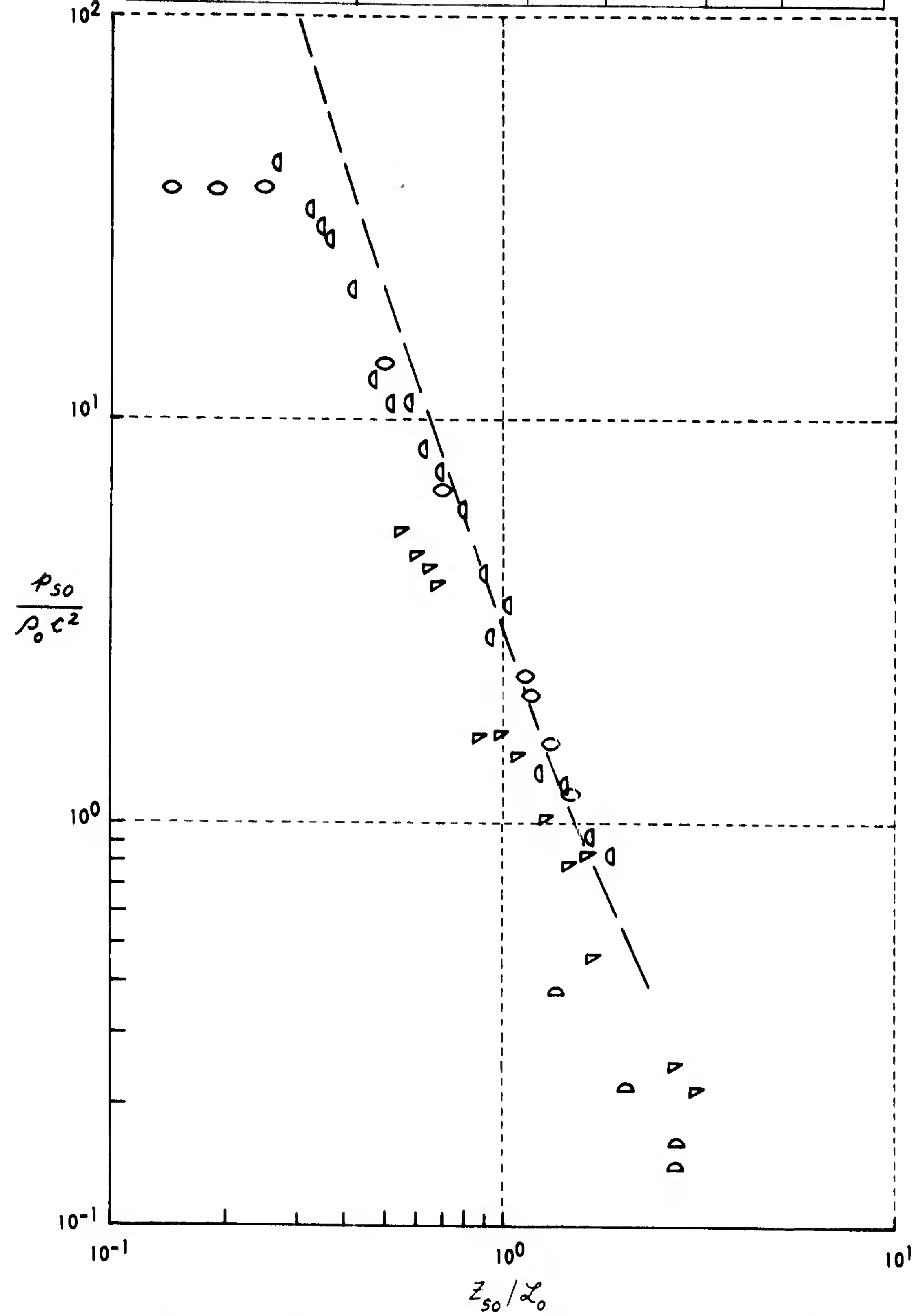

Figure 24 PEAK PRESSURE ON THE SYMMETRY AXIS, COMPARED WITH APPROXIMATE POINT-SOURCE-SIMILTUDE PREDICTION

aluminum. The present writer (54, 90) worked out the solution for the case where γ was allowed to vary with M_{so}, so as to match the quantities at the shock:

$$\gamma(M_{so}) = 2\frac{q_1}{f_s} - 1 = 2\frac{\rho_o q_s^2}{p_1} - 1 = \frac{\frac{\rho_1}{\rho_o}+1}{\frac{\rho_1}{\rho_o}-1} = \left\{\frac{2q_s^2}{e_1}\right\}^{1/2} - 1 \tag{186}$$

This functional dependence is then inserted in Eq. (140), which gives a relation between M_{so} and z_{so}/R_o, and a quadrature yields ct/R_o as a function of z_{so}/R_o, where the scaling length is defined as

$$R_o = \left(\frac{E}{2\pi\rho_o c^2}\right)^{1/3} \tag{187}$$

Except for a constant factor, this is what $\mathcal{L}_o$ would reduce to for $\nu = 2/5$.

Calculated shock trajectories are correlated by these parameters nearly as well as by $\mathcal{L}_o$ and c, as might be anticipated from the relatively small value of $2\nu-5$. In addition, the theoretical curves deduced from the quadrature mentioned above showed good agreement with the calculated data and led to the same conclusions (54, 91), regarding the various phases of the solution, as were presented in Section V B1 above. However, these symmetric-solution results are chiefly of historical interest today, in view of the general theoretical basis for the similitude based on $\mathcal{L}_o$.

3. Porzel-Zaker Method

Another approximate solution which attempts to account for nonsimilarity was developed by Porzel (92) for strong shock motion in gases, and was later adapted by Zaker (93) to the problem of a point-source explosion in a solid. The essence of the method is to assume the density distribution; the continuity equation can then be used to find the particle-velocity distribution. These two are then used in the momentum equation to find the pressure distribution.

The present writer treated this method briefly (54), using the equation of state of a C, S material. This treatment was carried out in full detail by Bach and Lee (94), who showed that the method gives a more realistic particle-velocity distribution than those of the other approximate methods mentioned above. However, its predictions of the shock trajectory are essentially the same as those of the latter methods.

VI. CONCLUDING REMARKS

A. PRESENT STATUS OF THEORY

Many of the features of the response of a half space of an inviscid, compressible, Mie-Grüneisen fluid to a point release of energy and momentum on its free surface can now be said to be well understood. The solution begins with a self-similar regime, in which the shock scale grows as a power of the time, where the power is slightly less than the value appropriate to a symmetric point-source explosion. This phase continues up to the point where $ct/\mathcal{L}_0$ is approximately 10^{-2}. Later, the logarithmic slope of the shock-scale, time curve begins to increase as the solution enters the nonsimilar regime, and tends toward one as the weak-wave limit is reached. This occurs at approximately $ct/\mathcal{L}_0 = 10$. Throughout the solution, results for all cases are correlated by the parameters $\mathcal{L}_0$ and c, with a relatively minor additional dependence on equation-of-state parameters. (This latter dependence is much greater in the plane-wave case).

In an actual impact, the projectile has nonzero size, and the shock trajectory begins with a constant-speed phase, which persists for a period on the order of the time required for a shock to travel through the projectile. After this period, the projectile becomes severely deformed and the solution makes a transition to the point-source trajectory. The point at which this transition is completed depends on the initial speed of the shock at the impact point. Unless this initial value of M_{so} is on the order of

50 or greater, the self-similar phase is not observed. This extremely large value is not likely to occur, except for impact speeds on the order of 50 km/sec. or greater. For most of the speed range of interest for meteroid impact, the transition to the point-source solution occurs in the nonsimilar range. A quantitative estimate of how long it takes to complete this transition is not available at present. After the transition is completed, the appropriate scaling factors are $\mathcal{L}_o$ and c, which originate in the self-similar phase.

Details of the two-dimensional flow pattern are available only in the self-similar regime, and even there, the structure of the flow near the shock and near the shock/free-surface intersection is not known with great precision. In the nonsimilar regime, there are essentially no details of the flow pattern available. Thus, despite the existence of a powerful similitude, the fact remains that calculations of the flow pattern must be repeated for any specific case of interest, if anything more than the shock trajectory is desired.

B. IMPLICATIONS FOR CRATER-SIZE PREDICTIONS

It must be emphasized that all of the solutions described in this review deal exclusively with an inviscid fluid. There is no mechanism by which such a fluid can be permanently brought to rest at a finite time after impact. Consequently, these solutions offer no direct information regarding the ultimate configuration in which the target comes to rest.

However, the inviscid solution has often been used as a basis for inferring the crater size by various auxiliary criteria. In applying such criteria, a clear distinction must be made between what is explicitly given by the inviscid solution, and what is inferred from it on the basis of the auxiliary criterion. A failure to recognize this distinction led to a lengthy disagreement (1) between Bjork (68) and Walsh (6) over the dependence of the crater size on impact velocity. In fact, the source of their difference lay in the crater-formation criteria, since the evidence then available indicated that the shock trajectories found by both of these writers could be correlated by the same scaling law(90), a law that was very close to the constant-energy, spherically symmetric result. The further evidence that has subsequently become available (some of which is shown in Fig. 22) serves to confirm this conclusion.

Walsh (6) adopts as his criterion the hypothesis that, if two different impacts generate the same flow pattern during the late stages of the inviscid motion, then the subsequent deformation during the strength-affected phases would also be the same. Thus, crater size would be scaled by the same parameters as those which govern the inviscid similitude, i.e., crater size would be proportional to impact speed raised to the α power.

Bjork in his earlier papers (68) identified the crater boundary as a locus of points where the pressure was low, and the particle velocities randomly oriented, a condition which he interpreted (Ref. 68, p. 512) as a finite-difference representation of a stationary region of zero pressure. From this criterion, he arrived at the conclusion that the crater size would grow with the 1/3-power of the impact speed.

As noted above, a permanent zero-velocity region is not possible in an inviscid-fluid model; on the other hand, the locus corresponding to any nonzero pressure would scale with the α -power of $\mathcal{U}$, since a given value of $p_1/\rho_0 c^2$ implies a fixed value of M_{s0} , which in turn yields a single value of $z_{s0}/\mathcal{L}_0$.

In later work, Bjork and his associates (78) have adopted a different criterion, defining the crater boundary as the locus along which the kinetic-energy density* $\frac{1}{2}\rho(u^2+v^2)$ is equal to the (temperature-dependent) yield stress of the material. The result is a prediction in which the crater size is proportional to a power of the impact speed. The power lies roughly between the limits 1/3 and 2/3, and depends on the density of the projectile.

As noted earlier, the power would have to be the same as the parameter α (approximately 0.58) if the temperature dependence of the yield strength were neglected, and if the crater boundary lay in a region of the flow field to which the point-source similitude applied. The fact that the criterion used by Bjork et al does not lead to a penetration prediction proportional to the α power of impact speed is presumably due in part to their incorporation of the temperature dependence of the yield strength. In addition, it is important to note the suggestion made by Bjork et al (Appendix D of Ref. 78) that the crater takes shape in a region to which the point-source similitude does not apply. If this assertion is true in general, it clearly

*They refer to this quantity as the dynamic pressure .

invalidates the criterion used by Walsh.* To decide whether the assertion is true, it is necessary to compare the flow field predicted by the point-source similitude with that calculated for a specific case. Unfortunately, the point-source solution is not available at present in sufficient detail to allow such a comparison. Thus it is not possible to make a definitive assessment of the boundaries in space and time within which the point-source solution is valid, nor how this region of validity varies with the size, shape, speed and composition of the projectile.

To put this discussion in proper perspective, it must be stressed that all of these attempts to predict a crater size on the basis of the inviscid solution represent a substantial further approximation. In the real case, quantities such as the temperature distribution in the flow are themselves affected by the material strength. To estimate the strength on the basis of an inviscid solution for the temperature is a complete decoupling of these effects; the error introduced by this decoupling cannot be judged on the basis of results available at the present time.

The skill and ingenuity displayed in successfully achieving numerical solutions of the Euler equations in three independent variables have properly been the object of considerable acclaim. It is sometimes difficult to appreciate the limits of validity of these solutions and, specifically, to realize that inferences drawn about crater formation do not in any sense share the same firm theoretical basis as do the inviscid solutions themselves.

*In addition, it would imply that the crater boundary should be sensitive to the shape of the projectile.

In the present writer's opinion, there is no reliable basis in the inviscid solutions available at present for selecting a dependence of crater size on impact velocity. A satisfactory resolution of this question will require solutions in which the effects of material strength are accounted for.

C. REMAINING PROBLEMS

Many problems remain to be solved before the inviscid-flow solution itself can be called complete. The two-dimensional pattern of flow contours in the nonsimilar range must be found. In addition, an improved definition of the flow near the shock, and near the shock/free-surface intersection is needed.

The effects of projectile shape play a dominant role in the period during which the transition to the point-source flow is occurring. The method of characteristics (82, 83) may prove particularly valuable in better defining this portion of the flow.

There are also certain target-shape effects which merit attention. This survey has ignored entirely the thin-plate perforation problem (see Refs. 95 and 96 , for example) and the intermediate-thickness regime in which spall fracture is the major damage mechanism (97), but in both these areas there are many unsolved problems. Even for a semi-infinite target, one unknown effect is that due to surface curvature, where some evidence (98) suggests that a convex surface leads to a more rapid decay of the shock than that encountered when the free surface is a plane.

The discussion above deals only with state equations of the Mie-Grüneisen type, and thus does not include many materials of technical importance, such as porous solids or materials which undergo a change of phase (99). The theory of impact-generated shock propagation in materials such as these is still very incomplete.

Finally, a continuing theoretical attack on the response of materials to high-speed impact must always look toward the development of solutions in which the material strength is accounted for. Many efforts have already been made in this direction (100-102), but a satisfactory understanding of the problem still lies some years in the future. In the meantime, it is hoped that the present survey will provide a convenient point of reference for evaluating future progress.

References

Note: Much of the hypervelocity-impact literature that has originated in the United States has appeared in the form of company reports. In most cases, these are available from the Clearinghouse for Federal Scientific and Technical Information (CFSTI) of the United States Department of Commerce, according to the N- and AD- serial numbers listed below.

1.) Eichelberger, R.J., "Summary: Theoretical and Experimental Studies of Crater Formation" pp 683-704 of the Proceedings of the Sixth Hypervelocity Impact Symposium, Volume 2, Part 2 (August, 1963) AD 423064

2.) Bethe, H.A., Fuchs, K., Hirschfelder, J.O., Magee, J.L., Peierls, R.E., and von Neumann, J.: "Blast Wave" Los Alamos Scientific Laboratory, Report No. LA-2000 (Aug. 1947) Available from CFSTI

3.) Sedov, L.I. Similarity and Dimensional Methods in Mechanics Academic Press, New York (1959)

4.) Taylor, G.I. "The Formation of a Blast Wave by a Very Intense Explosion. I. Theoretical Discussion" Proceedings of the Royal Society A201 (1950) 159-174

5.) Walsh, J.M., Johnson, W.E., Dienes, J.K., Tillotson, J.H., and Yates, D.R. "Summary Report on the Theory of Hypervelocity Impact" General Atomic Division, General Dynamics Corporation, Report No. GA-5119 (March 31, 1964) AD436251. Also published as pp. 343-387 of The Fluid Dynamics of Space Flight

AGARDograph 87, Volume I. Gordon and Breach, New York (1966).

6.) Walsh, J.M., and Tillotson, J.H., "Hydrodynamics of Hypervelocity Impact" General Atomic Division, General Dynamics Corp., Report No. GA-3827 (Jan. 22, 1963) AD 401023. Also available as pp. 59-104 of the Proceedings of the Sixth Symposium on Hypervelocity Impact, Volume II, Part I (Aug. 1963) AD 423063

7.) Walsh, J.M., and Johnson, W.E. "On the Theory of Hypervelocity Impact" pp. 1-75 of the Proceedings of the Seventh Hypervelocity Impact Symposium, Volume II (Feb. 1965) AD 463228

8.) See, for example: Bryan, George M. "Oblique Impact of High Velocity Steel Pellets on Lead Targets" pp. 511-534 of the Proceedings of the Fifth Symposium on Hypervelocity Impact, Volume I, Part 2 (April 1962) AD 284280

9.) Eichelberger, R.J., and Gehring, J.W. "Effects of Meteoroid Impacts on Space Vehicles" American Rocket Society Journal <u>32</u> (1962) 1583-1591

10.) Eichelberger, R.J., "Hypervelocity Impact" pp 155-187 of <u>Behavior of Materials under Dynamic Loading</u>, edited by N.J. Huffington. ASME, New York (1965)

11.) Deal, W.E. "Shock Wave Research on Inert Solids" pp 321-345 of the <u>Proceedings of the Fourth Symposium (International) on Detonation</u>. Available as Office of Naval Research, Report No. ACR-126, from the Superintendent of Documents, U.S. Government Printing Office, Washington, D.C.

12.) Kynch, G.J. "Blast Waves" <u>Modern Developments in Fluid</u>

Dynamics, Ed. by L. Howarth, Volume I, Part IV, Section II, Clarendon Press, Oxford (1953)

13.) See Reference 3, page 154.

14.) Zeldovich, Ya. B. "Motion of a Gas Due to a Pressure of Short Duration (Shock)" Akusticheskiy Zhurnal, 2 (1956) 28-38. Translation in Soviet Physics - Acoustics, 2 (1956) 25-35

15.) Rayzer, Yu. P. "Motion of a Gas Under the Influence of a Point-Impact Shock on its Surface (An Explosion on a Surface)" Zhurnal Prikladnoi Mekhaniki i Tekhnicheskoi Fiziki, No. 1, (Jan-Feb 1963) 57-66. Translation, by M. J. Nowak, available as General Atomic Division, General Dynamics Corp., Report No. GA-tr-5081, (May 28, 1964) AD 440513, and by Foreign Technology Division, Air Force Systems Command, as Report No. FTD MT 63-80, (24 Sept 1963) AD 434954

16.) Rae, W.J., and Kirchner, H.P. "Final Report on a Study of Meteoroid Impact Phenomena" Cornell Aeronautical Laboratory Report No. RM-1655-M-4 (February, 1963) N63-16887

17.) Häfele, W. "Zur Analytischen Behandlung Ebener, Starker, Instationarer Stosswellen" Zeitschrift fur Naturforschung 10a (1955) 1006-1016

18.) v. Hoerner, S. "Losung der Hydrodynamischen Gleichungen mit Linearem Verlauf der Geschwindigkeit" Zeitschrift fur Naturforschung 10a (1955) 687-692

19.) Adamskii, V.B. "Integration of a System of Autosimulating Equations for the Problem of a Short Duration Shock in a Cold Gas"

Akusticheskiy Zhurnal 2 (1956) 3-9. Translation in: Soviet Physics-Acoustics 2 (1956) 1-7

20.) Adamskii, V. B., and Popov, N. A. "The Motion of a Gas Under the Action of a Pressure on a Piston, Varying according to a Power Law" Prikladnaya Matematika i Mekhanika 23 (1959) 564-573. Translation in: Applied Mathematics and Mechanics 23 (1959) 793-806

21.) Zhukov, A. I., and Kazhdan, Ya. M. "Motion of a Gas Due to the Effect of a Brief Impulse" Akusticheskiy Zhurnal 2 (1956) 352-357. Translation in: Soviet Physics - Acoustics 2 (1957) 375-381

22.) Dienes, J. K. "Late-Stage Equivalence and Similarity Theory for One-Dimensional Impacts" General Atomic Division, General Dynamics Corp., Report No. GA-5755 (Nov. 11, 1964) AD 608870. Reprinted as pp. 187-219 of the Proceedings of the Seventh Hypervelocity Impact Symposium, Volume II (Feb 1965) AD 463228

23.) Mirels, H. "Hypersonic Flow Over Slender Bodies Associated with Power-Law Shocks" pp. 1-54 of Advances in Applied Mechanics, Volume VII, Ed. by H. L. Dryden and T. von Karman, Academic Press, New York (1962)

24.) Zeldovich, Ya. B., and Rayzer, Yu. P. Physics of Shock Waves and High-Temperature Hydrodynamic Phenomena, edited by W. D. Hayes and R. F. Probstein, Volume II, Academic Press, New York (1967)

25.) Yakura, J. K. "Theory of Entropy Layers and Nose Bluntness in Hypersonic Flow" pp 421-470 of Hypersonic Flow Research, edited by F. R. Riddell, Volume 7 of Progress in Astronautics and Rocketry, Academic Press, New York, (1962)

26.) Guiraud, J.P. "Asymptotic Theory in Hypersonic Flow" pp 70-84 of Fundamental Phenomena in Hypersonic Flow, edited by J.G. Hall. Cornell University Press, Ithaca, N.Y., (1966)

27.) Van Dyke, M.D. Perturbation Methods in Fluid Mechanics Academic Press, New York (1964)

28.) Chou, P.C., and Burns, B.P., "Late-Stage Equivalence in One-Dimensional Impacts" Journal of Applied Physics 38 (1967) 553-560

29.) Johnson, W.E., "OIL: A Continuous Two-Dimensional Eulerian Hydrodynamic Code" General Atomic Division, General Dynamics Corporation, Report No. GAMD-5580 (January 7, 1965) AD 477240

30.) Grib, A.A., Ryabinin, A.G., and Khristianovich, S.A. "On the Reflection of a Plane Shock Wave in Water from a Free Surface" Prikladnaya Matematika i Mekhanika 20 (1956) 532-544

31.) Ryzhov, O.S., and Khristianovich, S.A. "On Nonlinear Reflection of Weak Shock Waves" Prikladnaya Matematika i Mekhanika 22 (1958) 586-599. Translation in Applied Mathematics and Mechanics 22 (1958) 826-843

32.) Grib, A.A., Ryzhov, O.S., and Khristianovich, S.A. "Theory of Short Waves" Zhurnal Prikladnoi Mekhaniki i Tekhnicheskoi Fiziki, (1960) No. 1, 63-74

33.) Zaslavskii, B.I. "Some Particular Solutions of the Equations of 'Short Waves' " Zhurnal Prikladnoi Mekhaniki i Tekhnicheskoi

Fiziki (1962) No. 1, 34-38

34.) Zaslavskii, B.I. "On the Reflection of a Spherical Shock Wave in Water from a Free Surface" Zhurnal Prikladnoi Mekhaniki i Tekhnicheskoi Fiziki (1963) No. 6, 50-58

35.) Zaslavskii, B.I. "On the Nonlinear Interaction of a Spherical Shock Wave, Arising as the Result of the Explosion of a Submerged Charge, with a Free Water Surface" Zhurnal Prikladnoi Mekhaniki i Tekhnicheskoi Fiziki (1964) No. 4, 57-65

36.) Collins, R. "Intense Explosions at the Ocean Surface" College of Engineering, University of California, Berkeley, Report No. AS-66-9 (Aug 1966) AD 800347

37.) Collins, R., and Holt, M. "Intense Explosions at the Ocean Surface" Physics of Fluids 11 (1968) 701-713

38.) Hertzberg, A., and Kantrowitz, A.: "Studies with an Aerodynamically Instrumented Shock Tube" Journal of Applied Physics 21 (1950) 874-878

39.) See, for example: Streeter, V.L.: Fluid Dynamics, 1st Edition, Chapter 2, Section 8. McGraw-Hill, New York (1948)

40.) Frasier, J.T.: "Hypervelocity Impact Studies in Wax" Ballistic Research Laboratories Report No. 1124 (Feb 1961) AD255772. See also: Karpov, B.G.: "Transient Response of Wax Targets to Pellet Impact at 4 km/sec" Ballistic Research Laboratories Report No. 1226 (Oct 1963) AD 428221, Frasier, J.T., and Karpov, B.G.,: "The Transient Response of Wax Targets Subjected to Hypervelocity Impacts" Experimental Mechanics 5 (1965) 305-312, Frasier, J.T., Karpov, B.G., and Holloway, L.S.: "The Behavior of Wax Targets Subjected to Hypervelocity Impacts" Proceedings of the Seventh Hypervelocity Impact Symposium, Volume V, pp. 123-160 (Feb 1965) AD 463231, and: Frasier, J.T.: "The Transient Response of Targets Subjected to Hypervelocity Impacts" Ballistic Research Laboratories Report No. 1290 (July 1965) AD 474604

41.) Courant, R., and Friedrichs, K.O. Supersonic Flow and Shock Waves Interscience Publishers, New York (1948)

42.) Stanyukovich, K.P. Unsteady Motion of Continuous Media Pergamon Press, New York (1960) p. 362

43.) Liepmann, H.W., and Roshko, A. Elements of Gasdynamics Wiley and Sons, New York (1957) p. 99

44.) Johannesen, N.H., and Meyer, R.E. "Axially - Symmetrical Supersonic Flow near the Centre of an Expansion" Aeronautical Quarterly 2 (1950) 127-142

45.) Hakkinen, R.J. "Supersonic Flow Near Two-Dimensional and Axially Symmetric Convex Corners and Curvature Discontinuities" Douglas Aircraft Company Report No. SM-27747 (July 1958)

46.) Hakkinen, R.J. "Further Results on Supersonic Flow Near Convex Corners" Douglas Aircraft Company Report No. SM-35992 (March 1960)

47.) Weiss, R.F., and Weinbaum, S. "Hypersonic Boundary-Layer Separation and the Base Flow Problem" AIAA Journal 4 (1966) 1321-1330

48.) Deribas, A.A., and Pokhozhaev, S.I.: The Problem of an Explosion on the Surface of a Liquid" Doklady Akademii Nauk, SSSR 144 (1962) 524-526. Translation in: Soviet Physics-Doklady 7 (1962) 383-384.

49.) Minin, V.F., "Explosion on the Surface of a Liquid" Zhurnal Prikladnoi Mekhaniki i Tekhnicheskoi Fiziki (1964), No. 3, 159-161. Translation available as Air Force Systems Command, Foreign Technology Division, Rept No. MT-64-319 (Feb 28, 1966) 275-281. AD 636992

50.) Hayes, W.D., and Probstein, R.F. Hypersonic Flow Theory Academic Press, New York (1959). See especially Chapter 4.

51.) Taylor, J.L., "An Exact Solution of the Spherical Blast-Wave Problem" Philosophical Magazine 46 (1955) 317-320

52.) Latter, R.: "Similarity Solution for a Spherical Shock Wave" Journal of Applied Physics 26 (1955) 954-960

53.) Sakurai, A., "An Exact Solution of the Blast-Wave Problem" Journal of the Physical Society of Japan 10 (1955) 827-828

54.) Rae, W.J., "Nonsimilar Solutions for Impact-Generated Shock Propagation in Solids" Cornell Aeronautical Laboratory Report No. AI-1821-A-2 (March 1965) N65-21625

55.) Davids, N., Huang, Y.K., and Juanzemis, W., "Some Theoretical Models of Hypervelocity Impact" Proceedings of the Fifth Symposium on Hypervelocity Impact, Volume I, Part I, (April 1962) 111-132. AD 284282

56.) Davids, N., and Huang, Y.K. "Shock Waves in Solid Craters"

Journal of the Aerospace Sciences 29 (1962) 550-557

57.) Rice, M.H., McQueen, R.G., and Walsh, J.M., "Compression of Solids by Strong Shock Waves" pp. 1-63 of Solid State Physics, Advances in Research and Applications, Edited by F. Seitz and D. Turnbull, Volume 6. Academic Press, New York (1958)

58.) Bjork, R. L. "Analysis of the Formation of Meteor Crater, Arizona: A Preliminary Report" Journal of Geophysical Research 66 (1961) 3379-3387

59.) Tillotson, J.H. "Metallic Equations of State for Hypervelocity Impact" General Atomic Division, General Dynamics Corporation, Report No. GA-3216, (July 18, 1962) AD 486711

60.) Riney, T.D., "Solution of Visco-Plastic Equations for Axisymmetric Hypervelocity Impact. Second Summary Report, 3 Nov 1961-2 Nov 1962" APGC TDR-62-74 (Dec 1962) AD 294959

61.) Gylden, N., "On the Similarity between Compressible, Nonviscous Flows in Metals" Journal of Applied Physics 36 (1965) 2082

62.) Gogolev, V.M., Myrkin, V.G., and Yablokov, G.I. "Approximate Equation of State of Solid Bodies" Zhurnal Prikladnoi Mekhaniki i Tekhnicheskoi Fiziki, No. 5 (Sept-Oct 1963) 93-98. Translation in Air Force Systems Command, Foreign Technology Division, Report No. FTD-MT-64-61 (8 Feb 1965) 139-148. N65-30413

63.) Enig, J.W. "A Complete E, P, V, T, S, Theromodynamic Description of Metals Based on the P, u Mirror-Image Approximation" Journal of Applied Physics 34 (1963) 746-754

64.) Enig, J.W., and Petrone, F.J., "Equation of State and Derived Shock Initiation Criticality Conditions for Liquid Explosives" Physics of Fluids 9 (1966) 398-408

65.) Walsh, J.M., and Christian, R.H., "Equation of State of Metals from Shock Wave Measurements" Physical Review 97 (1955) 1544-1556

66.) Harlow, F.H., "The Particle-in-Cell Method for Numerical Solution of Problems in Fluid Dynamics" pp 269-288 of Experimental Arithmetic, High Speed Computing and Mathematics. Volume 15 of Proceedings of Symposia in Applied Mathematics. American Mathematical Society, Providence, Rhode Island (1963)

67.) For a sampling of articles describing the particle-in-cell method, various modifications of it, and other methods as well, see Fundamental Methods in Hydrodynamics, Volume 3 of Methods in Computational Physics, edited by B. Alder, S. Fernbach, and M. Rotenberg, Academic Press, New York (1964)

68.) Bjork, R.L., "Effects of a Meteroid Impact on Steel and Aluminum in Space" Tenth International Astronautical Congress Proceedings, Volume 2, pp 505-514. Springer Verlag, Vienna (1960)

69.) Brode, H.L., and Bjork, R.L., "Cratering from a Megaton Surface Burst" RAND Corporation Report RM-2600 (June 30, 1960) AD 250380

70.) Riney, T.D., "Theoretical Hypervelocity Impact Calculations Using the PICWICK Code" Interim Report, 24 June 1963 - 23 December 1963, ATL-TDR-64-8 (March 1964). AD 434220.

Also available as General Electric Space Sciences Laboratory Report R64SD13 (February 1964) AD 430606.

71.) Riney, T. D., "Behavior of Metals During Hypervelocity Impact Cratering" pp 419-445 of Developments in Mechanics, Volume 2, Part 2, Solid Mechanics. Pergamon Press, New York (1965)

72.) Riney, T. D., and Heyda, J. F., "Hypervelocity Impact Calculations and their Correlation with Experiment" General Electric Company Space Sciences Laboratory Report No. R64SD64 (September 1964) AD 606123

73.) Riney, T. D., and Heyda, J. F., "Hypervelocity Impact Calculations" pp 77-186 of the Proceedings of the Seventh Hypervelocity Impact Symposium, Volume 2 (February 1965) AD 463228

74.) Heyda, J. F., and Riney, T. D., "Peak Axial Pressures in Semi-Infinite Media under Hypervelocity Impact" pp. 75-122 of the Proceedings of the Seventh Hypervelocity Impact Symposium, Volume 3, (February 1965) AD 463229. Also available as General Electric Space Sciences Laboratory Report No. R64SD87 (February 1964) AD 452991

75.) Heyda, J. F., and Riney, T. D., "Peak Pressures in Thick Targets Generated by Reduced Density Projectiles" National Aeronautics and Space Administration Contractor Report No. CR-609 (September 1966) N66-36369

76.) Riney, T. D. "Depth of Penetration of Hypervelocity Projectiles" AIAA Journal 3 (1965) 52-60

77.) Cole, R. H., Underwater Explosions Princeton University Press, Princeton, N. J., (1948)

78.) Bjork, R. L., Kreyenhagen, K.N., and Wagner, M H., "Analytical Study of Impact Effects as Applied to the Meteoroid Hazard" NASA Contractor Report CR-757 (May 1967) N67-29028

79.) Fowles, G.R., "Attenuation of the Shock Wave Produced in a Solid by a Flying Plate" Journal of Applied Physics 31 (1960) 655-661

80.) Curran, D.R., "Nonhydrodynamic Attenuation of Shock Waves in Aluminum" Journal of Applied Physics 34 (1963) 2677-2685

81.) Chou, P.C., and Allison, F.E., "Strong Plane Shock Produced by Hypervelocity Impact and Late-Stage Equivalence" Journal of Applied Physics 37 (1966) 853-860

82.) Madden, R. "The Application of the Method of Characteristics in Three Independent Variables to the Hypervelocity Impact Problem" PhD Thesis, Virginia Polytechnic Institute, (June 1967)

83.) Madden, R., and Chang, T.S., "Axially Symmetric Hypervelocity Impact Calculations Using the Method of Characteristics" North Carolina State University, Report No. TSC-68-1 (February 1968)

84.) Oshima, K., "Blast Waves Produced by Exploding Wire" Aeronautical Research Institute, University of Tokyo, Report No. 358 (July 1960)

85.) Oshima, K., "Blast Waves Produced by Exploding Wires" pp 159-180 of Exploding Wires, Volume 2, Edited by W.G. Chace and H.K. Moore, Plenum Press, New York (1962)

86.) Oshima, K. "Quasi-Similar Solutions of Blast Waves"

Aeronautical Research Institute, University of Tokyo, Report No. 386 (March 1964)

87.) Lewis, C.H., "Plane, Cylindrical, and Spherical Blast Waves Based upon Oshima's Quasi-Similarity Model" Arnold Engineering Development Center TN 61-157 (December 1961) AD 268654

88.) Lee, B.H.K., "Nonuniform Propagation of Imploding Shocks and Detonations" AIAA Journal 5 (1967) 1997-2003

89.) Charest, J.A., "Measurements of Shock-Wave Pressures Generated by Hypervelocity Impacts in Aluminum" General Motors Corp., Defense Research Laboratories, Technical Report No. TR64-58, NASA Contractor Report CR-78399 (November 1964) N66-37523

90.) Rae, W.J., and Kirchner, H.P., "A Blast-Wave Theory of Crater Formation in Semi-Infinite Targets" Proceedings of the Sixth Symposium on Hypervelocity Impact, Volume 2, Part 1, (August 1963) 163-227 AD 423063

91.) Rae, W.J. "A Critical Review of Impact Theories" Paper presented at the Highwater Conference on Meteoroid Impact, Highwater, Quebec, (July 14-15, 1966) Available from the Library, Cornell Aeronautical Laboratory, and from CFSTI: AD 815234

92.) Porzel, F.B., "Height of Burst for Atomic Bombs, 1954. Part I, The Free-Air Curve" Los Alamos Scientific Laboratory Report LA-1664 (May 1954). Available from CFSTI.

93.) Zaker, T.A., "Point Source Explosion in a Solid" Armour

Research Foundation, Illinois Institute of Technology, Report No. A. F 4132-6 (November 1959) Available from CFSTI

94.) Bach, G.G., and Lee, J.H., "Shock Propagation in Solid Media" AIAA Paper No. 67-141 (January 1967)

95.) Friend, W.H., Murphy, C. L., and Shanfield, I., "Review of Meteroid-Bumper Interaction Studies at McGill University" McGill University, Space Research Institute Report No. SRI-R-15, NASA Contractor Report No. CR-54857 (August 1966) N67-35001

96.) Maiden, C.J., Gehring, J.W., and McMillan, A.R., "Investigation of Fundamental Mechanism of Damage to Thin Targets by Hypervelocity Projectiles" General Motors, Defense Research Laboratories Report No. TR 63-208 (March 1963) AD 404274

97.) Rae, W.J., "Comments on the Solution of the Spall-Fracture Problem in the Approximation of Linear Elasticity" Cornell Aeronautical Laboratory Report No. AI-1821-A-3, NASA Contractor Report CR-54250 (January 1965) N65-19848

98.) Loeffler, I.J., Lieblein, S., and Clough, N., "Meteroid Protection for Space Radiators" pp 551-579 of Power Systems for Space Flight, Edited by M.A. Zipkin and R.N. Edwards. Volume II of Progress in Astronautics, Academic Press, New York (1963)

99.) For an excellent summary, see: Doran, D.G., and Linde, R.K., "Shock Effects in Solids" pp 229-290 of Solid State Physics, Advances in Research and Applications, Edited by F. Seitz and D. Turnbull, Volume 19, Academic Press, New York (1966)

100.) Hopkins, H.G., "Dynamic Expansion of Spherical Cavities in Metals" pp 83-164 of Progress in Solid Mechanics, Volume 1. Ed. by I.N. Sneddon and R. Hill. North Holland Publishing Co., Amsterdam, (1960)

101.) Herrmann, W., Jones, A.H., and Percy, J.H., "The Inclusion of Material Strength in Hydrodynamic Calculations" U.S. Air Force, Special Weapons Center, Report No. TDR-63-12 (April 1963) AD 410386

102.) McDowell, E.L., "Deviatoric Effects in High Intensity Stress Waves" U.S. Air Force Weapons Laboratory Report No. TR-65-15 (August 1965) AD 620334

103.) Lees, L., and Kubota, T. "Inviscid Hypersonic Flow over Blunt-Nosed Slender Bodies" Journal of the Aeronautical Sciences 24 (1957) 195-202

Appendix 1

APPROXIMATE SOLUTION OF THE PLANE-WAVE, PERFECT-GAS CASE

A determinate solution can be found if the small amount of mass neglected, and the constant in Eq. (23) are used as two parameters to match the total energy and momentum. To actually evaluate these parameters, it is necessary to begin by finding the asymptotic form of the solution at large negative values of ζ. The fact that the pressure approaches zero in this region means that f' can be neglected in Eq. (52), leading to the approximate solution

$$\phi \simeq \zeta / N \tag{A-1}$$

This relation is now inserted in Eq. (51), to find the density:

$$\psi \simeq A_1 |\zeta|^{-\frac{1}{1-N}} \tag{A-2}$$

Finally, use of ϕ and ψ in Eq. (53) gives the asymptotic pressure formula

$$f \simeq A_2 |\zeta|^{2-\frac{\gamma}{1-N}} \tag{A-3}$$

The constants A_1 and A_2 are not independent. Lees and Kubota (103) have shown that the similarity equations have the first integral

$$\psi^{\gamma - \frac{2(1-N)}{N}} |\phi - \zeta|^{-2\frac{1-N}{N}} = \frac{\gamma+1}{2} \left(\frac{\gamma+1}{\gamma-1} \right)^{\gamma} f \tag{A-4}$$

Use of the asymptotic formulas in this relation shows that

$$A_2 = \frac{A_1^{\gamma}}{\frac{\gamma+1}{2}\left(\frac{\gamma+1}{\gamma-1}\right)^{\gamma}\left(\frac{1-N}{N}A_1\right)^{\frac{2(1-N)}{N}}} \tag{A-5}$$

The value of A_1 must be found by integrating the similarity equations out to a large negative value of ζ . For example, in the case $\gamma = 1.4$, the exact solution shows that $A_1 = 3/16$. In general, A_1 depends on γ .

The small amount of mass to be neglected, m_0 , will be to the left of a point $\zeta_0(t)$:

$$m_0 = \rho_0 A t^N \int_{-\infty}^{\zeta_0} \psi \, d\zeta \tag{A-6}$$

The integral appearing here can be evaluated directly. The expression stating the conservation of the mass lying between the shock and a control-surface position $z_{cs}(t)$ is

$$\frac{\partial}{\partial t}\int_{z_{cs}}^{z_{so}} \rho \, dz = \rho_1\left(\dot{z}_{so} - u_1\right) - \rho(z_{cs})\left[\dot{z}_{cs} - u(z_{cs})\right] \tag{A-7}$$

Sedov (3) has pointed out that this relation, expressed in terms of the self-similar functions leads to the integral

$$\int_{\zeta_a}^{\zeta_b} \psi \, d\zeta = -\Big[\psi(\phi - \zeta)\Big]_{\zeta_a}^{\zeta_b} \tag{A-8}$$

The same integral can be derived by integrating Eq. (51) by parts. If this relation is now used in Eq. (A-6), the result is

$$m_o = \rho_o A t^N \frac{1-N}{N} A_1 \left|\zeta_o\right|^{1-\frac{1}{1-N}} \tag{A-9}$$

The quantity m_o is made independent of time by choosing

$$\zeta_o = -K_1 t^{1-N} \quad , \quad K_1 > 0 \tag{A-10}$$

This gives

$$m_o = A A_1 K_1^{-\frac{N}{1-N}} \frac{1-N}{N} \rho_o \tag{A-11}$$

The parameters K_1 and A are the two that are used to match the quantities $\mathcal{E}$ and $\mathcal{P}$.

The energy-conservation integral, with m_o neglected, is

$$\mathcal{E} = \rho_o A t^N N^2 A^2 t^{2N-2} \int_{\zeta_o}^{1} \left(\frac{f}{\gamma-1} + \frac{1}{2} \psi \phi^2 \right) d\zeta \tag{A-12}$$

The integral appearing here can be evaluated from the expression for the conservation of the energy between the shock and the control-surface position:

$$\frac{\partial}{\partial t} \int_{z_{cs}}^{z_{so}} \rho \left(e + \tfrac{1}{2} u^2\right) dz = -\left[\rho \left(e + \tfrac{1}{2} u^2\right)\right]_{z_{so}} \left(u_1 - \dot{z}_{so}\right) - \left[p u\right]_{z_{so}}$$

$$+ \left[\rho \left(e + \tfrac{1}{2} u^2\right)\right]_{z_{cs}} \left[u\left(z_{cs}\right) - \dot{z}_{cs}\right] + \left[p u\right]_{z_{cs}} \tag{A-13}$$

Rewriting this in terms of the self-similar functions yields (3)

$$\int_{\zeta_a}^{\zeta_b} \left(\frac{f}{\gamma - 1} + \frac{1}{2} \psi \phi^2 \right) d\zeta = \frac{-N}{3N-2} \left[(\phi - \zeta) \left(\frac{f}{\gamma-1} + \frac{1}{2} \psi \phi^2 \right) + f \phi \right]_{\zeta_a}^{\zeta_b} \qquad \text{(A-14)}$$

As before, this integral can also be found by manipulation of the similarity equations.

If this integral and the asymptotic solutions are now used in Eq. (A-12), the result is

$$\mathcal{E} = \rho_0 A^3 \frac{A_1}{2} \frac{1-N}{2-3N} K_1^{\frac{2-3N}{1-N}} \qquad \text{(A-15)}$$

Finally, the momentum-conservation integral

$$\mathcal{P} = \rho_0 A t^N N A t^{N-1} \int_{\zeta_0}^{1} \psi \phi \, d\zeta \qquad \text{(A-16)}$$

is evaluated by expressing the conservation of momentum for the fluid lying between the shock and a control surface

$$\frac{\partial}{\partial t} \int_{z_{cs}}^{z_{so}} \rho u \, dz = \rho_1 u_1 (\dot{z}_{so} - u_1) - [\rho u]_{z_{cs}} \left[\dot{z}_{cs} - u(z_{cs}) \right] \qquad \text{(A-17)}$$

$$- [p]_{z_{so}} + [p]_{z_{cs}}$$

When this is rewritten in terms of the self-similar functions, the result is (again shown by Sedov (3) and derivable by manipulation of the similarity equations)

$$\int_{\zeta_a}^{\zeta_b} \psi \phi \, d\zeta = \frac{-N}{2N-1} \left[f + \phi \psi (\phi - \zeta) \right]_{\zeta_a}^{\zeta_b} \qquad \text{(A-18)}$$

With the use of this result, the momentum-conservation integral becomes

$$\mathcal{P} = \rho_0 N A^2 t^{2N-1} \frac{A_1}{N} \frac{1-N}{2N-1} \left|\zeta_0\right|^{2-\frac{1}{1-N}} \tag{A-19}$$

As $\zeta \to -\infty$, $\mathcal{P}$ vanishes. Thus, if all the mass were to be included in this integral, and described by the self-similar solution, its total momentum would be zero, as pointed out by Zeldovich (14). He takes the viewpoint that the solution should be interpreted in this light, namely, as one in which the input energy is matched to that of the flow by neglecting some of the mass, and in which the momentum acquired by the flow is considered to be zero, a condition guaranteed by including all of the mass in the momentum-conservation integral. If this viewpoint is taken, Eqs. (A-11) and (A-15) are solved for A and K_1 in terms of $\mathcal{E}$ and m_0; the resulting expression for the shock trajectory is

$$Z_{so}(t) = H(\gamma) \frac{m_0}{\rho_0} \left(\frac{\rho_0^2 \mathcal{E} t^2}{m_0^3} \right)^{N/2} \tag{A-20}$$

where

$$H(\gamma) = \left[\frac{2(2-3N)}{1-N} \right]^{N/2} \frac{1}{A_1^{1-N}} \left(\frac{N}{1-N} \right)^{\frac{2-3N}{2}} \tag{A-21}$$

An approximate result in which the length scale is determinate can be found (16) by neglecting m_0 in the momentum-conservation integral, which gives

$$\mathcal{P} = \rho_0 A^2 A_1 \frac{1-N}{2N-1} K_1^{\frac{1-2N}{1-N}} \tag{A-22}$$

Solving for A and K_1 in terms of $\mathcal{E}$ and P gives

$$A = G(\gamma) \frac{P^2}{\rho_0 \mathcal{E}} \left(\frac{\rho_0 \mathcal{E}^2}{P^3} \right)^N \tag{A-23}$$

$$K_1 = \left[\frac{4A_1 (1-N)(2-3N)^2}{(2N-1)^3} \; \frac{\mathcal{E}^2 \rho_0}{P^3} \right]^{1-N} \tag{A-24}$$

where

$$G(\gamma) = \frac{2(2-3N)}{2N-1} \left[\frac{(2N-1)^3}{4A_1 (1-N)(2-3N)^2} \right]^{1-N} \tag{A-25}$$

This solution then takes the form

$$Z_{so}(t) = G(\gamma) \frac{P^2}{\rho_0 \mathcal{E}} \left(\frac{t}{P^3/\rho_0 \mathcal{E}^2} \right)^N \tag{A-26}$$

For $\gamma = 1.4$, the values $A_1 = 3/16$, $N = 0.6$, lead to

$G(1.4) = (128/9)^{1/5}$.

CAL